

# UC San Diego

## UC San Diego Electronic Theses and Dissertations

### Title

Over-expression dominant negative mutagenesis identifies novel surfaces involved in telomerase regulation and an additional EST gene

### Permalink

<https://escholarship.org/uc/item/0781m0fx>

### Author

Lubin, Johnathan William

### Publication Date

2019

Peer reviewed|Thesis/dissertation

UNIVERSITY OF CALIFORNIA SAN DIEGO

Over-expression dominant negative mutagenesis identifies novel surfaces involved in telomerase regulation and an additional *EST* gene

A dissertation submitted in partial satisfaction of the requirements for the degree  
Doctor of Philosophy

in

Biology

by

Johnathan W. Lubin

Committee in charge:

Professor Vicki Lundblad, Chair  
Professor James Kadonaga  
Professor Amy Pasquinelli  
Professor Alan Saghatelian  
Professor Huilin Zhou

2019

©

Johnathan W. Lubin, 2019

All rights reserved.

The Dissertation of Johnathan W. Lubin is approved, and is acceptable in quality and form for publication on microfilm and electronically:

---

---

---

---

---

Chair

University of California San Diego

2019

## **DEDICATION**

I dedicate this dissertation to my parents, Richard and Kathleen, and to my brother, Michael.

My parents have always supported and believed in me, and made great sacrifices to ensure my happiness and success. They taught me the importance of education at an early age and provided me with opportunities to participate in after-school science, music, and sports programs. They allowed me to attend the best schools possible, and encouraged me to pursue my passions. They instilled in me the value of hard work and perseverance. And without all of that, I would not have been able to achieve this Ph.D.

My brother taught me to succeed by always making sure I failed. Growing up, he beat me at everything and never let me win. As a result, I learned never to give up and that one often improves more from failure than from first-time success. Science is full of failure, and without the life-lessons from an older brother, I may not have had the will to stay around long enough for success.

## **EPIGRAPH**

Success is not final, failure is not fatal: it is the courage to continue that counts.

Winston S. Churchill

## TABLE OF CONTENTS

Signature Page .....	iii
Dedication .....	iv
Epigraph.....	v
Table of Contents.....	vi
List of Figures.....	x
List of Tables .....	xv
Acknowledgements.....	xvi
Vita.....	xviii
Abstract of the Dissertation .....	xix
<b>Chapter One:</b> Introduction .....	1
An overview of telomerase in <i>S. cerevisiae</i> .....	4
Assembly of the holoenzyme.....	4
Recruitment to the telomere.....	5
Enzymatic activity .....	7
Additional telomerase associated proteins.....	8
Identifying <i>sof</i> mutations to understand protein function and regulation .....	9
<b>Chapter Two:</b> ODN mutagenesis, an efficient protocol for identifying separation-of-function mutations that encode structurally stable proteins, identifies two functionally distinct clusters of amino acids on the surface of Est3 .....	11
Abstract.....	12
Introduction.....	13
Results.....	16
An <i>in vivo</i> dominant-negative effect on telomere replication correlates with <i>in vitro</i> stability of mutant Est3 proteins .....	16
Mutagenesis of hydrophobic amino acids to alanine can often fail to identify functionally relevant residues.....	18
Comparing charge-swap and alanine mutagenesis of charged residues in Est3 .....	22
Structure-guided mutagenesis of the complete Est3 protein surface ....	25
Conservation does not fully predict functional interfaces .....	27
An entire surface of Est3 appears to be dispensable for telomere length maintenance, DNA replication, and repair .....	28
Discussion.....	29
Using ODN phenotypes to eliminate hypomorphic mutations due to unstable proteins .....	29
Alanine versus charge swap mutagenesis.....	31
The structure revealed there are two distinct functional surfaces on the Est3 protein.....	32
Figures .....	34
Materials and Methods.....	54

Acknowledgements.....	55
<b>Chapter Three: Using separation-of-function mutagenesis to define the full spectrum of activities performed by the Est1 telomerase subunit <i>in vivo</i></b> .....	57
Abstract.....	59
Introduction.....	60
Results.....	62
ODN-based mutagenesis identifies 11 candidate <i>sof</i> mutations in <i>EST1</i> .....	62
Identification of a novel RBD in Est1 that is conserved from yeast to humans .....	64
The Est1-Est3 interaction involves dual sites in the N- and C-terminal domains of Est1 .....	67
An expanded Est1 interface is required for the interaction with Cdc13.....	68
A newly discovered fourth function for Est1.....	70
Reexamining whether Est1 is regulated by proteasome-mediated degradation.....	72
Discussion.....	74
Are there more than four Est1 activities? .....	74
A working model for Est1 .....	76
Figures .....	79
Supplemental Figures .....	87
Materials and Methods.....	103
Acknowledgements.....	105
<b>Chapter Four: Over-expression dominant negative site-directed mutagenesis identifies a fifth <i>EST</i> gene</b> .....	106
Abstract.....	107
Introduction.....	108
Discovery of <i>EST</i> genes .....	108
Results.....	109
ODN mutagenesis identifies residues on the surface of an essential DNA replication gene involved in telomere length regulation.....	109
<i>EST5</i> is in the telomerase pathway .....	110
Identifying an external binding partner of Est5 .....	111
The interaction between Est5 and telomerase.....	113
The role of <i>EST5</i> in telomerase assembly.....	116
Discussion.....	116
The role of <i>EST5</i> in regulating telomerase .....	117
Figures .....	119
Materials and Methods.....	125
Acknowledgements.....	126



<b>Chapter Five: Conclusion</b> .....	127
Separation-of-function mutations in <i>EST1</i> , <i>EST2</i> , and <i>EST3</i> .....	129
Structural validations .....	130
Alanine versus charge swap mutagenesis.....	131
Applying ODN mutagenesis to other genes and pathways.....	132
Future directions .....	133
Figures .....	135
<b>Appendix A: Genetic approaches to reveal the <i>EST5</i> binding partner</b> .....	138
Abstract.....	139
Co-suppression by mutagenesis.....	139
Candidate genes .....	139
Genome-wide mutagenesis .....	141
Suppression by over-expression .....	141
Candidate genes .....	141
High-copy genome library .....	142
Conclusion .....	143
Figures .....	144
<b>Appendix B: Developing an assay to examine the effect of <i>EST5</i> on telomerase activity at collapsed replication forks</b> .....	148
Discussion.....	149
Figures .....	152
<b>Appendix C: Applying ODN to another gene: <i>RAD51</i></b> .....	154
Abstract.....	155
Results.....	155
A DNA polymerase delta temperature sensitive strain reveals ODN and ODP mutations .....	156
A lethal replication fork stability strain ( <i>sgs1-Δ mus81-Δ</i> ) is rescued by selected <i>rad51</i> missense mutations .....	156
Growth of ODN mutations exposed to hydroxyurea correlates with the other growth assays .....	157
Figures .....	158
<b>Appendix D: Applying the RepFC assay to monitor telomerase processivity <i>in vivo</i></b> .....	172
Abstract.....	173
Results.....	174
<i>tlc1-alt2</i> template mutations are incorporated in the RepFC assay ...	174
Both wild-type and mutant templates are incorporated in a single cell division.....	175
Template mutations affect telomere length homeostasis .....	175
Discussion.....	176

Figures .....	177
<b>References:</b> .....	180

## LIST OF FIGURES

Figure 2.1: Est3 mutant protein stability in vitro correlates with the ability of mutant proteins to confer a dominant-negative phenotype in vivo.....	34
Figure 2.2: Alignment of 20 Est3 protein sequences from the three sub-clades of <i>Saccharomytina</i> . .....	35
Figure 2.3: Analysis of mutations introduced into 18 highly conserved hydrophobic amino acids in Est3 .....	36
Figure 2.4: Loss of function (LOF) assay monitoring telomere length of <i>est3</i> - $\Delta$ yeast strains bearing single copy plasmids expressing mutations in hydrophobic residues from the native <i>EST3</i> promoter.....	37
Figure 2.5: Over-expression dominant (ODN) phenotypes assessed by monitoring telomere length. ....	38
Figure 2.6: An alternative assay for ODN phenotypes based on synthetic lethality in the presence of a <i>yku80</i> - $\Delta$ mutation. ....	39
Figure 2.7: Summary of LOF (loss of function) and ODN (over-expression dominant) phenotypes for mutations in hydrophobic residues mutated to either alanine (A) or glutamic acid (E). ....	40
Figure 2.8: Conservation of charged residues predicts the likelihood of generating a <i>sof</i> allele in <i>EST3</i> . ....	41
Figure 2.9: Comparison of LOF and ODN phenotypes displayed by a panel of mutations in charged residues in <i>EST3</i> . ....	42
Figure 2.10: Additional mutations in an alternative assay for ODN phenotypes, based on synthetic lethality in the presence of a <i>yku80</i> - $\Delta$ mutation .....	43

Figure 2.11: The severity of the ODN phenotype for an <i>est3<sup>-</sup></i> mutation, relative to the severity of the LOF phenotype, correlates with in vitro structural stability. ....	44
Figure 2.12: Two functionally distinct activities on the surface of Est3. ....	46
Figure 2.13: The surface of Est3 reveals two distinct contiguous patches. ....	47
Figure 2.14: Clustal Omega (Sievers et al. 2011) alignment of Est3 proteins from 22 yeast species used for conservation mapping by ConSurf (Ashkenazy et al. 2010; Glaser et al. 2003; Landau et al. 2005) in Fig. 3.4.....	48
Figure 2.15: Conserved surface on Est3 coincides with part of its functional activity Clustal. ....	49
Figure 2.16: DNA damage and replication stress response of selected <i>est3<sup>-</sup></i> mutations. ....	49
Figure 2.17: Three categories of <i>sof<sup>*</sup></i> mutations in the <i>EST3</i> gene. ....	50
Figure 3.1: ODN mutagenesis identifies 11 candidate separation-of-function mutations in <i>EST1</i> .....	79
Figure 3.2: Formation of the Est1-TLC1-Est2 subcomplex is unimpaired by 11 separation-of-function mutations in <i>EST1</i> .....	80
Figure 3.3: Identification of a novel 60-amino acid RNA-binding domain in Est1 .....	81
Figure 3.4: A cluster of residues in the C-terminal domain of Est1 mediate the Est1-Est3 interaction .....	82
Figure 3.5: An expanded interface on Est1 is required for binding to Cdc13 .....	83

Figure 3.6: Two mutations in the C-terminal domain of Est1 define a fourth novel function .....	84
Figure 3.7: Reinvestigating the role of proteasomal degradation on Est1 protein levels.. .....	85
Figure 3.8: A working model for Est1.....	86
Figure 3.S1: Mutations in <i>EST1</i> that were examined for ODN and/or LOF phenotypes.....	87
Figure 3.S2: ODN phenotypes of 11 separation-of-function mutations in <i>EST1</i> .....	91
Figure 3.S3: Loss-of-function analysis of telomere length for an extensive panel of <i>est1</i> <sup>-</sup> mutations .....	92
Figure 3.S4: Additional analysis of the RNA binding domain of Est1 .....	95
Figure 3.S5: Additional analysis of Est3-binding-defective alleles of <i>EST1</i> .....	97
Figure 3.S6: Additional analysis of the fourth function of Est1.....	98
Figure 4.1: ODN mutagenesis identifies residues on the surface of an essential DNA replication protein involved in telomere length regulation.....	119
Figure 4.2: <i>EST5</i> is in the telomerase pathway.....	120
Figure 4.3: Identifying an external binding partner of Est5 .....	121
Figure 4.4: Biochemical analysis of the interaction between Est5 and telomerase ....	122

Figure 4.5: Genetic analysis of the interaction between Est5 and telomerase.....	123
Figure 4.6: Biochemical analysis of the effect of <i>EST5</i> on telomerase assembly .....	123
Figure 5.1: ODN mutations identified in telomerase.....	135
Figure 5.2: Examples of ODN phenotypes in <i>EST1</i> that depend on amino acid substitution.....	135
Figure A.1: <i>cdc13</i> <sup>-</sup> mutations are not capable of suppressing the telomere length defect of <i>est5-1</i> .....	144
Figure A.2: Selected pictures of growth of genes over-expressed in an <i>est5-1</i> strain.....	145
Figure A.3: Over-expression of <i>RIF2</i> alleviates senescence .....	146
Figure A.4: Candidate plasmids from the 2 $\mu$ library retransformed into a <i>yku80</i> - $\Delta$ strain containing ADH- <i>est5-1</i> . .....	146
Figure B.1: The RepFC assay captures telomerase activity in a single cell division .	152
Figure C.1: Amino acid sequence alignment of Rad51 .....	158
Figure C.2: Over-expression of <i>rad51</i> <sup>-</sup> mutations in a <i>cdc2-2</i> strain.....	164
Figure C.3: Over-expression of <i>rad51</i> <sup>-</sup> mutations in an <i>sgs1</i> - $\Delta$ <i>mus81</i> - $\Delta$ strain. ....	237
Figure D.1: Mutation in the core template region of <i>TLCI</i> (adapted from Paschini Thesis 2015).....	177

Figure D.2: Alternative template sequence is incorporated by <i>tlc1-alt2</i> .....	177
Figure D.3: Both <i>TLC1</i> and <i>tlc1-alt2</i> add telomeric sequence at the same replication fork collapse event. ....	178
Figure D.4: Telomere length of the RepFC strains.....	179

## LIST OF TABLES

Table 2.1: List of mutations in surface-exposed Est3 residues. ....	45
Table 2.2: The parental plasmids used in Lubin et al. 2013 for all <i>in vivo</i> analysis were pVL1024 (2 $\mu$ <i>LEU2 ADH-EST3</i> ) and pVL2537 ( <i>CEN LEU2 EST3</i> ). ....	51
Table 2.3: Strains used in this chapter.....	52
Table 2.4: pVL2537 ( <i>EST3 CEN LEU2</i> ) plasmids used in Rao et al. 2014.....	52
Table 2.5: pVL2076 ( <i>EST3-(FLAG)<sub>3</sub> CEN LEU2</i> ) plasmids used in Rao et al. 2014. ....	52
Table 2.6: pVL1024 ( <i>ADH-EST3 2<math>\mu</math> LEU2</i> ) plasmids used in Rao et al 2014. ....	53
Table 3.1: Yeast Strains used in this chapter. ....	100
Table 3.2: Plasmids used in this chapter. ....	102
Table 4.1: Strains used in this chapter.....	124
Table 4.2: Plasmids used in this chapter. ....	124
Table 5.1: ODN mutations identified in telomerase. ....	137
Table A.1: Genes over-expressed in an <i>est5-1</i> strain.....	145
Table A.2: Genomic inserts of candidate plasmids from 2 $\mu$ library.....	147
Table C.1: Summary of the <i>rad51<sup>-</sup></i> mutant phenotypes. ....	169



## ACKNOWLEDGEMENTS

I would first like to thank my advisor, Vicki Lundblad. Vicki believed in my scientific abilities long before I did and her encouragement led me to pursue a career path I had never envisioned. Her continued mentorship and support was instrumental in my scientific, intellectual, professional, and personal growth. I could not have asked for a better mentor, especially at the start of my career, and I will be forever grateful and indebted to her for the success she helped me achieve.

I am also very grateful to several members of the Lundblad lab for their mentorship, friendship, and support. Tim Tucey was my first lab mentor when I started as an undergraduate intern. He had a great deal of patients and knowledge, and without that first positive lab experience, my path likely would have been different. Margherita Paschini was always a wealth of scientific knowledge and someone I frequently turned to for help and thoughtful deliberation. Cynthia Reyes always kept me humble and provided endless entertainment during the long hours and years in lab.

Debbie Wuttke and the members of her lab were incredible collaborators and the development of the ODN assay would not have been possible without them.

Thank you to my committee members for their support, encouragement, and time, for always being engaged at my committee meetings, and for making the scheduling of those meetings very easy.

I was fortunate to have several funding sources throughout my graduate career, and I would like to acknowledge all those who donated and/or paid taxes to the foundations, and those who sat on the funding committees. Thank you to the NIH, NSF, Glenn Foundation, and Rose Hills Foundation.

Some of Chapter 2 is a formatted reprint of portions of the material as it appears in Lubin, J.W., Rao, T., Mandell, E.K., Wuttke, D.S., Lundblad, V. (2013). Dissecting protein function: An efficient protocol for identifying separation-of-function mutations that encode structurally stable proteins. *Genetics* 193: 715-725, of which the dissertation author was the co-primary investigator and author, and Rao, T., Lubin, J.W., Armstrong, G.S., Tucey, T.M., Lundblad, V., Wuttke, D.S. (2014). Structure of Est3 reveals a bimodal surface with differential roles in telomere replication. *PNAS* 111: 214–218.

Chapter 3 is a formatted reprint of the material as it appears in Lubin, J.W., Tucey, T.M., Lundblad, V. Using separation-of-function mutagenesis to define the full spectrum of activities performed by the Est1 telomerase subunit *in Vivo*. *Genetics* 208: 97-110 (2018). The dissertation author was the co-primary investigator and author of this paper.

Chapter 4 contains unpublished material. Margherita Paschini contributed Figure 4.2B. The dissertation author was the primary investigator and author of this chapter.

## VITA

### EDUCATION

**University of California, San Diego, La Jolla, CA**  
Ph.D. in Biology. 2019.

**University of California Extension, San Diego, La Jolla, CA**  
Certificate in Business Management, 2018.

**San Diego State University, San Diego, CA**  
B.S. in Biology, 2009.

### RESEARCH

**Salk Institute for Biological Studies, La Jolla, CA**  
Telomere Maintenance and Telomerase Regulation  
Professor Vicki Lundblad  
2009-2019

### PUBLICATIONS

Paschini, M., Toro, T. B., **Lubin, J.W.**, Braunstein-Ballew, B., Morris, D. K., and Lundblad, V. (2012). A naturally thermolabile activity compromises genetic analysis of telomere function in *Saccharomyces cerevisiae*. *Genetics* 191: 79–93.

**Lubin, J.W.**, Tucey, T. M., and Lundblad, V. (2012). The interaction between the yeast telomerase RNA and the Est1 protein requires three structural elements. *RNA* 18: 1597–1604.

**Lubin, J.W.**, Rao, T., Mandell, E.K., Wuttke, D.S., and Lundblad, V. (2013). Dissecting protein function: An efficient protocol for identifying separation-of-function mutations that encode structurally stable proteins. *Genetics* 193: 715–725.

Rao, T., **Lubin, J.W.**, Armstrong, G. S., Tucey, T. M., Lundblad, V., and Wuttke, D.S. (2014). Structure of Est3 reveals a bimodal surface with differential roles in telomere replication. *Proc. Natl. Acad. Sci. USA* 111: 214–218.

**Lubin, J.W.**, Tucey, T.M., and Lundblad, V. (2018). Using separation-of-function mutagenesis to define the full spectrum of activities performed by the Est1 telomerase subunit *in Vivo*. *Genetics* 208: 97-110.

## **ABSTRACT OF THE DISSERTATION**

Over-expression dominant negative mutagenesis identifies novel surfaces involved in telomerase regulation and an additional *EST* gene

by

Johnathan W. Lubin

Doctor of Philosophy in Biology

University of California San Diego 2019

Professor Vicki Lundblad, Chair

A leading objective in biology is to identify the complete set of activities that each gene performs *in vivo*. For many years, the telomere biology field has sought define the functional regulatory surface of telomerase, a goal that eluded many researchers due to the lack of structural data for any of the protein subunits. A major goal of this thesis

work has been to develop of a rapid genetic approach that can identify amino acids on the surfaces of proteins (even in the absence of structural data) that, when mutated, surgically eliminate single biochemical activities. I used over-expression dominant negative (ODN) phenotypes to identify mutant proteins that disrupt function in an otherwise wild-type strain. This approach is based on the assumption that such mutant proteins retain an overall structure that is comparable to that of the wild-type protein and are therefore able to compete with the endogenous protein (Herskowitz 1987). To test these assumptions, the *in vivo* phenotypes of mutations in the Est3 telomerase subunit from *Saccharomyces cerevisiae* were compared with the *in vitro* secondary structure of these mutant proteins as analyzed by circular-dichroism spectroscopy (in collaboration with the Wuttke lab), which demonstrates that ODN is a more sensitive assessment of protein stability than the commonly used method of monitoring protein levels from extracts.

Using reverse mutagenesis to target highly conserved charged residues in the ODN assay has been efficient and extremely fruitful. By applying this strategy to all three protein subunits of telomerase, I have been able to define multiple biochemically distinct activities, including identifying two novel surfaces (one in Est3 and one in Est1) required for unknown regulatory functions.

I also supervised several undergraduate students and summer interns to apply the ODN strategy to various essential genes involved in DNA replication and repair, which led to the discovery of *EST5*. This is the first identification in over twenty years of a gene involved in the telomerase pathway that causes progressive telomere shortening and cellular senescence.

## **CHAPTER ONE:**

### Introduction

Telomeres are characterized as the repetitive, TG-rich sequence at the ends of eukaryotic chromosomes comprised of a duplex region and a 3' over-hang. Both the telomeric repeat sequence, as well as structure, is conserved from budding yeast to humans (Blackburn 1991) implying how important the telomere is in maintaining chromosomal integrity and cellular proliferation. The telomere plays an essential role in distinguishing the end of the chromosome from a double strand break, and loss of the telomere can lead to end-to-end fusions (Palm and de Lange 2008). Telomeric DNA also serves two other important purposes - it acts as a binding site for specific telomere-associated proteins that prevent unregulated resection of the chromosome end, and it also creates a buffer for DNA lost in each cell cycle due to the end replication problem. Because DNA is only replicated in the 5' to 3' direction, some amount of DNA is lost from the lagging strand with each cell division. Additionally, distal portions of the chromosome can be lost due to an unresolved fork collapse occurring during DNA replication (Paschini et al. submitted). As cells continue to proliferate, telomeres become increasingly shorter until they reach a critically short length, leading to a halt in cell division, or senescence (Levy et al. 1992). While the majority of human somatic cells age, in part, due to a loss of telomeric DNA, some stem cells, as well as ~90% of cancers are able to maintain their telomeres with a specialized enzyme called telomerase (Stewart and Weinberg 2006).

The enzyme telomerase is capable of adding telomeric repeats to the single-stranded over-hangs at chromosome ends, using an RNA template and the mechanism by which telomerase adds these repeats is conserved from yeast to humans. While all of the accessory subunits of telomerase are not fully conserved, the catalytic core, consisting of

the RNA template and a reverse transcriptase-like protein subunit, are conserved (Greider and Blackburn 1987). In fact, most of the telomerase discoveries were first made in yeast and ciliates (Greider and Blackburn 1987; Lingner et al. 1997), and then later identified in humans (Feng et al. 1995; Nakamura et al. 1997). Even though telomerase was first identified almost 30 years ago, we still lack a precise understanding of how telomerase is regulated *in vivo*.

During each cell cycle, telomerase only elongates a small subset of telomeres, and it has generally been accepted that telomerase preferentially elongates the shortest telomeres after being fully replicated (Teixeira et al. 2004). However, new evidence, from the Lundblad lab, suggests that telomerase has a second substrate, which is created when a fork collapse occurs as replication moves through the telomere (Paschini et. al submitted). These two substrates may be subject to different regulatory pathways, which is not a concept previously considered by the field. The average telomere length within a species remains constant, with yeast maintaining their telomeres at ~300 base pairs, while human telomere length is consistent at several kilobases (Blackburn 2001). Even though it is clear telomerase maintains a stable average telomere length, what regulates this length remains unknown. Furthermore, it is also now clear that while the average telomere length in a population of cells remains constant, individual telomere lengths vary greatly (Paschini et. al submitted). There is also still uncertainty as to how many telomeric repeats telomerase adds per cell cycle *in vivo*.



## **An overview of telomerase in *S. cerevisiae***

In *S. cerevisiae*, telomerase is comprised of three protein subunits and an RNA that serves as a scaffold and template. Telomerase is recruited to its substrate and regulated in three ways – assembly of the holoenzyme, recruitment to the telomere, and enzymatic activity.

While only the RNA, TLC1, and the catalytic protein subunit, Est2, are required for telomerase activity *in vitro* (Cohn and Blackburn 1995; Lingner et al. 1997), the other two protein subunits, Est1 and Est3, are required for telomerase function *in vivo* (Lendvay et al. 1996). Deletion of any of the four subunits results in the exact same phenotype upon propagation – progressively shorter telomeres and eventual senescence. Clearly, Est1 and Est3, as well as Est2, are playing some role in how telomerase action is regulated; however, very little is known about the *in vivo* regulation of telomerase. The following chapter outlines what is currently known and unknown about the three ways in which telomerase is regulated.

### *Assembly of the holoenzyme*

In budding yeast, the catalytic core of telomerase is comprised of the RNA subunit, TLC1, as well as the reverse transcriptase-like catalytic protein Est2. Bound to the complex are two regulatory subunits, Est1 and Est3, which are required for telomerase function *in vivo* (Lendvay et al. 1996), but are dispensable for catalytic function *in vitro* (Cohn and Blackburn 1995; Lingner et al. 1997).

TLC1 not only provides the template for telomere repeat addition, but also a flexible scaffold for binding the protein subunits (Zappulla and Cech 2004). Est1 and

Est2 bind TLC1 independently, on distinct arms of the RNA (Evans and Lundblad 2002; Livengood et al. 2002; Seto et al. 2002; Chappell and Lundblad 2004), forming a complex throughout most of the cell cycle (Tucey and Lundblad 2013). However, the holoenzyme is not formed until late in S phase when Est3 binds Est1 and Est2, and after which Est2 disassociates from the complex (Tucey and Lundblad 2014).

While the temporal aspects of telomerase assembly are somewhat understood, we still lack a complete spatial understanding. Whether Est3 binds to form the holoenzyme before or after telomerase is at the telomere is unknown. Additionally, we are unaware of the positive or negative regulatory signal Est3 receives to cause it to bind telomerase.

The work in this dissertation attempts to elucidate the regulation of telomerase by first identifying the functionally important surface residues of each protein subunit. Identification of each amino acid involved in telomerase function provides an incredibly useful set of reagents for identifying exactly how the complex forms and what additional regulatory interactions may occur.

### *Recruitment to the telomere*

The most well defined regulatory step of yeast telomerase is the direct interaction between the Est1 subunit and the telomere-bound protein Cdc13, which results in recruitment of telomerase to the telomere. This regulatory step was ultimately discovered as a result of first identifying mutant alleles that gave rise to the Est (ever-shorter telomere) phenotype (Lendvay et al. 1996). A mutation in *CDC13* (*cdc13-2*), as well as a mutation in *EST1* (*est1-60*), both result in the Est phenotype; however, introducing both mutations simultaneously results in a rescue of the phenotype, indicating a restoration of

a direct interaction (Nugent et al. 1996; Pennock et al. 2001). Additionally, fusing the mutant Cdc13 and telomerase can rescue the phenotype (Evans and Lundblad 1999). Furthermore, this loss of interaction, and restoration, can also be observed biochemically by co-immunoprecipitation followed by western blotting (Tucey and Lundblad 2013).

Interestingly, the direct interaction between Cdc13 and Est1 is not dependent on Est1 being bound to telomerase (via TLC1). Mutations in *EST1*, or *TLC1*, that abolish the Est1-Tlc1 interaction does not affect the Est1-Cdc13 interaction (Chapter 3). This observation, then, begs the question of when the Est1-Cdc13 interaction occurs, and leaves open several possibilities for when telomerase is recruited to the telomere. For instance, it has been proposed that telomerase may travel with the replication fork as it moves through telomeric DNA (Greider 2016). This would mean telomerase is recruited prior to it having a substrate on which to act (collapsed replication fork or fully replicated chromosomal ends). Alternatively, Est1 could bind to Cdc13, during DNA replication of the telomere, prior to Est1 binding the Est2-TLC1 complex.

It is also possible that Est3 plays a role in telomerase recruitment. Est3 is structurally very similar to the OB-fold of the human protein (Rao et al. 2014), Tpp1, which has been shown to recruit telomerase to the telomere through an interaction with the reverse transcriptase, hTERT (Zhong et al. 2012). In yeast, Est3 does not bind telomerase to form the holoenzyme until late in S phase, when telomerase is known to act (Tucey and Lundblad 2014). Perhaps before the formation of the holoenzyme, Est3 is at the telomere and is involved in recruiting telomerase through its interaction with Est1 and Est2.

Presented in this dissertation is work that identifies a novel surface on Est3 that is

essential for telomerase to function *in vivo*, yet is not required for Est3 to bind telomerase. This patch of residues likely binds a yet-to-be-identified partner of Est3, which could be bringing Est3 to the telomere in order to recruit telomerase. Other possibilities include Est3 receiving a regulatory signal to bind and form the holoenzyme, or perhaps a regulatory signal after the formation of the holoenzyme that results in telomerase being recruited to the telomere. The novel Est3 interaction could occur even further downstream, and disruption prohibits telomerase from acting on its substrate after the holoenzyme is already at the telomere. Identification of this novel surface provides an excellent set of reagents to test these possibilities.

#### *Enzymatic activity*

Telomerase is also regulated through its enzymatic activity. There are 32 telomeres in the budding yeast genome, but telomerase is predicted to act only on 7% in cell division (Teixeira et al. 2004). While the long-standing belief was that telomerase acted on the shortest telomeres, it is now becoming clear that the preferred substrate for telomerase is a collapsed replication fork (Paschini et al. submitted). However, telomerase does not act every time a replication fork collapse occurs at a telomere, and we do not yet understand why this is the case.

Previous work also argued that when telomerase does act, it is only capable of adding a small number of telomeric repeats (Cohn and Blackburn 1995), but we can now see *in vivo* that telomerase can actually add up to ~200 base pairs in a single cell division (Lundblad lab, unpublished data). The amount of nucleotides added by telomerase in on cell division is quite variable, though, and regulation is unknown.

Studying yeast telomerase *in vitro* has not been effective for gaining an understanding of its regulation, as the regulatory subunits, Est1 and Est3, are dispensable for enzymatic activity (Cohn and Blackburn 1995; Lingner et al. 1997). Luckily, we now have an assay in the Lundblad lab that is capable of capturing the footprint of telomerase in a single cell division, allowing us to observe how frequently telomerase is acting at a collapsed replication fork and how many nucleotides it is adding. Examining the effect of different telomerase mutations in this assay should allow for a greater understanding of the role different proteins play in regulating telomerase activity.

#### *Additional telomerase-associated proteins*

Telomerase is also known to have several interacting factors involved in biogenesis, recruitment, and regulation. In *S. cerevisiae*, the heterodimer Ku70/80 binds the TLC1 RNA and affects Est1 and Est2 association and possibly recruitment (Fisher et al. 2004); the Sm proteins provide RNA stability (Seto et al. 1999); and another complex, Pop1-Pop6-Pop7, was shown to interact with telomerase, most likely as a chaperone (Lemieux et al. 2016).

Many other proteins have also been implicated to either directly or indirectly associate with telomerase. The t-RPA complex (Cdc13-Stn1-Ten1) in *S. cerevisiae* has been shown to interact with telomerase (Nugent et al. 1996), but the RPA complex has also been suggested as a regulator of telomere length (Schramke et al. 2004). Structural data from *Tetryhymena* support the idea that RPA interacts with telomerase (Jiang et al. 2015), as the crystal structure of telomerase is bound to homologs of both t-RPA and RPA.

Work in this dissertation shows that yeast telomerase has other interacting factors that have not yet been identified, as well as identifies an additional *EST* gene.

### **Identifying *sof* mutations to understand protein function and regulation**

The above questions regarding how telomerase is regulated *in vivo* have remained unanswered due to a number of limitations. Because obtaining soluble, structurally stable telomerase proteins has been extremely challenging (Rao et al. 2014), leading to a lack of structural data, the surface of yeast telomerase has previously been a largely unexplored territory. We believe that there are regulatory activities of telomerase that have not yet been identified; however, the separation-of-function (*sof*<sup>+</sup>) mutations on the surface of telomerase, identified by my work, will help lead to their discovery. Targeting the surface of the complex for *sof*<sup>+</sup> mutations proved to be difficult in the absence of protein structures, but, to overcome this obstacle, I developed an over-expression dominant negative (ODN) assay (Herskowitz 1987; Lubin et al. 2013), to rapidly identify *sof*<sup>+</sup> mutations. In this assay, large panels of mutant proteins are over-expressed in a completely wild type strain. Mutants that present an ODN phenotype, then, are bonafide *sof*<sup>+</sup> alleles. In collaboration with Deborah Wuttke's lab, we showed that every mutant protein with an ODN phenotype is structurally stable (Lubin et al. 2013) and on the surface of the protein (Rao et al. 2014).

We now have a large data set of functionally important surface residues on yeast telomerase. While many of these amino acids are responsible for interactions with previously known binding partners, there are residues on each of the three protein subunits of telomerase that are novel regulatory sites required for proper *in vivo* function.

These novel mutant alleles will serve as an extremely valuable set of reagents for providing additional insights into the regulation of telomerase. Use of these alleles in further experiments to elucidate telomerase regulation will be discussed in this thesis.

Additionally, through the use of the ODN assay, mutations in protein complexes involved in DNA replication have revealed novel insights about their regulatory roles. For instance, we have found that the RPA complex has two critical roles in telomere homeostasis, as both a positive regulator and a negative regulator of telomere length. Pursuing an understanding of the mechanism by which this complex is regulating telomerase and telomere length will undoubtedly lead to insights about telomerase activity.

A greater understanding of the regulation of yeast telomerase will most certainly translate to a better knowledge of human telomerase, as well. This can eventually lead to treatments, or at least more comprehension, of telomere related diseases, such as Dyskeratosis congenita, Aplastic anemia, or Idiopathic pulmonary fibrosis, as well as shed light on cancer and aging.

Expanding the use of the ODN assay to mutate a wide range of protein complexes involved in DNA replication, repair, and recombination, we have been able to identify additional separation-of-function alleles, many in previously unrealized pathways. My thesis work specifically focused on attempts to identify novel regulators of telomere length. ODN mutagenesis screens have allowed us to uncover alleles in the telomerase complex, as well as other complexes that play important roles in telomere length regulation and will be discussed in detail throughout this thesis.

## **CHAPTER TWO:**

ODN mutagenesis, an efficient protocol for identifying separation-of-function mutations that encode structurally stable proteins, identifies two functionally distinct clusters of amino acids on the surface of Est3



A common genetic approach to identifying protein function involves deleting a gene and investigating the affect that has on the cell. However, eliminating an entire protein usually has an effect on multiple pathways or processes, so understanding a specific function among the pleotropic effects is difficult, if not impossible. Another genetic approach to overcome the problems inherent with pleotropic effects would be to make single amino acid mutations to create separation-of-function (*sof*) alleles to perturb a specific interaction or pathway. However, if a mutation is made that simply unfolds the protein, the cell then lacks that entire protein, similar to null situation. Targeting amino acids for mutagenesis that are on the surface of the protein is especially challenging for proteins that lack a known structure, as was the case for telomerase at the start of my research work. To over-come these challenges, and more efficiently screen the surface of telomerase for *sof* alleles, I developed a genetic approach that employs an over-expression dominant negative (ODN) approach and does not rely on the necessity for structural data. The following chapter details the validations for this protocol and how it was applied to the Est3 subunit of telomerase.

Some of Chapter 2 is a formatted reprint of portions of the material as it appears in Lubin, J.W., Rao, T., Mandell, E.K., Wuttke, D.S., Lundblad, V. (2013). Dissecting protein function: An efficient protocol for identifying separation-of-function mutations that encode structurally stable proteins. *Genetics* 193: 715-725, of which the dissertation author was the co-primary investigator and author, and Rao, T., Lubin, J.W., Armstrong, G.S., Tucey, T.M., Lundblad, V., Wuttke, D.S. (2014). Structure of Est3 reveals a bimodal surface with differential roles in telomere replication. *PNAS* 111: 214–218.

## **Introduction**

A fundamental tool for in vivo analysis of biological pathways employs gene inactivation. Prior to the availability of genome-wide resources, mutations in individual genes were commonly recovered from forward mutagenesis screens. Although labor-intensive, such approaches had the benefit of recovering rare novel alleles that conferred the loss of a single biochemical property. More recently, with the completion of the genome sequence of *Saccharomyces cerevisiae*, high-throughput methods have been used to generate a collection of mutant strains that inactivate gene products either through deletion of nonessential genes or conditional depletion of essential genes (Winzeler et al. 1999; Ben-Aroya et al. 2008; Yan et al. 2008; Li et al. 2011). The availability of these genome-wide reagents has permitted the analysis of genetic networks on a large scale, with the resulting information used to place genes in pathways, identify points of intersection between different pathways, and assign gene function to novel ORFs (Tong et al. 2001; Dixon et al. 2009; Chuang et al. 2010). However, an inherent caveat of these studies stems from the nature of the genetic reagents. Many proteins have more than one biochemical activity [for example, more than one interaction with other proteins (Venkatesan et al. 2009)], and thus complete inactivation of gene function is potentially pleiotropic (Costanzo et al. 2010); an additional source of pleiotropy is the aneuploidy that has been observed in a subset of yeast deletion strains (Hughes et al. 2000). Furthermore, conditional depletion of essential genes through the use of temperature-sensitive alleles or degrons requires a temperature shift (Hartwell et al. 1970; Dohmen et al. 1994), which can itself confer a phenotype even in the wild-type situation (Paschini et al. 2012).

A potential solution is to employ missense mutations, referred to as separation-of-

function (*sof*<sup>-</sup>) alleles, which surgically eliminate a single biochemical function while leaving other activities (and presumably the structural integrity of the protein) intact. The advantages of this particular class of mutations in elucidating biological pathways, particularly in essential genes, can be substantial (Zhou and Elledge 1992; Nugent et al. 1996; Umezu et al. 1998). However, recovery of *sof*<sup>-</sup> alleles has been a logistic hurdle even for single genes, as such mutations are most often recovered from genetic screens that employ loss-of-function phenotypes, followed by careful analysis to ensure that only one function has been impaired (for examples, see Rudge et al. 2001; Laurençon et al. 2003; Bertuch and Lundblad 2003; Mu et al. 2008). As a consequence, the amount of experimental effort necessary to identify and characterize *sof*<sup>-</sup> mutations has been a substantial barrier to recovering such mutations on a large scale. The obstacles stem from two technical hurdles. The first challenge is identifying the rare mutations that alter a specific biochemical property of a protein among the much larger set of hypomorphic mutations that alter nonspecific properties (such as protein stability/folding). A second hurdle is the presumption that a large number of mutations must be screened, since very few amino acids are likely to yield a separation-of-function phenotype when mutated. If candidate mutations are generated by reverse genetics, the problem is further confounded by the decision of which amino acid substitution(s) would be most likely to result in *sof*<sup>-</sup> defects.

Toward the goal of developing a widely applicable protocol for generating *sof*<sup>-</sup> alleles, I examined several approaches that might alleviate the two obstacles described above. My first experimental system was the *EST3* gene, which encodes a small (181 amino acid) subunit of yeast telomerase with two distinct categories of *sof*<sup>-</sup> alleles and

loss-of-function (LOF) as well as overexpression dominant-negative (ODN) phenotypes that can be easily monitored (Hughes et al. 2000; Lee et al. 2008, 2010). Est3 can also be expressed as a soluble structurally stable protein in *Escherichia coli* (Lee et al. 2010), thereby providing an opportunity to assess the secondary structure of mutant and wild-type proteins by circular dichroism (CD). In collaboration with the Wuttke lab, I examined the properties of a large panel of mutant Est3 proteins and revealed a striking correlation between *in vivo* ODN phenotypes and *in vitro* protein stability, resulting in the conclusion that ODN assays can provide a facile means of identifying mutant proteins that are structurally intact. We also used a systematic set of mutations introduced into ~20% of the amino acids in the Est3 protein to assess the phenotypic consequences of mutating different categories of amino acids to alanine vs. a residue with a high potential to disrupt protein folding. Alanine mutagenesis has been the default option for reverse mutagenesis (Cunningham and Wells 1989; Baase et al. 1992; Wertman et al. 1992) on the assumption that such a substitution should have a minimal effect on protein structure (Dao-Pin et al. 1991; Lim et al. 1992). We showed instead that introduction of a residue that is potentially disruptive to protein structure is in fact more useful in distinguishing between mutant proteins that are unfolded (and thus do not have a ODN phenotype) vs. proteins that have a defect in a specific activity (with a strong ODN phenotype). Based on our analysis of several different categories of mutations, we proposed that charge-swap mutagenesis directed at highly conserved charged amino acids, combined with an assessment of ODN phenotypes to eliminate unstable proteins, is an effective strategy for identifying *sof*<sup>+</sup> alleles in proteins.

Once the Wuttke lab was able to solve the structure of the Est3 protein, I probed this structure with saturation mutagenesis of the complete surface of Est3. This comprehensive approach, which is only possible once structural information is available, allows identification of all functionally relevant residues on the surface of the protein. Strikingly, residues that mediated telomere replication *in vivo* clustered to a single face of the Est3 protein, which is distinct from the normal ligand-binding surface used by OB-fold proteins. This surface could be divided into two adjacent yet functionally distinct regions. The first is a telomerase interaction surface of Est3 that is shared with its closest structural homolog, HsTPP1 (formerly known as TINT1, PTOPI, and PIP1) (Sexton et al. 2012; Zhong et al. 2012; Nandakumar et al. 2012), which has been called the “TEL patch.” We find that immediately adjacent to this TEL patch is a second functional surface that is required for yeast telomere replication *in vivo*. The strong structural similarities between Est3 and HsTPP1 suggest that this second surface might be functional on TPP1. This study illustrates how structure-driven mutagenesis of the surface of a protein, performed at saturation levels, reveals unexpected insights into the function of the protein.

## **Results**

*An in vivo dominant-negative effect on telomere replication correlates with in vitro stability of mutant Est3 proteins*

The Lundblad lab previously proposed that the overall structure of mutant Est3 proteins should be largely intact for those proteins that are capable of disrupting telomere replication when over-expressed in a wild-type strain (i.e., ODN), whereas the inability to

confer an ODN phenotype would indicate an improperly folded protein (Lee et al. 2008). To test this assumption directly, the Wuttke lab assessed the *in vitro* properties of mutations in four amino acids of the Est3 protein: *est3-W21A*, *est3-D86A*, *est3-R110A*, and *est3-V168E*. As shown previously, strains expressing these four alleles exhibit severe LOF phenotypes, comparable to that of an *est3-Δ* null strain (Lee et al. 2008). Two of these mutations (*est3-R110A* and *est3-V168E*) also represent distinct categories of *sof*<sup>+</sup> alleles: V168 is part of a group of residues that provide a binding site on Est3 for interaction with telomerase whereas R110A defines a separate activity that is not required for either association with telomerase or enzyme activity (Lee et al. 2008, 2010). Despite comparable LOF phenotypes, these four mutations show striking differences with regard to their ODN phenotypes. Overexpression of either Est3-R110A or Est3-V168E conferred a substantial telomere length decline in a wild-type strain (i.e., in the presence of the wild-type Est3 protein expressed from its native genomic locus), whereas overexpression of the Est3-W21A or Est3-D86A proteins had no impact (Lee et al. 2008 and Figure 2.1A).

To examine whether this differential ODN response was a reflection of protein stability, the Wuttke lab examined recombinant versions of the Est3-W21A, Est3-D86A, Est3-R110A, and Est3-V168E proteins relative to the wild-type Est3 protein following expression in *E. coli*. Structure stability was initially assessed based on expression and solubility of His<sub>10</sub>-SUMO-tagged Est3 mutant proteins by evaluating the partitioning of *E. coli*-expressed protein into insoluble vs. soluble fractions after cell lysis by Western blot analysis (Figure S1, Lubin et al. 2013). The wild-type Est3 protein expressed well, whereas expression of Est3-D86A was markedly reduced, exhibiting expression levels

only 30% of the wild-type and yielding very little, if any, soluble protein. Although expression of Est3-W21A was less impaired, subsequent purification revealed that it formed soluble aggregates. Thus, both of these mutant proteins exhibited a marked loss of structural stability *in vitro*, providing a potential explanation for their failure to disrupt wild-type yeast telomere replication *in vivo* when overexpressed.

In contrast, the mutant Est3-R110A and Est3-V168E proteins were readily expressed and yielded sufficient soluble protein to allow secondary structure analysis by CD. Comparison of the spectra of the Est3- R110A and Est3-V168E mutant proteins with wild-type Est3 revealed a strikingly similar secondary structure content and thermal stability, as indicated by the spectra shown in Figure 2.1B and Figure S2 (Lubin et al. 2013) and by the melting curves at 208 and 222 nm in Figure S3 (Lubin et al. 2013). In fact, the Est3-V168E protein appeared to be slightly more stable than Est3 or Est3-R110A (Figure 2.1B). The ability of these two mutant proteins to assume an overall structure that was essentially indistinguishable from that of the wild-type Est3 protein supports the correlation between structure stability and the ability of these two mutant proteins to exert a dominant-negative impact on telomere length when overexpressed.

*Mutagenesis of hydrophobic amino acids to alanine can often fail to identify functionally relevant residues*

In the example above, changing valine 168 to a charged residue resulted in a mutant protein with a profound effect on Est3 function. However, mutating this same residue to alanine had no effect on telomere replication (Lee et al. 2008 and see below). This result runs counter to the usual convention, in which mutation to alanine is the

default choice when assessing the potential contribution of an amino acid to protein function to minimize any possible perturbation of protein structure (Cunningham and Wells 1989; Moreira et al. 2007). However, an alternative premise is that amino acid changes that are likely to be highly detrimental to protein folding would provide a more effective means of distinguishing between residues that are important for stability vs. those that perform a discrete biochemical function. This approach is based on the rationale that, if a residue is located in the interior of the protein, mutating it to a charged residue is likely to disrupt the structural integrity of a protein (Dao-Pin et al. 1991; Lim et al. 1992); this destabilized mutant protein should confer a LOF phenotype but will be phenotypically silent in the ODN assay. In contrast, mutating a surface residue that is critical for a specific activity (such as a protein interaction) to a nonconservative amino acid substitution is less likely to affect protein structure; as a consequence, such mutations should exhibit defects in both the LOF and ODN assays.

To assess this idea in a systematic manner, I examined the behavior of mutations introduced into hydrophobic amino acids; although such apolar residues are frequently solvent-inaccessible, hydrophobic patches on protein surfaces can contribute to protein-protein interfaces (Lijnzaad and Argos 1997). A total of 18 hydrophobic amino acids in Est3 that exhibited a high degree of conservation (Figure 2.2) were selected for mutagenesis to either alanine or glutamic acid. The resulting panel of mutations was examined for both LOF and ODN phenotypes following transformation into *est3-Δ* and *EST3* strains, respectively (Figure 2.3; Figures 2.4, 2.5, and 2.6). Figure 2.3A compares the consequences on telomere length in the LOF assay, which shows that this panel of conserved hydrophobic residues was remarkably tolerant to alanine mutagenesis, with



very modest declines in telomere length observed in a limited subset of the mutant strains. Not unexpectedly, introduction of a glutamic residue in place of these 18 hydrophobic residues had a far more substantial impact on Est3 function, with 12 mutant strains displaying a severe impairment in telomere length maintenance. The differential response to alanine vs. glutamic acid mutagenesis suggested that the more severe phenotypes were due to disruption of protein structure. However, when this collection of hydrophobic/glutamic acid mutations was examined in the ODN assay, four mutant proteins were capable of conferring an effect on telomere replication in the presence of the wild-type Est3 protein (Figure 2.3B; Figures 2.5 and 2.6). Notably, the extent of the ODN defect paralleled the magnitude of the LOF defect for each of these four mutations. For example, *est3-V75E* and *est3-V168E*, which both behaved like null mutations when introduced into an *est3-Δ* strain in the LOF assay (Figure 2.3A and Lee et al. 2008), had a pronounced impact in the ODN assay (Figure 2.3B). Similarly, *est3-L6E* and *est3-L18E* exhibited comparable effects in both the LOF and the ODN assays (Figure 2.3A; Figures 2.5 and 2.6), although the modest phenotypes in both assays indicate that these two residues are less critical for Est3 function.

The fact that the ODN phenotype was comparable to that of the corresponding LOF phenotype in each case argues that the glutamic acid residues introduced at these four sites did not interfere with protein structure. Consistent with this, the CD spectra of the purified Est3-L6E mutant protein, as well as the midpoint of the melting curves at 208 and 222 nm, were indicative of an overall structure that was highly similar to that of the wild-type Est3 protein (Figures S2, S3, and S8, Lubin et al. 2013), similar to the results for the Est3-V168E protein (Figure 2.1). The remaining mutations that conferred

extremely short telomeres in the LOF assay were phenotypically silent in the ODN assay (Figures 2.5 and 2.6), suggesting that their *in vivo* defects were due to impaired structural stability. This was confirmed for *est3-I22E* and *est3-V157E*, as the comparable mutant proteins expressed very poorly in *E. coli* and with greatly reduced solubility (Figure S1, Lubin et al. 2013), indicating that these hydrophobic residue side chains are likely internalized and important for structural integrity of the protein. These observations provide additional support for the premise that the ODN assay can provide a rigorous means of distinguishing between mutations that impair structural stability of a protein vs. those that are potential separation-of-function alleles (Figure 2.3C). The results with this panel of 36 mutations (the *in vivo* data set is summarized in Figure 2.7) also demonstrate that mutagenesis to residues other than alanine may be necessary to identify hydrophobic residues that are important for function. In particular, the potential contribution of valine 168 to Est3 function would have been overlooked in a mutagenesis strategy that relied only on alanine substitutions.

One unexpected observation from this analysis was that expression and solubility of the Est3-V157A protein in *E. coli* was reduced, and the Est3-I22A protein formed soluble aggregates (Figure S1, Lubin et al. 2013 and data not shown). This was unanticipated, as the *est3-I22A* and *est3-V157A* yeast strains were indistinguishable from a wild-type strain with regard to telomere function, at least as assessed under laboratory conditions (Figure 2.3A). Presumably, additional features of the *in vivo* milieu (such as association with other subunits of the telomerase complex) that are not recapitulated in the *E. coli* expression system contribute to function (and presumably to stability) of these two mutant Est3 proteins in yeast. This indicates that an examination of the properties of

wild-type and mutant Est3 proteins expressed in *E. coli* provides a very stringent assessment of protein stability.

### *Comparing charge-swap and alanine mutagenesis of charged residues in Est3*

Although the above analysis supports the ODN assay as a strategy for identifying functionally important residues, hydrophobic residues proved to be an inefficient target, as only two (V75 and V168) among 18 residues qualified as strong *sof<sup>+</sup>* alleles. Moreover, neither V75 nor V168 could be distinguished on the basis of amino acid conservation (Figures 2.2 and 2.7), arguing that this criterion would not be helpful in restricting mutagenesis to a more limited subset of hydrophobic amino acids.

Because charged residues are often located on the surface of a protein, mutagenesis of this class of amino acids might provide a more enriched category of candidate *sof<sup>+</sup>* alleles. To test this, I conducted a similar systematic analysis of 18 charged residues in Est3, which were mutated either to alanine or to a charged residue (as a charge swap) and analyzed for ODN and LOF phenotypes. Unlike the situation with the hydrophobic residues, amino acid conservation was a strong predictor of whether a charged residue would generate a potential *sof<sup>+</sup>* mutation, as shown by the summary in Figure 2.8. In particular, mutations in four (K68, K71, R110, and D166) of the six invariant or highly conserved residues conferred a strong LOF phenotype that was also accompanied by a pronounced ODN phenotype. In contrast, only one residue (D164) of the eight moderately conserved amino acids gave rise to a notable telomere replication defect when mutated (although mutations in two additional residues in this category conferred more modest phenotypes).

For the charged residue mutations that gave rise to a moderate-to-strong phenotype in the LOF assay, I assessed whether each mutation conferred an ODN phenotype of equivalent magnitude by monitoring telomere length under the appropriate genetic conditions. This comparison identified eight mutations (*est3-K3E*, *est3-K68A*, *est3-K71A*, *est3-K71E*, *est3-R110A*, *est3-R110E*, *est3-D164A*, and *est3-D166R*) with ODN phenotypes that were strikingly similar to their corresponding LOF phenotypes (Figures 2.1 and 2.9; Figure 2.10; data not shown). To further test our hypothesis that these mutations should encode structurally stable proteins, the protein stability of six of these mutant proteins was examined (since *est3-K71A* has a weaker phenotype than *est3-K71E*, Est3-K71A was not included; similarly, only Est3-R110A was tested as *est3-R110A* and *est3-R110E* have essentially identical LOF and ODN phenotypes). Consistent with this prediction, the spectra for five of these mutant Est3 proteins were comparable to that of the wild-type protein (Figure 2.1B and Figure 2.9C; Figure S2, Lubin et al. 2013), with a thermal denaturation pattern that was either highly similar (Est3-K71E, Est3-R110A, Est3-D164A, and Est3-D166R) or only slightly reduced at 36 (Est3-K68A) relative to the wild-type Est3 protein. The spectra for the sixth protein in this group (Est3-K3E) also closely resembled that of the wild-type Est3 protein at temperatures up to 36 (Figures S2 and S8, Lubin et al. 2013), indicating that the Est3-K3E protein exhibited a secondary structure that was also highly similar to that of the wild-type protein under conditions that were permissive for yeast growth. Curiously, however, the thermal denaturation pattern for Est3-K3E protein from 45 to 75 indicated that this mutant protein unfolded into an anomalous structure (Figure S8, Lubin et al. 2013). The biological relevance of this deviation from the wild-type denaturation pattern is unclear, since it was

observed only at temperatures that were well above laboratory growth conditions for *S. cerevisiae*. This demonstrates that these six mutations encoded proteins with secondary structure content that was highly similar to that of the wild-type Est3 protein, as predicted by their comparable *in vivo* LOF and ODN phenotypes (summarized in Figure 2.11).

Figure 2.9 also identified a second category of mutations in which the magnitude of the ODN phenotype was less than that predicted by the LOF phenotype. The first example was the *est3-D164R* strain, which exhibited a more pronounced telomere length defect in the LOF assay than in the ODN assay (compare telomere length indicated by the medium-size box in Figure 2.9, A and B). This predicted that the *in vivo* defect displayed by the *est3-D164R* strain could be attributed at least in part to a partially unstable mutant protein, which was consistent with its thermal denaturation profile (Figures S2 and S3, Lubin et al. 2013). The most notable contrast between LOF and ODN phenotypes in Figure 2.9 was exhibited by the *est3-E104R* mutation. In the LOF assay, the *est3-E104R* strain displayed a null phenotype, with telomeres reaching a critically short length after a limited period of growth (small box, Figure 2.9A). However, the ODN phenotype conferred by the *est3-E104R* mutation was notably less severe, as telomeres were shortened to only an intermediate length by overexpression of this mutant protein (small box, Figure 2.9B). This contrasts with the *est3-R110A* mutation [which, like *est3-E104R*, exhibited a null phenotype in the LOF assay (Lee et al. 2008)], as overexpression of the Est3-R110A mutant protein resulted in the appearance of senescence and the recombination-dependent telomeric rearrangements that are a hallmark of critically short telomeres (Figure 2.9B and data not shown). The incomplete correlation between the LOF and ODN phenotypes therefore suggested that the Est3-E104R mutant protein was

partially destabilized *in vivo*. To test this prediction, the *in vitro* properties of the bacterially expressed mutant protein were examined by the Wuttke lab and the Est3-E104R spectra indicated reduced stability. Both the reduced *in vitro* structural stability and the attenuated ODN phenotype argues that the magnitude of the LOF phenotype displayed by the *est3-E104R* strain was due in part to a loss of structural integrity of the mutant protein, rather than solely due to loss of a single biochemical property. This example illustrates how a diminished ODN phenotype can be used to eliminate certain alleles as candidate *sof* mutations for future studies.

#### *Structure-guided mutagenesis of the complete Est3 protein surface*

The Wuttke lab was able to solve the the Est3<sup>ΔN</sup> structure (Rao et al. 2014), allowing me to pursue an unbiased comprehensive survey of the entire surface of the Est3 protein by examining the *in vivo* consequences of mutations introduced into every solvent-accessible surface residue identified in the structure. Analysis of surface exposed residues revealed 112 residues with side chains touching the surface envelope and therefore these were designated as surface-exposed side chains of Est3 (Table 2.1). These surface residues were mutated by the introduction of a charged amino acid [rather than mutagenesis to alanine, which can often fail to detect functionally important residues (Lubin et al. 2013)], and the resulting mutant collection was examined for effects on telomere replication as previously described (Lubin et al. 2013; Lee et al. 2008). Strikingly, this comprehensive analysis revealed that much of the protein surface is dispensable for the functions tested. We clearly identified a total of 15 surface residues which, when mutated, resulted in an inability to maintain telomere length *in vivo* (Lubin

et al. 2013; Lee et al. 2008) (Figure 2.12 and summarized in Table 2.1). Notably, these 15 residues map to a noncanonical surface of the Est3 protein which is not commonly used by OB-fold-containing proteins for ligand binding.

Coimmunoprecipitation of wild-type and mutant Est3 proteins with the Est2 catalytic subunit of telomerase revealed that this collection of surface residues comprised two functionally distinct groups of residues that could be distinguished by their impact on association of Est3 with the telomerase complex (Figure 2.12 A and C). Mutations in one set of residues resulted in a greatly reduced ability of Est2 to coimmunoprecipitate with Est3 (Figure 2.12A), which was accompanied by a telomere length defect (Figure 2.12B), whereas a second set of residues did not impair association of Est3 with telomerase when mutated (Figure 2.12C) but nevertheless conferred a profound telomere maintenance defect in vivo (Figure 2.12D). Mapping these residues on the surface of Est3 revealed that the residues that mediated association with the telomerase complex defined a narrow contiguous interface, which extended along one face (Figure 2.13 A–C) of the Est3 surface along the base of the  $\beta$ -barrel. The second set of residues (Lys71 and Leu171), although distant in sequence, also form a contiguous interface (TELR) located immediately adjacent to this telomerase interaction surface, thereby defining a second, unique function for Est3 (Figure 2.13 A–C).

Recent genetic and biochemical studies in human cells have also identified a telomerase interaction surface on the human TPP1 protein, the TEL patch (Sexton et al. 2012; Zhong et al. 2012; Nandakumar et al. 2012) (Figure 2.13 E and F). Comparison of this surface with the functionally analogous surface on Est3 reveals that these surfaces are essentially completely coincident (Figure 2.13D). Furthermore, the second functional

Est3 patch (TELR) maps to chemically similar amino acids in TPP1, which predicts that there is a second function for TPP1 that is yet to be elucidated.

*Conservation does not fully predict functional interfaces*

An additional striking conclusion from the surface saturation mutagenesis was that a surprisingly large portion of the Est3 surface appeared to be dispensable for telomere length maintenance in vivo. This opens the possibility that Est3 performs a non-telomere-related function not assessed in our assays. Alternatively, it may be that a large segment of the surface is simply superfluous. As one means of distinguishing between the two possibilities, we compared a map of the functional surface of Est3 with a map of conserved residues on the surface of Est3. Conserved residues (based on a multiple sequence alignment of Est3 proteins from 22 different yeast species) (Figure 2.14) were mapped onto the structure of Est3 (Figure 2.15 A and B). As expected, most of the highly conserved residues are internal and thus appear to contribute to structure integrity, evident from the sequence conservation in the core OB-fold region ( $\beta$ 1– $\beta$ 5 and H5) (Figure 2.15A, colored in pink). Indeed, several of these core residues were already identified as being critical to structural integrity, including Trp21, Ile22, and Val157, based on their intolerance to mutation (Lubin et al. 2013). Notably, an assessment of conservation of surface residues indicated that the region of Est3 dispensable for telomere-length regulation displayed a low level of conservation. In contrast, the functional map overlapped, although not precisely, with the region of the surface that displayed the highest degree of conservation. This lack of precise overlap is considered further in Discussion.



*An entire surface of Est3 appears to be dispensable for telomere length maintenance, DNA replication, and repair*

Mapping of the functional residues to the surface of Est3 revealed two distinct contiguous patches (Figure 2.13), but strikingly, comprehensive mutagenesis of all surface residues revealed that an entire side of the Est3 protein was dispensable for telomere length maintenance. We then wanted to ask whether these amino acids might play a role in non-telomere-related functions related to DNA replication or repair. To do so, I assessed cell viability in wild-type yeast when these *EST3* mutations were over-expressed and the cells were subjected to DNA damage and replication stress.

To test how the mutant cells would respond to DNA mutagenesis by irradiation, cells were exposed to 5K, 10K, and 15K  $\mu$ J of UV radiation. Additionally, mutant cells were exposed to .0025%, 0.05%, and 0.1% Methyl methanesulfonate (MMS) to assess the response to DNA damage (Beranek et al. 1990), as well as 25mM, 50mM, and 100mM Hydroxyurea (HU) to assess the response to DNA replication stress (Koc et al. 2003). Somewhat surprisingly, none of the mutant *EST3* genes showed any noticeable growth defect compared to wild-type *EST3* when subjected to these treatments (Figure 2.16).

From these experiments, it appears that one side of Est3 does not play any functional interactive or regulatory role, both in telomere length maintenance, as well as in DNA replication or repair. However, the possibility does still exist that the assays we chose were not capable of detecting these regulatory roles, or that this surface on Est3 is involved in some other pathway we did not examine.

## Discussion

Reverse mutagenesis of a protein is usually driven by two technical assumptions: (i) target highly conserved residues and (ii) introduce alanine substitutions. In collaboration with the Wuttke lab, I tested these two assumptions with the Est3 protein by conducting a systematic *in vivo* analysis of how two different categories of amino acids—hydrophobic and charged residues—respond to mutation to alanine vs. a residue with a high potential to disrupt protein folding. The results, summarized in Figure 2.7 and Figure 2.8, demonstrate that mutation to a charged residue has a higher probability of generating a severe LOF phenotype; of the 18 amino acids that conferred short or very short telomeres when mutated, 15 had a more pronounced telomere replication defect in response to a charged residue substitution than mutation to alanine. In collaboration with the Wuttke lab, we subsequently used two complementary assays to assess whether the resulting phenotypes were simply due to destabilization of protein structure by examining *in vivo* ODN phenotypes in yeast as well as *in vitro* structural stability of proteins expressed in *E. coli*. This second aspect of the analysis indicates that an ODN assay can be used to identify structurally stable mutant Est3 proteins with defined biochemical defects (summarized in Figure 2.11 and Figure 2.17).

### *Using ODN phenotypes to eliminate hypomorphic mutations due to unstable proteins*

Classically, separation-of-function alleles have been defined, based on *in vivo* characteristics, as mutations that confer a restricted subset of the full range of phenotypes displayed by the null mutation. This is often accompanied by the assumption that such mutations have eliminated a single biochemical property (such as a protein-binding

surface) without impairing overall protein stability. If so, such alleles can be powerful genetic reagents for subsequent studies designed to identify the interacting partner. However, defining *sof*<sup>+</sup> alleles based solely on the range of LOF phenotypes potentially fails to identify those mutations that encode (partially) destabilized proteins. One aspect of this *EST3* study, therefore, was to examine the potential correlation between *in vitro* protein stability and *in vivo* phenotypes as a means of asking whether an ODN phenotype could predict structural stability. Toward this goal, 16 mutant Est3 proteins, corresponding to 7 mutations in hydrophobic residues and 9 in charged residues, were examined for structural stability following expression in *E. coli*, as summarized in Figure 2.11. This collection of mutant proteins represented the full range of *in vivo* phenotypes for *est3*<sup>-</sup> mutations: null LOF but no ODN (3 mutations); moderate LOF but no ODN (1 mutation); an attenuated ODN relative to LOF (2 mutations); and null, strong, or moderate LOF with comparable ODN (2, 4, and 2 mutations, respectively). As Figure 2.11 illustrates, the correlation between mutations with comparable ODN and LOF phenotypes and wild-type *in vitro* protein stability was striking. In contrast, for *est3*<sup>-</sup> mutations that conferred an ODN phenotype that was less severe than the corresponding LOF phenotype, the corresponding proteins exhibited a degree of structural instability that reflected the discrepancy between the ODN and LOF phenotypes.

These observations also suggest that ODN potentially provides a far more sensitive means of assessing whether a protein is properly folded than monitoring steady-state protein levels in yeast extracts. In the case of Est3, only those variants that behaved as completely unfolded proteins following expression in *E. coli* (Est3-W21A and Est3-D86A; Figure S1, Lubin et al. 2013) displayed readily detectable reductions in protein

levels from yeast extracts (3- and 10-fold, respectively) (Lee et al. 2008). In contrast, measurements of steady-state levels of the Est3-E104R protein from yeast extracts did not uncover any evidence of protein instability, even though the CD spectra and melting curves for the bacterially expressed Est3-E104R protein demonstrate that this mutant protein does not retain a wild-type secondary structure. This indicates that, while monitoring protein levels in extracts can be a useful tool in excluding substantially destabilized mutant proteins, it fails to discriminate against partially unstable proteins that would be less-than-ideal reagents for subsequent analyses.

#### *Alanine versus charge swap mutagenesis*

These *EST3* studies, as well as a prior one (Lee et al. 2008), identified 16 amino acids in *EST3* that display ODN and LOF phenotypes of comparable magnitude when mutated. These 16 residues can be divided into three categories based on their response to either alanine substitution or mutation to a charged residue (Figure 2.17). Class I residues exhibit the same degree of impairment *in vivo* when mutated, regardless of whether the amino acid change is an alanine substitution or a charge swap. In contrast, the majority category (class II) contains both hydrophobic and charged amino acids that result in a strong phenotype when mutated to a charged residue (as indicated by red bars in Figure 2.6) but are unaffected (or only modestly impaired in the case of V75) by an alanine substitution (as indicated by gray bars in Figure 2.17). The third category contains two residues that are severely impaired by mutation to alanine, whereas a charge swap results in an attenuated ODN phenotype indicative of a partially destabilized protein. This distribution suggests that the simple notion of substitution with alanine as a side chain

“null” is overly simplistic. Instead, the effectiveness of an alanine substitution in revealing the role of the targeted amino acid is context-dependent based on the structural environment.

*The structure revealed there are two distinct functional surfaces on the Est3 protein*

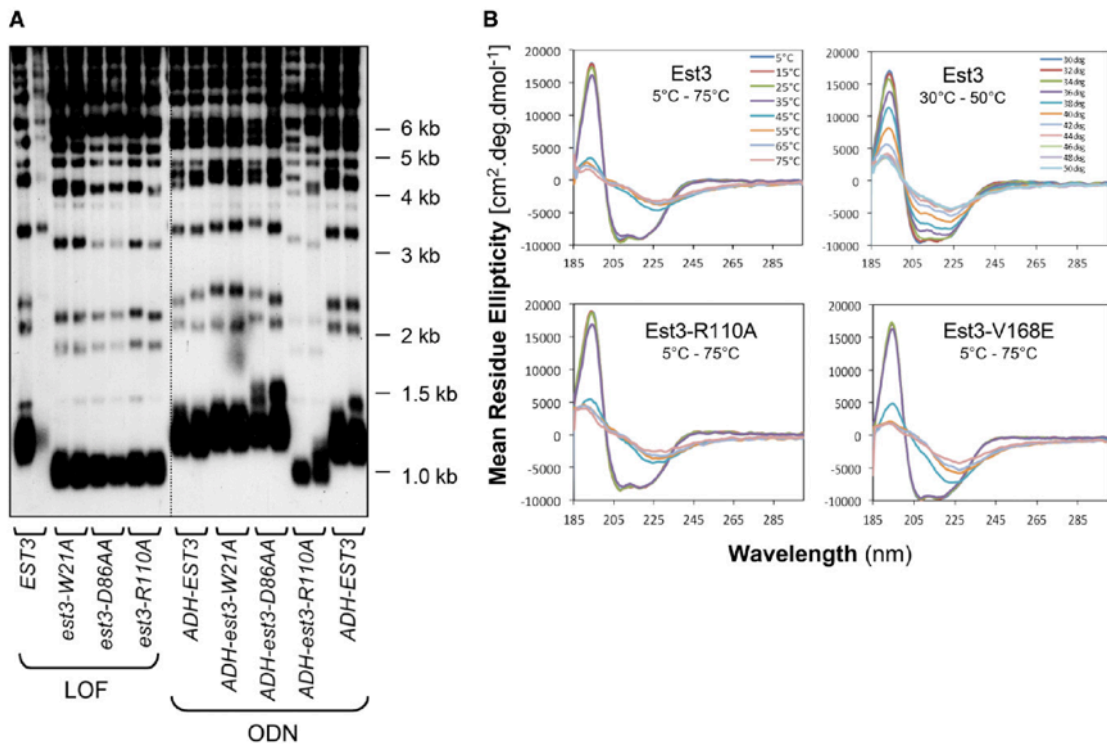
The Wuttke lab found that Est3 adopts an OB-fold with certain distinctive features. The most notable discrepancy between Est3 and other OB-fold proteins is that the canonical OB-fold ligand-binding surface is dispensable for telomere function in Est3, which explains the lack of robust nucleic acid-binding activity exhibited by Est3 (Lee et al. 2010). Instead, a complete genetic survey of the experimentally defined protein surface revealed two contiguous regions with differential functions in telomere maintenance. Whereas one surface facilitates association with the telomerase holoenzyme, the second serves a separate function in mediating telomerase action. That these surfaces do not fully correspond to those predicted based on conservation alone points to the importance of conducting a comprehensive evaluation of the available surface.

Although a protein fold for Est3 similar to that of TPP1 was accurately predicted on the basis of threading algorithms (Lee et al. 2008; Lue et al. 2013; Yu et al. 2008), the topology of the predicted Est3 protein surface was nevertheless strikingly inaccurate. This prior model placed the relevant Est3 surface residues across a wide surface area (Figure 2.15C). In contrast, the Wuttke lab structure showed that Est3 mediates its telomere functions through two tightly clustered patches located on a novel face of the OB-fold (Figure 2.13C). This illustrates the limitations of homology models, which can be particularly poor at predicting loop conformations in cases where the proteins share

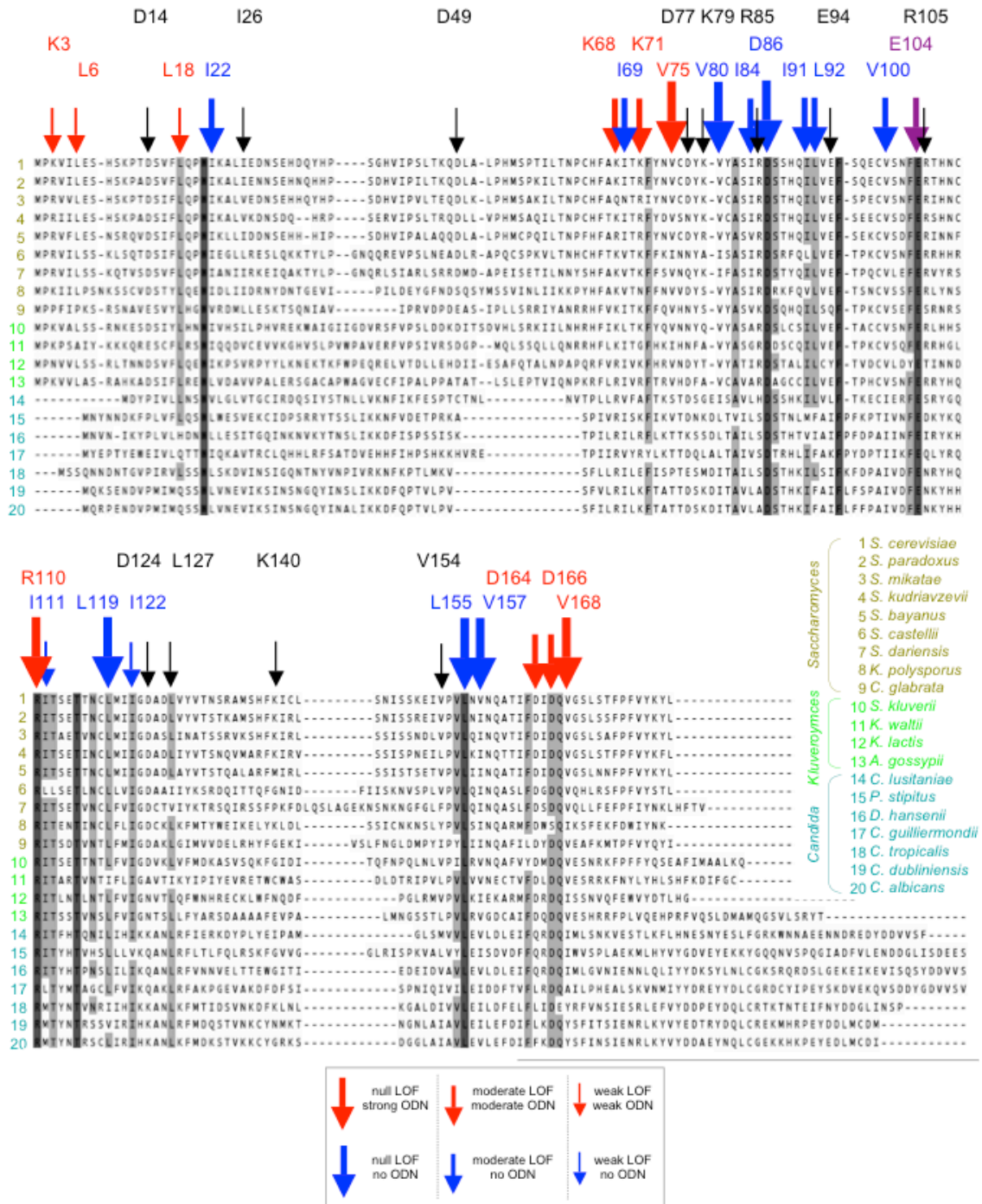
scant sequence identity.

Although HsTPP1 and Est3 localize to telomeres through distinct mechanisms, HsTPP1 through the shelterin complex and Est3 as a component of the yeast telomerase holoenzyme, the coincidence of the TEL patches suggests these divergent factors share a common surface for telomerase association. Furthermore, the discovery of a second cluster of functional residues on the surface of Est3 points to the use of additional mechanisms of telomerase regulation by HsTPP1. A full understanding of the activities performed by these surfaces on both Est3 and HsTPP1 may also address whether these two proteins share a common ancestry or instead arose as the result of convergent evolution.

## Figures

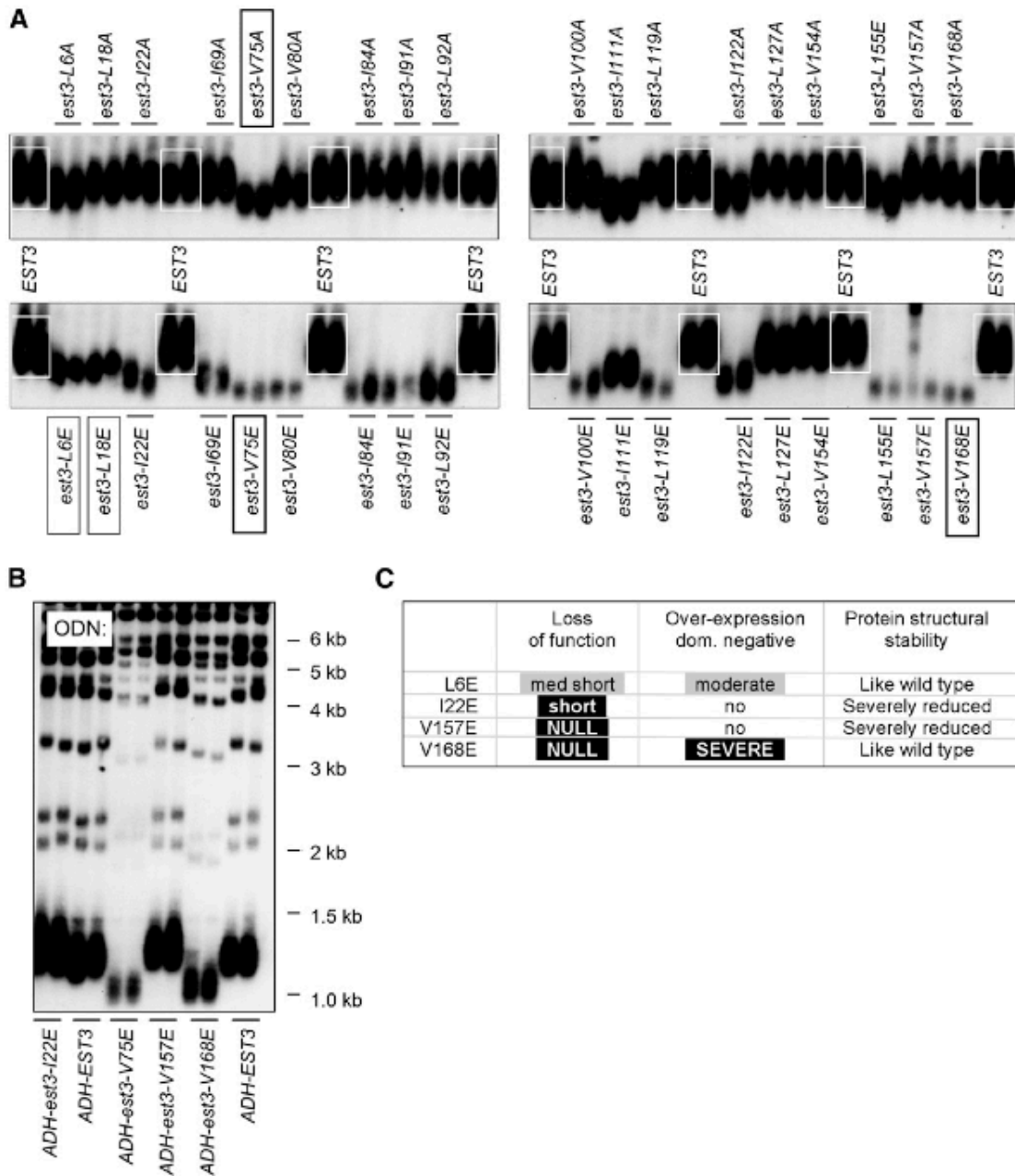


**Figure 2.1: Est3 mutant protein stability in vitro correlates with the ability of mutant proteins to confer a dominant-negative phenotype in vivo.** (A) LOF phenotypes were assessed by monitoring telomere length of *est3-Δ* strains with single-copy plasmids expressing wild-type *EST3* or the indicated mutations from the native *EST3* promoter, whereas ODN phenotypes measured telomere length of wild-type strains containing high-copy plasmids expressing the same set of wild-type or mutant alleles from the constitutive ADH promoter. (B) Spectra of the wild-type Est3 protein collected from 30 to 50 with a step size of 2 (top right) and spectra of the wild-type Est3, Est3-R110A, and Est3-V168E proteins collected from 5 to 75 with a step size of 10; the temperature color code is shown in the inset of the wild-type Est3 protein plot. Proteins were expressed and purified as shown in Figure S1 (Lubin et al. 2013).

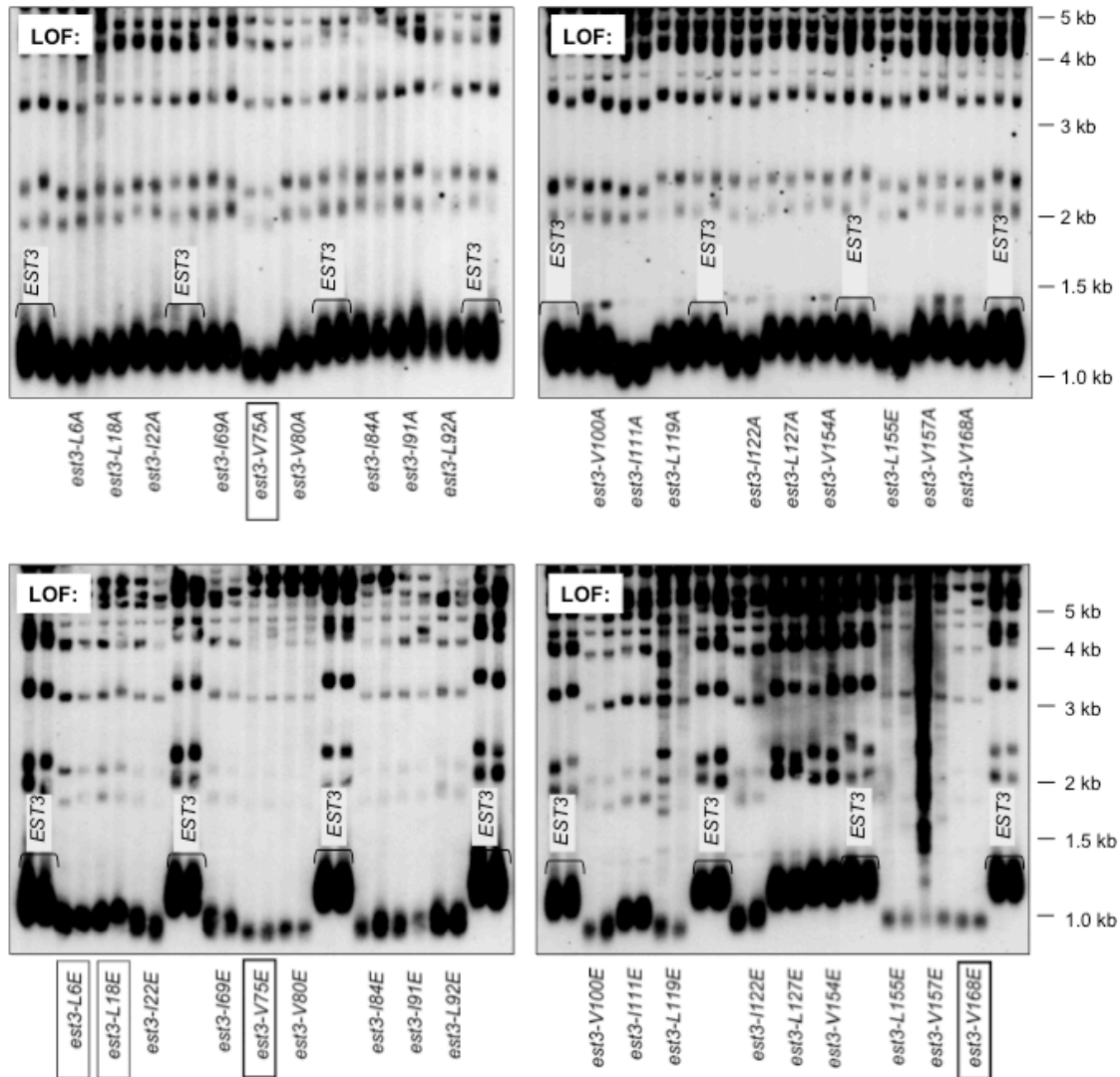


**Figure 2.2: Alignment of 20 Est3 protein sequences from the three sub-clades of *Saccharomytina*.** The position of the 36 hydrophobic and charged residues that were subjected to mutagenesis indicated. Arrow size and color as described to the right; black arrows = wild type. E104, with a partially attenuated ODN phenotype relative to LOF, is indicated in maroon.

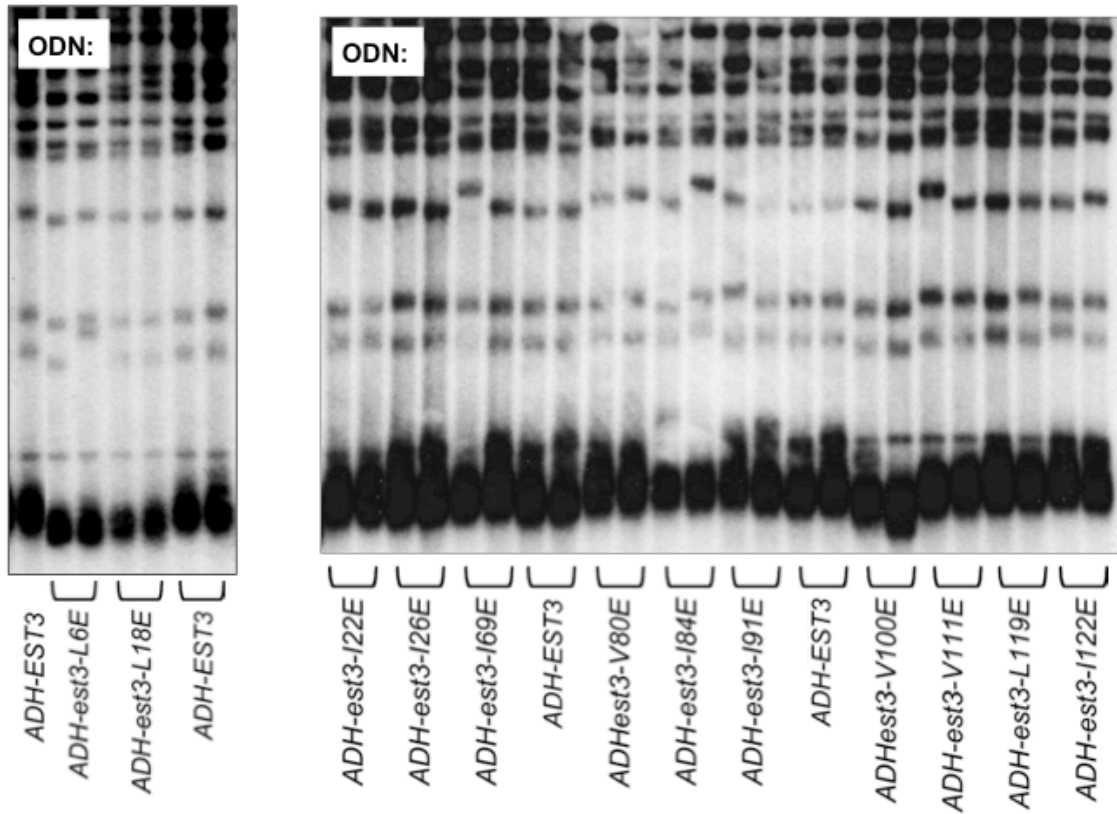




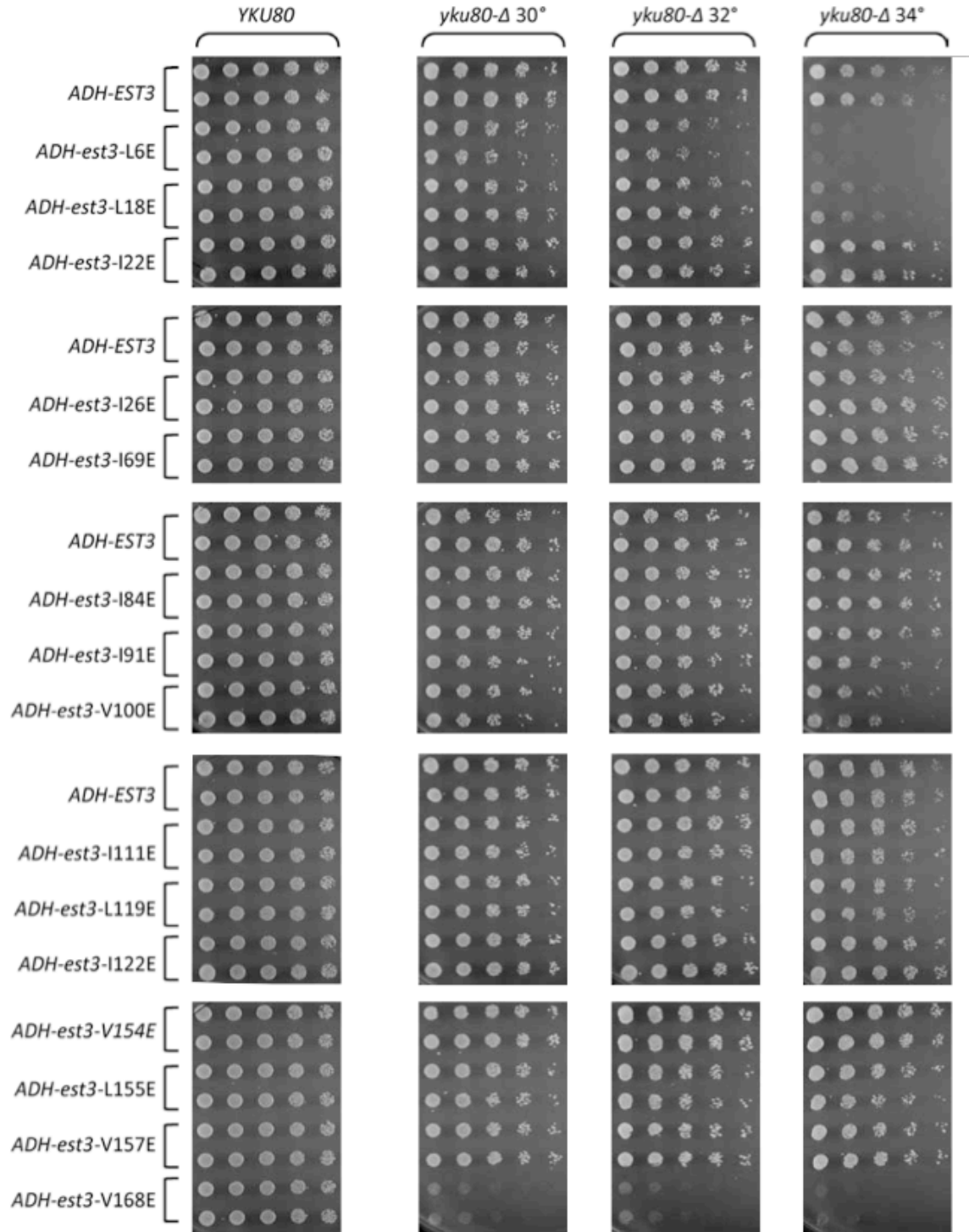
**Figure 2.3: Analysis of mutations introduced into 18 highly conserved hydrophobic amino acids in Est3.** (A) LOF assay monitoring telomere length of *est3-Δ* yeast strains bearing single-copy plasmids expressing mutations in hydrophobic residues (mutation to alanine, top panels; mutation to glutamic acid, bottom panels) from the native *EST3* promoter. The broad telomeric restriction fragment that corresponds to  $\sim 2/3$  of the 32 yeast telomeres is shown; the intact Southern blots can be viewed in Figure 2.4. Telomeres of wild-type *EST3* strains (boxed in white) provide multiple reference points. The genotypes of mutations that conferred a strong phenotype in the ODN assay are boxed in black. (B) An ODN assay showing telomere length of wild-type *EST3* strains containing high-copy plasmids expressing mutations of the indicated genotype from the constitutive ADH plasmid. (C) Summary of the comparison between in vivo and in vitro properties of missense mutations in four hydrophobic residues. Spectra for Est3-V168E and Est3-L6E are shown in Figure 2.1 and Figure S8 (Lubin et al. 2013), respectively, and expression and solubility levels for the His<sub>10</sub>-SUMO-Est3-I22E and His<sub>10</sub>-SUMO-V157E proteins are shown in Figure S1 (Lubin et al. 2013). ODN phenotypes for Est3-L6E are shown in Figures 2.5 and 2.6.



**Figure 2.4: Loss of function (LOF) assay monitoring telomere length of *est3*- $\Delta$  yeast strains bearing single copy plasmids expressing mutations in hydrophobic residues from the native *EST3* promoter. The genotypes of mutations that conferred a strong phenotype in the ODN assay are boxed. Mutations to alanine, upper panels; Mutations to glutamic acid, lower panels.**



**Figure 2.5: Over-expression dominant (ODN) phenotypes assessed by monitoring telomere length.** *EST3* yeast strains bearing high copy plasmids expressing the indicated mutations in hydrophobic residues under control of the ADH promoter. The effects of the two mutations (*est3*-V75E and *est3*-V168E) that exert a strong ODN phenotype are shown in Figure 2.3.



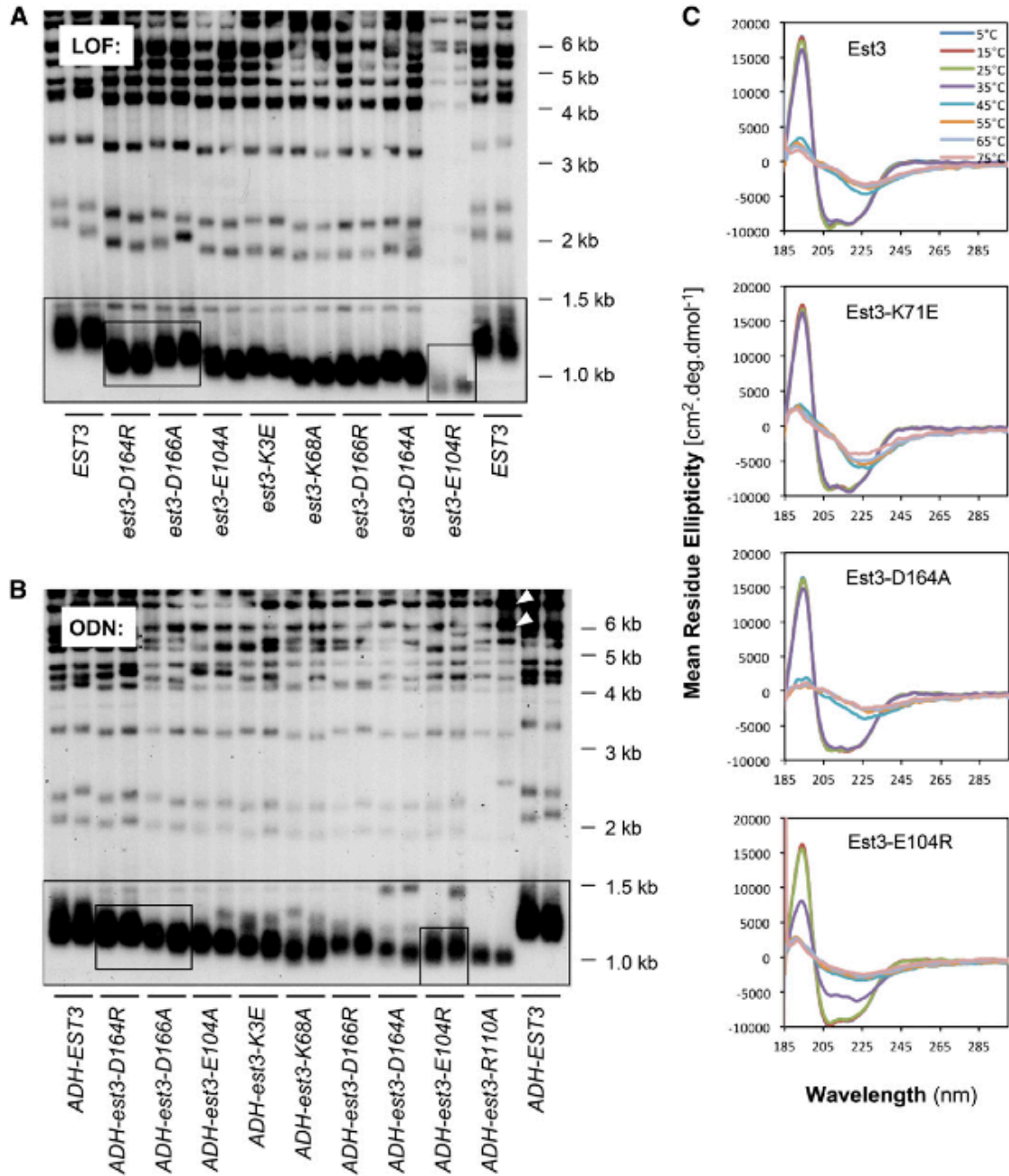
**Figure 2.6: An alternative assay for ODN phenotypes based on synthetic lethality in the presence of a *yku80-Δ* mutation.** As previously described (Evans and Lundblad 2001; Lee et al. 2008). Growth of *YKU80* or *yku80-Δ* strains (generated by plating on media that selects either for or against a *YKU80 URA3* plasmid) which also contain high copy plasmids expressing the indicated mutations in hydrophobic residues, under control of the ADH promoter. As predicted from the lack of an ODN effect on telomere length (Figure 2.5), the majority of the mutations in hydrophobic residues similarly have no effect in this assay.

	→ A loss of function	→ E loss of function	→ E ODN	Level of conservation
L6	slightly shorter	med short	moderate	moderate
L18	wild type	med short	moderate	high
I22	wild type	short	no	high
I26	wild type	wild type	no	high
I69	wild type	short	no	high
V75	med short	NULL	SEVERE	high
V80	slightly shorter	NULL	slight	high
I84	wild type	short	no	high
I91	wild type	short	no	high
L92	wild type	short	no	high
V100	wild type	short	slight	high
I111	med short	med short	no	high
L119	wild type	NULL	no	high
I122	slightly shorter	med short	no	INVARIANT
L127	wild type	wild type	no	high
V154	wild type	wild type	no	high
L155	slightly shorter	NULL	no	INVARIANT
V157	wild type	NULL	no	high
V168	wild type	NULL	SEVERE	high

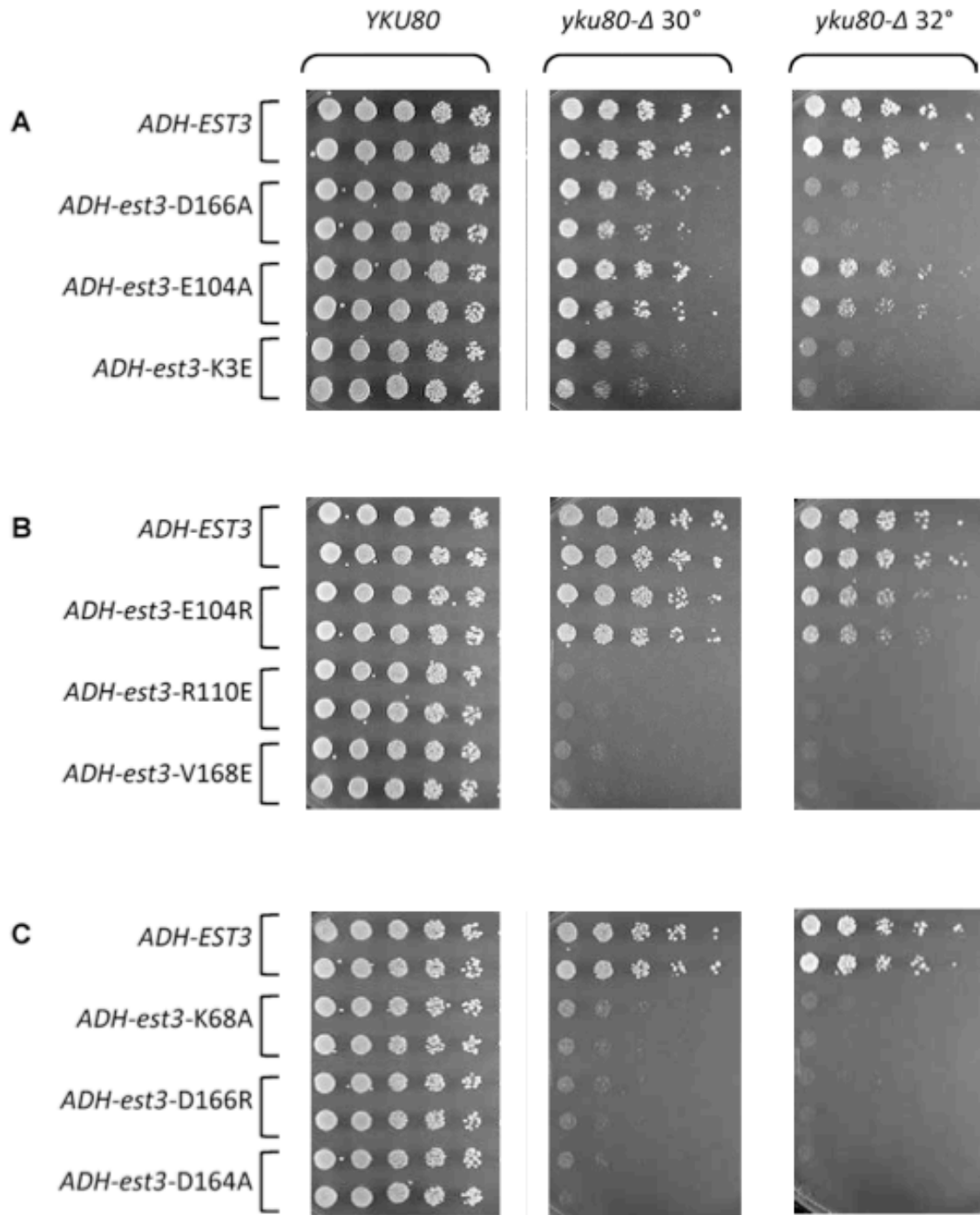
**Figure 2.7: Summary of LOF (loss of function) and ODN (over-expression dominant) phenotypes for mutations in hydrophobic residues mutated to either alanine (A) or glutamic acid (E).** Based on data shown in Figures 2.3, 2.4, 2.7 and 2.6. Level of conservation was determined as described in the legend for Figure 2.8 and based on the alignment shown in Figure 2.2.

	Alanine mutation; loss of function	Alanine mutation; ODN	Charge swap mutation; loss of function	Charge swap mutation; ODN	Level of conservation
D86	NULL	no	n.t.	n.t.	INVARIANT
R110	NULL	SEVERE	NULL	SEVERE	INVARIANT
E104	med short	weak	NULL	moderate	INVARIANT
K71	med short	moderate	short	strong	HIGH
D166	sl/med short	weak	short	strong	HIGH
K68	short	strong	med short	weak	HIGH
D164	short	strong	med short	no	moderate
K3	wild type	no	med short	moderate	moderate
E114	med short	moderate	med short	moderate	moderate
D14	wild type	no	wild type	no	moderate
D49	wild type	no	wild type	no	moderate
R85	slightly short	no	slightly short	no	moderate
E94	wild type	no	wild type	no	moderate
R105	wild type	no	wild type	no	moderate
D77	wild type	n.t.	wild type	n.t.	low
K79	wild type	n.t.	wild type	n.t.	low
D124	wild type	no	wild type	no	low
K140	wild type	n.t.	slightly short	n.t.	low

**Figure 2.8: Conservation of charged residues predicts the likelihood of generating a *sof* allele in *EST3*.** Results from Figure 2.9, Lee et al. (2008), and data not shown (corresponding to residues that did not have a telomere defect when mutated) are summarized. For LOF phenotypes, “medium short” and “short” correspond to a 100- to 130-bp or to a 140- to 160-bp reduction in telomere length, respectively, and “null” refers to mutants with telomeres that are >175 bp shorter than wild type with an accompanying senescence phenotype. For ODN phenotypes, “moderate,” “strong,” and “severe” correspond to the “medium short,” “short,” and “null” LOF phenotypic categories. The two different nomenclatures emphasize that the LOF and ODN phenotypes are not directly comparable (since the ODN assay measures telomere length in a strain expressing both wild-type and mutant variants of *EST3*, the phenotypic lag until steady-state telomere length is reached is different in the LOF and ODN assays). Degree of amino acid conservation was determined based on an alignment of 20 Est3 protein sequences encompassing the *Saccharomyces*, *Kluyveromyces*, and *Candida* clades (Figure 2.2), where “high,” “moderate,” or “low” correspond to 75–95%, 50–75%, or <50% identity and/or highly similar amino acid structure (i.e., arginine vs. lysine or aspartic acid vs. glutamic acid); “invariant” corresponds to 100% amino acid identity in all 20 Est3 proteins.



**Figure 2.9: Comparison of LOF and ODN phenotypes displayed by a panel of mutations in charged residues in *EST3*.** (A and B) LOF and ODN assays were performed as described in Figure 2.1, except that strains were propagated for an additional ~25 generations. As a result, the *est3-E104R* strain exhibited a more severe telomere length defect in the LOF assay than the comparable null mutants shown in Figure 2.1A; similarly, the ODN phenotype of the *est3-R110A* mutation was also more pronounced, as indicated by the amplification of subtelomeric elements (white arrowheads in B), which is a characteristic feature of extensively propagated telomerase-defective strains (Lundblad and Blackburn 1993). A second assay to measure ODN phenotypes, which monitors synthetic lethality in a *yku80-Δ* background, is shown in Figure 2.10. (C) CD spectra of wild type and the indicated mutant Est3 proteins were collected from 5 to 75 in parallel with the spectra shown in Figure 2.1.



**Figure 2.10: Additional mutations in an alternative assay for ODN phenotypes, based on synthetic lethality in the presence of a *yku80-Δ* mutation.** (Described in Figure 2.6) Effects on viability in a *yku80-Δ* strain of a subset of the same mutations shown in Figure 2.9B present on high copy plasmids and under control of the ADH promoter. The sensitivity range of this assay is such that “strong” vs. “severe” ODN phenotypes (using the nomenclature defined in the legend for Figure 2.9) of the mutations shown in (C), above cannot be distinguished. However, differences between the mutations shown in (A), above, provide a more sensitive assay than telomere length, as shown in Figure 2.9B.

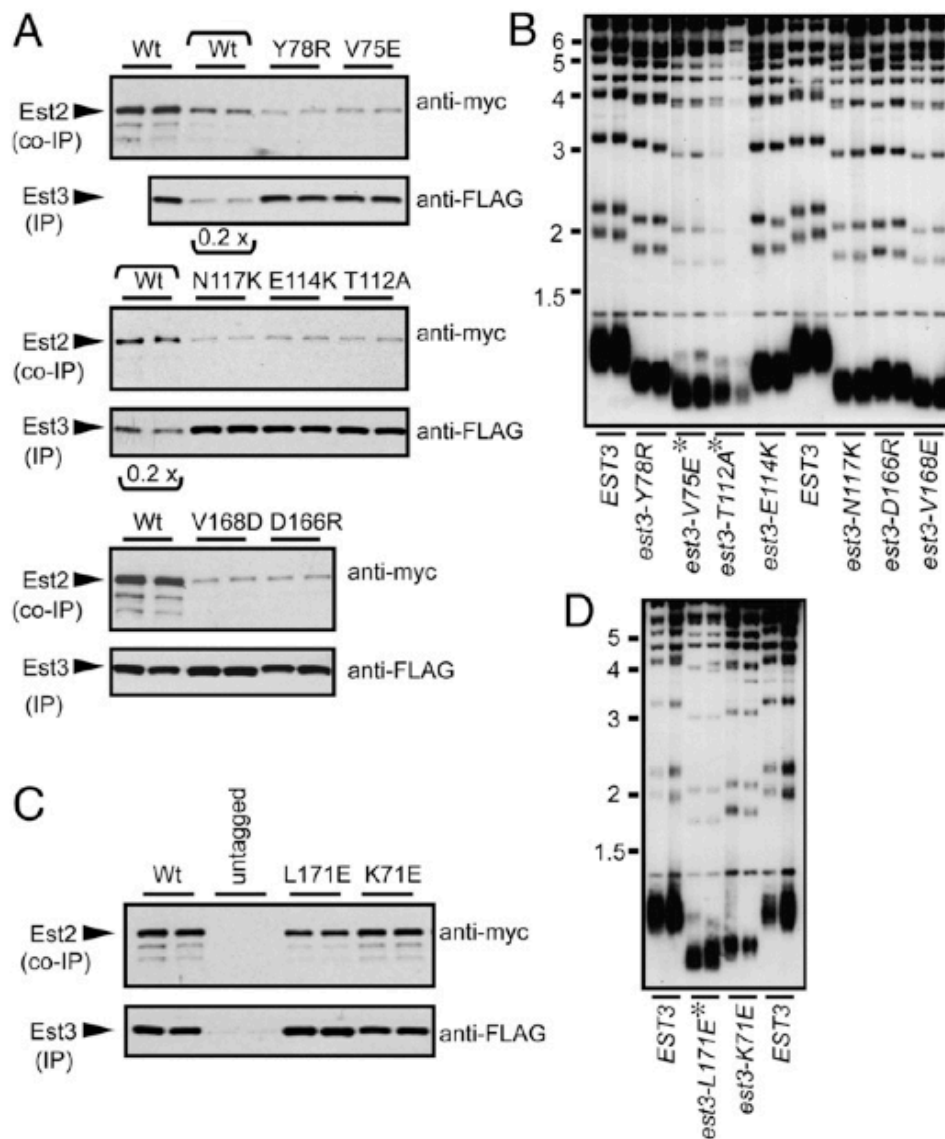


	Loss of function	Over-expression dom. negative	Protein structural stability
D86A	<b>NULL</b>	no	Severely reduced
W21A	<b>NULL</b>	no	Severely reduced
V157E	<b>NULL</b>	no	Severely reduced
I22E	<b>short</b>	no	Severely reduced
I22A	wild type	no	Reduced
V157A	wild type	no	Reduced
E104R	<b>NULL</b>	moderate	Partially destabilized
D164R	med short	no	Partially destabilized
K3E	med short	moderate	<b>Like wild type*</b>
L6E	med short	moderate	<b>Like wild type</b>
K68A	<b>short</b>	<b>strong</b>	<b>Like wild type</b>
K71E	<b>short</b>	<b>strong</b>	<b>Like wild type</b>
D164A	<b>short</b>	<b>strong</b>	<b>Like wild type</b>
D166R	<b>short</b>	<b>strong</b>	<b>Like wild type</b>
R110A	<b>NULL</b>	<b>SEVERE</b>	<b>Like wild type</b>
V168E	<b>NULL</b>	<b>SEVERE</b>	<b>Like wild type</b>
* exhibited an atypical thermal denaturation pattern at $\geq 45^\circ$			

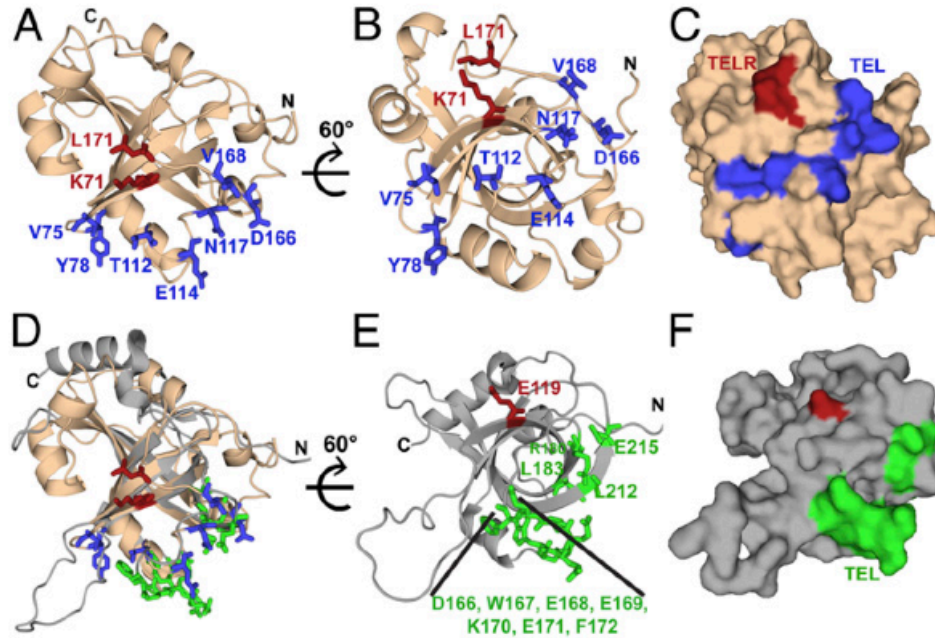
**Figure 2.11: The severity of the ODN phenotype for an *est3*<sup>-</sup> mutation, relative to the severity of the LOF phenotype, correlates with in vitro structural stability.** The LOF and ODN phenotypes corresponding to the 16 mutant Est3 proteins tested for stability following expression in *E. coli* are indicated as two subgroups based on protein stability; subjecting these two sets of data to a correlation test resulted in Pearson correlation coefficients of 0.32 and 1.0, respectively.

**Table 2.1: List of mutations in surface-exposed Est3 residues.** Surface residues were mutated by the introduction of a charged amino acid (rather than to alanine), to maximally disrupt function, and assessed for effects on telomere replication as described in Supporting Materials and Methods. Mutations with moderate to severe effects on telomere replication are highlighted in red, with more modest phenotypes indicated in pink; residues marked by an asterisk have been analyzed in previous studies (Lee et al. 2008, Lubin et al. 2013). For the three alleles that are highlighted in lavender, we have previously argued that charge-swap mutations introduced into these three residues result in partial destabilization of the mutant protein (Lubin et al. 2013).

D14R	D49R	Q90R	S137E
S15E	L52E	E94R	H138R, H138E
V16E	H54R, H54E	S96E, S96R	K140E
F17R, F19E	M55E	Q97R	C142E
Q19R	S56R	E98R	S144R
P20E	P57R	S101R	N146R
K23E	T58R	N102R	I146E
A24R	L60E	E104R*	S148E
L25E	T61R	R105E	K149E
E27R	N62R	T106R	E150R
D28R	P63R	H107E, H107R	I151E
N29R	C64R	N108R	N156R
E31R	K68E*	C109R	N158R
H32R, H32E	T70E	R110E*	Q159R
D33R	K71E*	T112A, T112I**	R161R
Q34R	Y73R, Y73E	S113R	F163R, F163E
Y35R, Y35E	N74R	E114	D164R*
H36E	V75E*	T116E	D166R*
P37E	C76R	N117K*	Q167R
S38R	D77R	D124R	V168E*
G39R	Y78R, Y78E	D126R	L171E
H40R, H40E	K79E	V128E	S172E
V41E	Y81R, Y81E	V130E	T173E
P43R	S83E	T131R	P175E
S44R	R85E	N132R	F176R, F176E
T46R	S87E	S133E	K179E
K47E	S88E	R134E	Y180R, Y180E
Q48R	H89E	M136E	L181E



**Figure 2.12: Two functionally distinct activities on the surface of Est3.** (A and C) Coimmunoprecipitation of wild-type (Wt) and mutant Est3 proteins with the catalytic Est2 subunit, bearing (FLAG)<sub>3</sub> and (myc)<sub>12</sub> epitopes, respectively; the functionality of these two tagged proteins is shown in Fig. 3.S5B. In a subset of the wild-type lanes (indicated by a bracket), 0.2× volume of immunoprecipitate was loaded, to illustrate the detection range. (B and D) Telomere length (assessed after ~75 generations of growth) of *est3*-Δ strains transformed with single copy plasmids expressing wild-type EST3 or the indicated *est3*<sup>-</sup> missense mutations; mutations that resulted in a telomere maintenance defect severe enough to confer senescence are indicated by an asterisk.



**Figure 2.13: The surface of Est3 reveals two distinct contiguous patches.** (A) Residues in Est3<sup>ΔN</sup> that mediate binding to telomerase (TEL patch: V75, Y78, T112, E114, N117, D166, and V168) (Fig. 2.12A) are displayed as sticks in blue, whereas residues not involved in telomerase interaction (TELR patch: K71 and L171) are displayed as sticks in red. (B) Sixty-degree rotation around a horizontal axis shows that the telomerase-interacting residues cluster at the base of the β-barrel. (C) A surface representation demonstrates that the interacting residues form a continuous protein–protein interaction surface. (D) Est3 and TPP1 have a common mode of telomerase association. Superposition of the structure in 3A on HsTPP1-OB (PDB ID code 2I46) with recently identified residues in HsTPP1-OB that mediate binding to telomerase (D166, E168, and K170) (11), (D166-F172, L183 and E215) (Sexton et al. 2012), and (E168, E169, E171, R180, L183, L212, and E215) (Nandakumar et al. 2012) are shown as sticks in green. The telomerase interaction surface from the two proteins coincides perfectly, indicating structural as well as functional similarity between the two. (E) HsTPP1 structure from D is rotated 60° to show the cluster of telomerase-interacting residues at the base of the β-barrel. Residue E119, identified from structural superposition with K71 of Est3, is displayed as a stick in red. (F) Surface representation of HsTPP1 (same orientation as E), displays two distinct functional patches on its surface. For simplification, the N-term tail has been removed from this view; the structure starts at R96 instead of S90 in the PDB 2I46 structure.

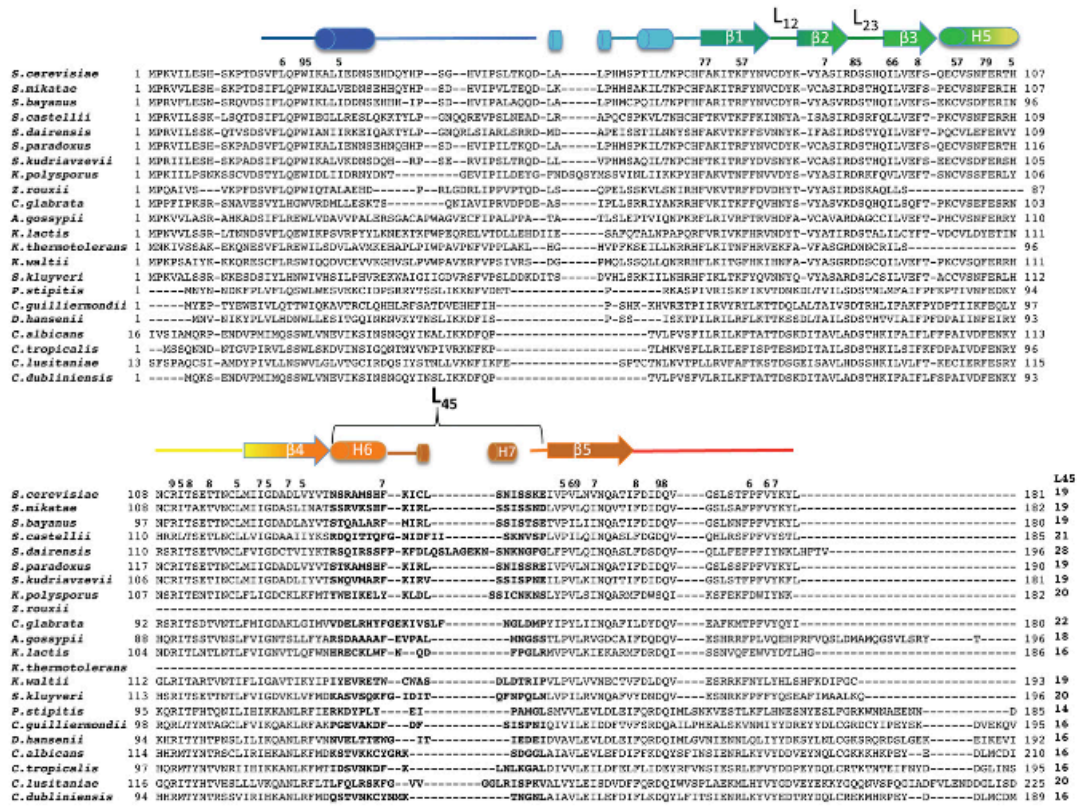
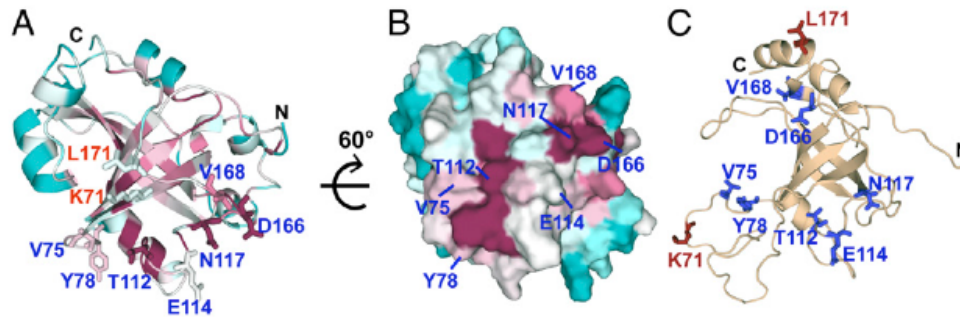
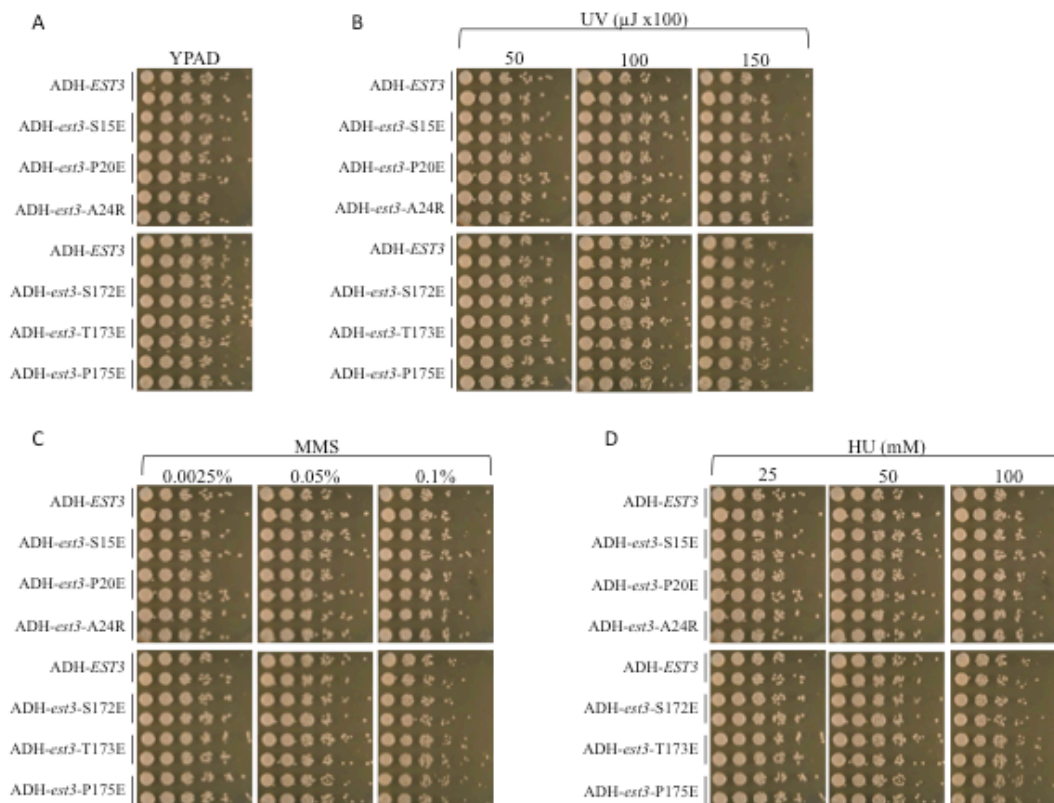






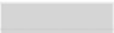

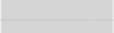

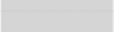

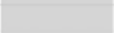









Figure 2.14: Clustal Omega (Sievers et al. 2011) alignment of Est3 proteins from 22 yeast species used for conservation mapping by ConSurf (Ashkenazy et al. 2010; Glaser et al. 2003; Landau et al. 2005) in Fig. 3.4. Medium to highly conserved residues are indicated by numbers 5–9 on top of the alignment, with 9 indicating the most conserved. Secondary structure elements from RASREC Rosetta structure of Est3<sup>AN</sup> are drawn on top of the sequence alignment. The extended loop L45 is highlighted in bold.



**Figure 2.15: Conserved surface on Est3 coincides with part of its functional activity.** (A) Conserved residues in Est3 (Fig. 2.14) are mapped on the structure. Residues are color-coded maroon through turquoise indicating conserved through variable residues based on phylogenetic conservation as evaluated by the ConSurf server (Glaser et al. 2003). Residues involved in telomere maintenance are displayed. (B) A view of the structure rotated 60° to match Fig. 3.3C shows the co-occurrence of the Tel patch with the conserved surface of Est3. (C) The predicted 3D model significantly differs from the calculated structure. The model generated by the PS<sup>2</sup> structure prediction server (Chen et al. 2006) is the same as a recently reported model of Est3 (Lue et al. 2013). As a result of these differences, functionally important residues (same as A) map to scattered locations on the predicted model's surface unlike Fig. 2.13 where a contiguous functional surface was identified.



**Figure 2.16: DNA damage and replication stress response of selected *est3*<sup>-</sup> mutations.** Growth of wild-type strains containing high-copy plasmids expressing wild-type *EST3* or mutations, under the control of the ADH promoter. Saturated cultures were serially diluted 1:5 and microtitered onto plates containing (A) rich media, (B) rich media subject to ultra violet radiation, (C) rich media containing MMS, or (D) rich media containing HU.

		In vivo telomere phenotype		Telomerase association	
		Mutation to alanine	Mutation to charged	Mutation to alanine	Mutation to charged
Class I	R110	 *		wild type	wild type
	E114			REDUCED	REDUCED
Class II	K3		 *	n.a.	wild type
	L6		 *	n.t.	n.t.
	K71		 *	wild type	wild type
	V75			n.t.	n.t.
	N117			wild type	REDUCED
	D166		 *	n.t.	REDUCED
V168		 *	n.t.	REDUCED	
Class III	K68	 *	unstable	wild type	reduced
	D164	 *	unstable	wild type	reduced

\* = examined for structural stability following expression in *E. coli*

**Figure 2.17: Three categories of *sof* mutations in the *EST3* gene.** Mutations in 11 Est3 amino acids confer in vivo ODN and LOF phenotypes of comparable magnitude, indicated by colored bars, with red corresponding to the more severe set of phenotypes for each residue (note that the absolute magnitude of each phenotype among mutations is not conveyed; for example, *est3-E114A* imparts a far more modest phenotype than *est3-R110A*). Telomerase association is based on prior observations (Lee et al. 2008) or unpublished data (J. W. Lubin and V. Lundblad, data not shown). The term “unstable” indicates those mutations that exhibit an attenuated ODN phenotype relative to the respective LOF phenotype, indicating that the resulting mutant protein is partially destabilized *in vivo*. The *est3-N117* mutation, which was analyzed in our prior study (Lee et al. 2008), is included to provide a more complete summary of *sof* mutations in *EST3*.

**Table 2.2: The parental plasmids used in Lubin et al. 2013 for all *in vivo* analysis were pVL1024 (2 $\mu$  *LEU2 ADH-EST3*) and pVL2537 (*CEN LEU2 EST3*). Described previously (Lee et al. 2008).**

Lee, J.S., Mandell, E.K., Tucey T.M. Morris, D.K. and Lundblad, V., 2008 The Est3 protein associates with yeast telomerase through an OB-fold domain. *NSMB* 15:990-997.

<i>Parent</i>	<i>pVL2537</i>	<i>pVL1024</i>		<i>pVL2537</i>	<i>pVL1024</i>
<b>Mutation</b>	<b>pVL#</b>	<b>pVL#</b>	<b>Mutation</b>	<b>pVL#</b>	<b>pVL#</b>
K3A	5982	N.A.	E94A	6081	6088
K3E	3718	3765	E94R	6082	6089
L6A	5984	N.A.	V100A	6065	N.A.
L6E	5983	4632	V100E	6064	6271
D14A	6076	6083	E104A	3656	3499
D14R	6077	5797	E104R	3657	3495
L18A	6106	6098	R105A	6190	6183
L18E	6100	6264	R105E	6191	6184
W21A	3720	3544	R110A	3658	3492
I22A	5988	N.A.	R110E	3659	3494
I22E	5987	6265	I111A	6099	6093
I26A	5990	N.A.	I111E	6101	6272
I26E	5989	6266	E114A	3660	3496
D49A	5992	6084	E114K	3661	3545
D49R	6078	6085	L119A	6067	N.A.
K68A	5993	6090	L119E	6066	6273
K86E	3648	3713	I122A	6004	N.A.
I69A	6061	N.A.	I122E	6003	6274
I69E	6060	6267	D124A	6192	6185
K71A	3652	3706	D124R	6193	6186
K71E	3653	3707	L127A	6006	N.A.
V75A	6194	6187	L127E	6005	N.A.
V75E	6195	6210	K140A	6008	N.A.
D77A	5995	N.A.	K140E	6007	6235
D77K	5994	6211	V154A	6069	N.A.
K79A	5997	N.A.	V154E	6068	6275
K79E	5996	6215	L155A	6010	N.A.
V80A	6063	6092	L155E	6009	6276
V80E	6062	6268	V157A	6012	N.A.
I84A	5999	N.A.	V157E	6011	6277
I84E	5998	6269	D164A	3721	3497
R85A	6079	6086	D164R	3733	3500
R85E	6080	6087	D166A	3722	2715
D86A	3654	3766	D166R	3723	3646
I91A	6001	N.A.	V168A	3729	3805
I91E	6000	6270	V168E	6013	6278
L92A	6196	6188			
L92E	6197	6189			



**Table 2.3: Strains used in this chapter.**

<b>Strain</b>	<b>Genotype</b>
YVL2967	MATa <i>ura3-52 lys2-801 trp-Δ1 his3-Δ200 leu2-Δ1</i>
YVL3057	MATa <i>ura3-52 lys2-801 trp-Δ1 his3-Δ200 leu2-Δ1 est3-Δ::LYS2</i>
YVL3485	MATa <i>leu2 trp1 ura3-52 GAL+ prb- prc- pep43 myc12-G6-Est2</i>

**Table 2.4: pVL2537 (*EST3 CEN LEU2*) plasmids used in Rao et al. 2014.**

<b>Mutation</b>	<b>pVL#</b>
K71E	3653
V75E	6194
Y78R	6497
T112A	6501
E114K	3661
N117K	3816
D166R	3723
V168E	6013
L171E	6598

**Table 2.5: pVL2076 (*EST3-(FLAG)<sub>3</sub> CEN LEU2*) plasmids used in Rao et al. 2014.**

<b>Mutation</b>	<b>pVL#</b>
K71E	3454
V75E	7823
Y78R	6497
T112A	7824
E114K	3473
N117K	3472
D166R	3404
V168D	3464

**Table 2.6: pVL1024 (ADH-EST3 2 $\mu$  LEU2) plasmids used in Rao et al 2014.**

<b>Mutation</b>	<b>pVL#</b>	<b>Mutation</b>	<b>pVL#</b>	<b>Mutation</b>	<b>pVL#</b>
V16E	6198	K140E	6235	H107R	6362
F17E	6199	N145R	6236	C109R	6370
L25E	6200	I146E	6237	T116E	6371
Y35R	6201	K149E	6238	T131R	6372
Y35E	6202	E150R	6239	S133E	6373
V41E	6203	I151E	6240	S137E	6374
Q48R	6204	N156R	6241	H138R	6375
L52E	6205	N158R	6242	H138E	6376
M55E	6206	Q159R	6243	C142E	6377
L60E	6207	F163E	6244	S144R	6378
Y73R	6208	L171E	6245	S148E	6379
Y73E	6209	F176A	6246	T161R	6380
V75E	6210	F176R	6247	S172E	6381
D77K	6211	F176E	6248	T173E	6382
Y78A	6212	K179E	6249	P175E	6383
Y78R	6213	Y180R	6250	N62R	6384
Y78E	6214	Y180E	6251	N74R	6385
K79E	6215	L181E	6252	P43R	6386
Y81R	6216	P20E	6253	P57R	6400
Y81E	6217	A24R	6254	T58R	6401
Q90R	6218	H32R	6255	T61R	6402
S96E	6219	H36E	6256	C64R	6403
S96R	6220	S38R	6257	V75R	6404
Q97R	6221	G39R	6348	R110V	6405
E98R	6222	H40R	6349	V75R R110V	6406
N102R	6223	H40E	6350	K179E+K71A	6407
R105E	6224	S44R	6351	F176R+K179E	6408
N108R	6225	T46R	6352	T70E+K71A	6409
T112A	6226	H54E	6353	D124R+N158R	6461
T112I	6227	C76R	6354	R134E+S137E	6462
D124R	6228	S83E	6355	K79E+Y81E	6463
D126R	6229	S87E	6356	L92E+E94R	6464
V128E	6230	S88E	6357	Y73R+N74R	6465
V130E	6231	H89E	6358	S15A	6466
N132R	6232	S101R	6359	N108A	6467
R134E	6233	T106R	6360	T116A	6468
M136E	6234	H107E	6361	I146A	6469
L171A	6470	S172A	6471		

## Materials and Methods

### *Yeast strains and plasmids*

All genetic analyses were performed in two isogenic strains, YVL2967 (*MATa ura3-52 lys2-801 trp1-Δ1 his3-Δ200 leu2- Δ1*) or YVL3057 (*MATa est3-Δ ura3-52 lys2-801 trp1-Δ1 his3-Δ200 leu2-Δ1/p EST3 CEN URA3*). Missense mutations in *EST3* were introduced into either pVL1024 (2m *LEU2 ADH-EST3*) or pVL2537 (*CEN LEU2 EST3*); a complete list of the yeast plasmids used in this study is shown in Supporting Information, Table 2.S2. Standard genetic methods were used to introduce plasmids into yeast, and telomere length was assayed as described previously (Lendvay et al. 1996; Paschini et al. 2010).

### *Telomerase Coimmunoprecipitation Assays*

Wild-type and mutant Est3 proteins, bearing an in-frame (FLAG)<sub>3</sub> epitope and under control of the native *EST3* promoter, which were expressed from the previously described single-copy plasmid, pVL2076 (Lee et al. 2008), were introduced into a protease-deficient strain bearing an integrated (myc)<sub>12</sub>–(Gly)<sub>6</sub>–Est2 construct. Extract preparation and coimmunoprecipitation of Est3 and Est2 were assessed as previously described (Tucey & Lundblad 2013; Lee et al. 2008).

### *In Vivo Assessment of Telomere Function*

Effects of missense mutations in *EST3* were assessed by two assays, which measured (i) the ability to complement an *est3-Δ* strain in a standard loss-of- function (LOF) assay and (ii) the ability to disrupt telomere replication when over-expressed in the

presence of the wild-type *EST3* gene [overexpression dominant negative (ODN)]. This latter assay used a yeast strain which was sensitized to defects in telomerase (due to a mutation in YKU80), thereby permitting rapid initial detection of *est3*<sup>-</sup> defects as an immediate reduction in viability (Evans et al. 2002; Lee et al. 2008; Lubin et al. 2013). Missense mutations that exhibited an ODN phenotype in this viability assay were subsequently shown to have ODN effects on telomere length, as well telomere length defects in the LOF assay.

#### *In Vivo Assessment of Non-Telomere Function*

Effects of missense mutations in *EST3* were assessed by the ability to disrupt DNA replication or repair when over-expressed in the presence of the wild-type *EST3* gene [overexpression dominant negative (ODN)]. This used a wild-type yeast strain which was subjected to UV, MMS, or HU as cells were plated on rich media (YPAD).

#### **Acknowledgements**

The development for the ODN assay was a large collaboration between the Lundbald lab and the Wuttke lab. I would first like to thank all of the members of the Wuttke lab for their biochemical and structural work and expertise. Former members of the Lundblad lab, particularly Jeasung Lee and Ed Mandell, laid the foundation and made key initial observations for this assay. Finally, I worked closely with Tim Tucey and Lisa Nguyen in generating the data to prove the concept.

The authors of Lubin et al. 2013 thank Chris Lima at the Memorial Sloan-Kettering Cancer Center for the generous gift of the pET- His-Smt3 vector and Karen

Lewis for assistance with the CD instrument. This research was supported by National Institutes of Health grants R37 AG11728 (to V.L.), R01 GM059414 (to D.S.W.), T32 GM08759 (to T.R.), and by Cancer Center Core grant P30 CA014195 (the Salk Institute).

The authors of Rao et al. 2014 thank Chris Lima (Memorial Sloan–Kettering Cancer Center) for the generous gift of the pET-His10-Smt3 vector, Jayakrishnan Nandakumar and Oliver Lange for useful discussions and protocols, David McKay for assistance with the Phoenix protein drop setter for high-throughput buffer screening, and Thayne Dickey for helpful suggestions on the manuscript. We gratefully acknowledge time on the JANUS supercomputer (Research Computing Facility, University of Colorado Boulder) for RASREC Rosetta structure calculations and thank the National Institutes of Health (R01GM059414 to D.S.W., R37AG11728 to V.L., T32GM08759 to T.R., and T32GM007240 to T.M.T.), the National Science Foundation, and a Rose Hills Foundation Fellowship (to T.M.T.) for financial support of this research.

Some of Chapter 2 is a formatted reprint of portions of the material as it appears in Lubin, J.W., Rao, T., Mandell, E.K., Wuttke, D.S., Lundblad, V. (2013). Dissecting protein function: An efficient protocol for identifying separation-of-function mutations that encode structurally stable proteins. *Genetics* 193: 715-725, of which the dissertation author was the co-primary investigator and author, and Rao, T., Lubin, J.W., Armstrong, G.S., Tucey, T.M., Lundblad, V., Wuttke, D.S. (2014). Structure of Est3 reveals a bimodal surface with differential roles in telomere replication. *PNAS* 111: 214–218.

### **CHAPTER THREE:**

Using separation-of-function mutagenesis to define the full spectrum of activities  
performed by the Est1 telomerase subunit *in vivo*

Chapter 3 is a formatted reprint of the material as it appears in Lubin, J.W., Tucey, T.M., Lundblad, V. Using separation-of-function mutagenesis to define the full spectrum of activities performed by the Est1 telomerase subunit *in Vivo*. *Genetics* 208: 97-110 (2018). The dissertation author was the co-primary investigator and author of this paper.

## Abstract

A leading objective in biology is to identify the complete set of activities that each gene performs in vivo. In this study, we have asked whether a genetic approach can provide an efficient means of achieving this goal, through the identification and analysis of a comprehensive set of separation-of-function (*sof*<sup>\*</sup>) mutations in a gene. Toward this goal, we have subjected the *Saccharomyces cerevisiae* *EST1* gene, which encodes a regulatory subunit of telomerase, to intensive mutagenesis (with an average coverage of one mutation for every 4.5 residues), using strategies that eliminated those mutations that disrupted protein folding/stability. The resulting set of *sof*<sup>\*</sup> mutations defined four biochemically distinct activities for the Est1 telomerase protein: two temporally separable steps in telomerase holoenzyme assembly, a telomerase recruitment activity, and a fourth newly discovered regulatory function. Although biochemically distinct, impairment of each of these four different activities nevertheless conferred a common phenotype (critically short telomeres) comparable to that of an *est1-Δ* null strain. This highlights the limitations of gene deletions, even for nonessential genes; we suggest that employing a representative set of *sof*<sup>\*</sup> mutations for each gene in future high- and low-throughput investigations will provide deeper insights into how proteins interact inside the cell.



## Introduction

Telomeres—the ends of linear chromosomes, which are composed of G-rich repeats bound by an array of telomere-specific proteins—are essential for high-fidelity maintenance of linear chromosomes. Severe telomere dysfunction has catastrophic consequences for genome organization, but even modest reductions in telomere length can also have a genome-destabilizing effect. As a result, in cells that depend on long-term proliferation, a carefully regulated mechanism ensures that telomeres are stably maintained at an average length (Hug and Lingner 2006). In most eukaryotic species, a key player in this process is the enzyme telomerase. This telomere-dedicated enzyme is responsible for adding telomeric G-rich repeats onto the ends of chromosomes, thereby providing a counterbalance against sequence loss that arises due to incomplete DNA replication or other DNA-processing activities (Schmidt and Cech 2015; Wu et al. 2017). Although telomerase has been a topic of intense investigation, a detailed mechanistic picture of how telomerase-mediated elongation is regulated at individual telomeres is incomplete. For example, yeast telomerase only elongates a small subset of telomeres in a cell cycle, with a preference for shorter telomeres (Teixeira et al. 2004), a bias that also extends to mammalian telomeres (Britt-Compton et al. 2009). However, the molecular mechanism that restricts telomerase to a particular subset of telomeres has not yet been elucidated. Telomere length is also dictated by the number of telomeric repeats that are added each time telomerase interacts with its substrate, but how this enzymatic step is regulated *in vivo* is still poorly understood.

This incomplete picture suggests that there may be as-yet-undiscovered mechanisms that are critical for telomerase regulation. As one approach toward

addressing this, we are constructing a functional surface map of yeast telomerase, by identifying functionally important amino acids on the surface of each telomerase subunit that, when mutated, disrupt specific activities. To facilitate the identification of these separation-of-function (*sof*<sup>\*</sup>) mutations, we have employed a strategy that relies on overexpression dominant negative (ODN) phenotypes (i.e., disruption of function in a wild-type strain in response to an overexpressed mutant protein) as a rapid means of identifying the rare subclass of mutations that target a specific biochemical property without affecting protein stability. The rationale is based on the premise, first elucidated by Ira Herskowitz (Herskowitz 1987), that mutant proteins must be structurally intact in order to compete with the endogenous wild-type protein. In contrast, the much larger class of mutations that encode unstable/unfolded proteins will be phenotypically silent (or greatly attenuated) in an ODN-based assay.

We first applied this strategy to the Est3 subunit of telomerase, both as a proof-of-principle experiment and with the goal of identifying novel Est3 regulatory activities, by analyzing ODN phenotypes of a systematic set of mutations introduced into 20% of the amino acids in the Est3 protein. Notably, those mutant Est3 proteins with strong ODN phenotypes demonstrated a remarkably similar secondary structure content and thermal stability when compared to the wild-type protein (Lubin et al. 2013). Once the Est3 structure was solved (Rao et al. 2014), this revealed that every residue identified in our genetics-driven ODN screen was located on the Est3 protein surface. This provided a striking validation of this methodology, and argued that ODN-directed mutagenesis is capable of selectively identifying mutations in functionally important amino acids on the surface of a protein, even in the absence of structural information.

In this study, we have applied this protocol to the second of the three telomerase protein subunits, by analyzing a large panel of missense mutations in *EST1* for ODN effects on telomere length maintenance. The *sof*<sup>+</sup> mutations recovered from this ODN screen correspond to three biochemically distinct activities: (i) a dual Est3-binding site that involves regions in both the N- and C-terminal halves of the Est1 protein; (ii) an expanded surface that mediates the Est1-Cdc13 interaction; and (iii) a newly defined regulatory activity that is not required for telomerase biogenesis or recruitment. In parallel, we performed an extensive loss-of-function (LOF) screen, which identified a novel 60-amino acid RNA-binding domain (RBD) that was phenotypically silent in the ODN assay. This combined ODN plus LOF analysis has provided a representative set of *sof*<sup>+</sup> alleles that define four discrete activities performed by Est1. This provides a set of genetic reagents for *EST1* that has the potential to uncover activity-specific genetic interactions in future low- and high-throughput analyses, which would be otherwise masked by a complete deletion of the *EST1* gene.

## Results

### *ODN-based mutagenesis identifies 11 candidate sof<sup>+</sup> mutations in EST1*

To identify and characterize functional surfaces on the Est1 protein, an ODN protocol was employed, whereby *est1*<sup>-</sup> mutations were screened for the ability to disrupt telomere replication when overexpressed in the presence of the wild-type *EST1* gene. A total of 134 missense mutations were introduced by reverse mutagenesis into the *EST1* gene, which was present on a high-copy plasmid and under the control of the constitutive ADH promoter (Figure 3.S1). Amino acids were selected for mutagenesis based on

sequence conservation (data not shown) and emphasized: (i) charged amino acids, based on our analysis indicating that mutation in residues in this category were more likely to encode a protein that retained structural stability (Lubin et al. 2013), and (ii) aromatic residues, which frequently mediate nucleic acid interactions (Jones et al. 2001; Baker and Grant 2007). This collection of 134 overexpressed *estI*<sup>-</sup> mutations was transformed into a *yku80-Δ/p CEN URA3 YKU80* strain, and transformants were screened for viability following loss of the *YKU80* plasmid, based on earlier observations showing that increased expression of mutant telomerase subunits confers inviability in a *yku80-Δ* strain (Lee et al. 2008; Lubin et al. 2013). This strategy identified 11 *estI*<sup>-</sup> mutations that conferred a moderate to severe impact on viability when overexpressed in the *yku80-Δ* strain (Figure 3.S2), and also reduced telomere length when overexpressed in a wild-type (i.e., *EST1 YKU80*) strain (Figure 3.1, A–C). There was a strong correlation between these two ODN phenotypes; for example, mutations with the most pronounced effects on viability in the *yku80-Δ* strain (Figure 3.S2) also conferred substantially shorter telomeres (Figure 3.1A), consistent with our prior observations with *EST3* (Lee et al. 2008; Lubin et al. 2013). These 11 *estI*<sup>-</sup> mutations were subsequently assessed for effects on telomere length in a standard LOF assay, in which each allele, expressed by the *EST1* promoter on a single-copy plasmid, was transformed into an *estI-Δ* strain. Seven mutations conferred a severe impact on telomere length (Figure 3.1, D and E), whereas four mutations resulted in more intermediate phenotypes in the LOF assay (Figure 3.1, F and G). In each case, the severity of the ODN telomere length phenotype closely correlated with the strength of the corresponding LOF telomere length phenotype (compare Figure 3.1, A–C with Figure 3.1, D–G).

We have previously argued that an ODN phenotype can distinguish between a mutation that encodes a structurally intact protein vs. a mutation that results in a nonspecific effect on protein stability/folding (Lubin et al. 2013). Consistent with this expectation, steady-state protein levels for each of these Est1 mutant proteins were comparable to that of the wild-type Est1 protein (Figure 3.2A). This was assessed in a strain bearing identical (myc)<sub>12</sub> epitopes on Est1 and Est2, as well as a (FLAG)<sub>3</sub> epitope on Est2, with each of the 11 *est1*<sup>-</sup> mutations integrated into the genome. This allowed simultaneous detection of both proteins on the same anti-myc western, thereby providing highly accurate determination of the level of each mutant Est1 protein relative to the wild-type Est2 protein. As previously observed (Tucey and Lundblad 2013), the Est1 protein was present in at threefold excess, relative to Est2, in extracts prepared from asynchronous cultures; this ratio was unchanged in each of the mutant strains (Figure 3.2A). The Est1:Est2 ratio in the telomerase complex was also determined, following anti-FLAG IP of Est2. Examination of Est1 and Est2 protein levels in anti-FLAG IPs showed that each of the 11 mutant Est1 proteins was capable of forming a complex in a 1:1 ratio with Est2, in a manner that was indistinguishable from that of the wild-type Est1 protein (Figure 3.2B). Collectively, the observations shown in Figure 3.1 and Figure 3.2 argue that these mutations in *EST1* confer an in vivo defect without impairing protein stability and are candidates for sof<sup>-</sup> mutations. The positions of these 11 mutations are indicated on a schematic diagram of the Est1 protein in Figure 3.2C.

#### *Identification of a novel RBD in Est1 that is conserved from yeast to humans*

Notably, none of these 11 mutations affected the ability of Est1 to form the Est1-

TLC1-Est2 preassembly complex (Tucey and Lundblad 2014), indicating that the ODN-based approach had failed to uncover mutations in the RNA-binding activity of Est1. As a first step toward identifying the region of Est1 responsible for RNA binding, the ability of two subdomains of Est1 to form a complex with TLC1 was examined. N- and C-terminal domains expressing amino acids 1–340 and 340–699, respectively, with an in-frame (myc)<sub>12</sub> epitope, were integrated into the genome in place of the full-length Est1 protein, in a strain that also expressed the (FLAG)<sub>3</sub>-(myc)<sub>12</sub>- Est2 protein; domain boundaries were chosen based on a region of low sequence conservation around amino acids 340–350 (data not shown). Since TLC1 bridges the association between Est1 and Est2 through independent Est1-TLC1 and Est2-TLC1 interactions (Livengood et al. 2002; Lubin et al. 2012), the ability of an Est1 domain to co-IP with the Est2-TLC1 catalytic core reflects a direct interaction with TLC1. Following IP, the N-terminal domain of Est1 retained association with the Est2-TLC1 subcomplex, whereas the C-terminal domain was undetectable in anti-Est2 IPs (Figure 3.3A), indicating that RNA-binding activity localized to the N-terminal half of the Est1 protein.

Therefore, we subjected the N-terminal region of Est1 to conventional LOF analysis, by examining the telomere length of 84 *est1*<sup>-</sup> mutations spanning amino acids 1–350 (Figures 3.S1 and 4.). Each mutation, expressed on a single-copy plasmid by the *EST1* promoter, was introduced into an *est1*-Δ strain, and telomere length was examined after ~75 generations of growth. This identified mutations in a cluster of five aromatic amino acids (from amino acids 40 to 146) that resulted in significant telomere shortening (Figure 3.3B; see also in Figure 3.S3, A–N). To assess potential effects on RNA binding, these five mutations were introduced into the genome of the Est-(myc)<sub>12</sub> (FLAG)<sub>3</sub>-

(myc)<sub>12</sub>-Est2 strain in place of the wild-type *EST1* gene, and the relative ratio of Est1 to Est2 in anti-Est2 immunoprecipitates was examined. We have previously shown that this assay provides a very sensitive read-out of the interaction between Est1 and TLC1, due to the ability to simultaneously detect Est1 and the Est2 subunit of the Est2-TLC1 catalytic core on the same anti-myc western; this assay has also been validated by our prior identification of a panel of mutations in TLC1 that disrupt Est1-TLC1 binding (Lubin et al. 2012; see also Figure 3.S4). Using this assay, all five mutant Est1 proteins exhibited a reduced ability to bind TLC1 to form an Est1-TLC1-Est2 subcomplex (Figure 3.3C). This was not simply a consequence of reduced Est1 protein levels, as shown by anti-myc westerns of extracts from these mutant strains (Figure 3.3C); in fact, the Est1-Y136D mutant protein reproducibly displayed a slight increase in protein levels, relative to wild-type Est1. There was also a striking correspondence between the degree of biochemical impairment and the *in vivo* consequences for telomere replication. Three mutations with a pronounced telomere length defect (*est1-W87E*, *est1-F98D*, and *est1-Y136D*) exhibited a substantial reduction in the interaction between Est1 and TLC1, whereas *est1-F40* and *est1-Y146D* were only modestly diminished in both assays. When tested for ODN phenotypes, these five mutations failed to exhibit an ODN phenotype (Figure 3.S4 and data not shown), which explains our failure to identify this category of mutations in our ODN screen.

The recovery of five RNA-binding-defective *est1*<sup>-</sup> mutations in residues with aromatic side chains, which are used extensively in RNA–protein interactions (Baker and Grant 2007), was not due to a mutation bias, as this region of Est1 was extensively mutagenized (Figure 3.S1). Furthermore, the region of Est1 that encompassed four of the

residues identified by this analysis (Trp87, Phe98, Tyr136, and Tyr146) was highly conserved, as shown by the alignment that encompasses budding yeast, fission yeast, and human sequences (Figure 3.3D). These observations argue that we have uncovered a conserved, novel 60-amino acid RBD that does not exhibit sequence motifs characteristic of canonical RBDs (Helder et al. 2016). The position of the mutations that define the Est1 RBD are shown in Figure 3.2C. We note that the results presented here differ from observations from an earlier study, which reported that a different domain of the fission yeast Est1 protein was employed for RNA binding (Webb and Zakian 2012); Figure 3.S4 provides more information regarding the differences between these two studies.

*The Est1-Est3 interaction involves dual sites in the N- and C-terminal domains of Est1*

To characterize the biochemical activities of the 11 *est1<sup>-</sup>* mutations identified by ODN mutagenesis, we examined how each of these mutations affected binding to two known Est1-binding partners, Est3 and Cdc13. We previously showed that Est1 contains a binding site for the Est3 telomerase subunit, located in the N-terminal domain of Est1 in a region distinct from the RBD (Figure 3.2C; Tucey and Lundblad 2014); this Est1-Est3 interaction was defined by the *est1-R269E* mutation, which was recovered in our ODN screen (Figure 3.1 and Figure 3.S2). Although the Est1-R269E mutant protein formed a preassembly complex that was indistinguishable from wild-type (Figure 3.2B), subsequent association of Est3 with the mutant Est1-R269E-TLC1-Est2 subcomplex to form the telomerase holoenzyme was reduced (Tucey and Lundblad 2014; Figure 3.S5). To ask if additional *sof<sup>+</sup>* mutations identified by ODN mutagenesis affected the interaction between Est1 and Est3, we integrated *sof<sup>+</sup>* alleles into an Est1-(myc)<sub>12</sub> Est3-



(FLAG)<sub>3</sub> strain and examined the interaction between Est1 and Est3 following anti-FLAG IPs. This identified a cluster of three mutations in the C-terminal region of Est1 that were substantially impaired for the Est1-Est3 interaction (Figure 3.4A). The severity of this biochemical defect was reflected in the in vivo phenotype of the mutant strains bearing these three alleles, which exhibited critically short telomeres in all three cases (Figure 3.1E). Notably, other *sof*<sup>\*</sup> mutations in the C-terminal domain with pronounced in vivo phenotypes had no impact on the Est1-Est3 association (Figure 3.4B). This Est1-Est3 association was also dependent on prior formation of the Est1-TLC1-Est2 subcomplex; if Est1 was unable to bind the TLC1 RNA due to a mutation in the Est1 RBD, the Est1-Est3 interaction was abolished (Figure 3.4C). These results, combined with the identification of the RBD in Figure 3.3, show that the Est1 protein contains three distinct binding sites that are required for the formation of the quaternary enzyme complex: the RBD in the extreme N-terminus of Est1, and a bimodal Est3-binding interface that employs Est3-interacting residues in both the N- and C-terminal halves of Est1.

*An expanded Est1 interface is required for the interaction with Cdc13*

Mutations recovered from the ODN mutagenesis were also tested for whether they affected the interaction between Est1 and Cdc13, using a strain with (myc)<sub>12</sub> and (FLAG)<sub>3</sub> tags on Est1 and Cdc13, respectively. We have previously reported that an interaction between Est1 and Cdc13 can be detected in anti-Cdc13 immunoprecipitates. This biochemical association recapitulates the genetic interaction between these two proteins (Pennock et al. 2001), as Est1-Cdc13 binding is eliminated by the recruitment-

defective *cdc13-2* mutation, but restored in a *cdc13-2* strain containing a cosuppressing *est1-60* mutation (Tucey and Lundblad 2013; Figure 3.5A), providing strong support for a direct interaction between Est1 and Cdc13. The *est1-60* mutation (*est1-K444E*) was also identified in our ODN-directed mutant screen, as well as a second mutation in an immediately adjacent residue (*est1-R447E*; Figure 3.1 and Figure 3.S2); both mutations strongly reduced the Est1-Cdc13 interaction (Figure 3.5A). An additional cluster of mutations (at amino acids 555–566) made a more modest contribution to the association between Est1 and Cdc13 (Figure 3.5B). As was observed for mutations that affected Est1-TLC1 and Est1-Est3 interactions, the extent of the Est1-Cdc13-binding defect in the *in vitro* assay (Figure 3.5) correlated well with the impact on telomere length *in vivo* (Figure 3.1).

In contrast to the Est1-Est3 interaction (Figure 3.4C), the association between Est1 and Cdc13 was not dependent on the Est1-TLC1 interaction, as two mutant Est1 proteins (Est1-W87E and Est1-Y136D) that were defective for RNA binding, and thus incapable of associating with the telomerase complex (Figure 3.3C), still bound Cdc13 at wild-type levels (Figure 3.5C). Reciprocally, the Est1-Est3 and Est1-Cdc13 interactions were not interdependent, as mutant Est1 proteins that could not bind Cdc13 (Est1-K444E and Est1-R447E) were able to form the Est1-TLC1-Est2 preassembly complex (Figure 3.2B) and associate with Est3 to form the subsequent Est3-Est1-TLC1-Est2 holoenzyme (Figure 3.4B). Similarly, the mutant Est1-D510R and Est1-F511D proteins, which had lost association with Est3 (Figure 3.4A), were still capable of binding Cdc13 (Figure 3.S5), which is also consistent with a prior report showing that an Est1 mutant protein bearing a different ODN missense mutation in one of these residues (*est1-F511S*; Virta-

Pearlman et al. 1996) still retains association with telomeric chromatin (Sealey et al. 2011). This provides strong support for a model in which assembly of the telomerase holoenzyme and the interaction between Cdc13 and Est1 are biochemically independent events, as evidenced by the fact that an interaction between Cdc13 and Est1 occurs in G1 phase (Tucey and Lundblad 2013), at a point when Cdc13 cannot be detected at telomeres and the holoenzyme has not yet assembled.

#### *A newly discovered fourth function for Est1*

The analysis of the effects of these 11 *sof* mutations on binding to TLC1, Est1, or Cdc13 identified mutations in two closely spaced amino acids (*est1-R485E* and *est1-R488E*) that were unaffected for interaction with these three well-characterized binding partners of Est1. The mutant Est1-R485E and Est1-R488E proteins were indistinguishable from the wild-type Est1 protein in their ability to associate to form the Est1-TLC1-Est2 preassembly complex (Figure 3.2B), to bind Est3 to form the holoenzyme (Figure 3.4B), or to interact with the Cdc13 recruitment factor (Figure 3.6A). Furthermore, the telomerase disassembly pathway was unperturbed in strains bearing either of these two mutations (Figure 3.S6 and data not shown). The robust ODN phenotype exhibited by these two mutations was also reversed by the presence of an RNA-binding-defective allele (Figure 3.S6), arguing that Est1 performs this fourth activity as a component of the telomerase holoenzyme. These data, combined with the strong in vivo phenotype displayed by the *est1-R485E* and *est1-R488E* strains (Figure 3.1D), argues that telomerase has a fourth Est1-dependent activity that is critical for telomere replication.

Numerous factors besides TLC1, Cdc13, or Est3 have been proposed as direct interactors with either Est1 or the telomerase holoenzyme, and thus could be candidates that mediate this fourth activity. The strength of the *in vivo* phenotype displayed by the *est1-K485E* and *est1-K488E* strains suggests that a defect in this proposed factor will also exhibit an *Est<sup>-</sup>* phenotype (i.e., critically short telomeres and an accompanying senescence phenotype). This prediction potentially rules out candidates encoded by nonessential genes, since the only nonessential genes that have an *Est* phenotype when mutated are previously identified telomerase components (encoded by *EST1*, *EST2*, *EST3*, and *TLC1*; Askree et al. 2004). Therefore, we turned our attention to two previously described telomerase-interacting complexes encoded by essential genes: the Sm complex (Seto et al. 1999) and the Pop protein complex (Lemieux et al. 2016). Strains bearing a (myc)<sub>12</sub> tag on Est1 and a (FLAG)<sub>3</sub> tag on a subunit of either of these two complexes (Pop1 or Sme1) were constructed and subjected to anti-FLAG IP. As shown in Figure 3.6, B and C, both the Pop1 and Sme1 proteins exhibited a robust co-IP association with Est1. However, this co-IP signal was abolished if Est1 was unable to bind the TLC1 RNA, due to the introduction of the TLC1-binding-defective *est1-Y136D* mutation (Figure 3.6, B and C). Furthermore, the interaction between telomerase and the Sm and Pop complexes was not affected in *est1-R485E* and *est1-R488E* strains (Figure 3.6, B and C and data not shown). Thus, the association of the Sm and Pop complexes with telomerase is not mediated through a direct interaction with Est1.

We also reexamined proteins encoded by nonessential genes, which have been proposed to physically associate with yeast telomerase, using co-IP (Figure 3.S6). Somewhat surprisingly, we failed to detect an interaction between telomerase and a number of

factors previously proposed to associate with telomerase (Pif1, Ebs1, and Sir4), including proteins that have been proposed to directly interact with Est1 (Yku80 and Msp3).

*Reexamining whether Est1 is regulated by proteasome-mediated degradation*

Several prior studies have shown that Est1 protein levels are regulated through the cell cycle (Osterhage et al. 2006; Tucey and Lundblad 2013). In G1 phase, Est1 and Est2 protein levels are equivalent, but as cells progress into S phase, Est1 protein levels increase by almost threefold, whereas Est2 protein levels remain constant; nevertheless, the Est1-TLC1-Est2 subcomplex, which forms early in S phase with Est1 and Est2 in a 1:1 ratio, remains unchanged through the rest of the cell cycle (Tucey and Lundblad 2013). This cell cycle-dependent regulation of Est1 protein levels has been proposed to rely on proteasome-mediated degradation, whereby targeted ubiquitination of Est1 contributes to telomere homeostasis (Osterhage et al. 2006; Ferguson et al. 2013; Lin et al. 2015). This predicts that one or more lysine residues in Est1 should be substrates for ubiquitination, with consequences for telomere length regulation if ubiquitination is blocked. However, despite the inclusion of a large number of lysine residues in our ODN screening strategy (Figure 3.S1), only three lysines (K444, K555, and K559) were recovered that, when mutated, exhibited an effect on telomere length maintenance. Based on our biochemical analysis, these three lysine residues mediate the interaction between Est1 and Cdc13 (Figure 3.5); furthermore, since Est1 protein levels and assembly of the Est1-TLC1-Est2 sub-complex were unaffected in these three mutant strains (Figure 3.2), this argues that none of these three lysines were involved in proteasome-mediated degradation of Est1.

However, lysines that are targets for ubiquitination might be overlooked by an ODN strategy. To address this possibility, we examined the effect on telomere length of mutations in every lysine residue that was conserved in ~3 species within the *Saccharomyces sensu stricto* group (a closely related set of species descended from a common ancestor that underwent a whole-genome duplication; Wolfe and Shields 1997), using an LOF assay. As shown in Figure 3.S3, none of these mutant strains bearing K / A mutations exhibited any marked defects in telomere length. Although this single- residue mutational analysis does not rule out the possibility that modification at multiple lysines is required, we were also unable to detect a change in Est1 protein levels in response to a defect in Ufd4 (Figure 3.7A), which was suggested to be the E3 ubiquitin ligase that targets Est1 for degradation (Lin et al. 2015). Several candidate Destruction boxes in Est1 have also been proposed to mediate the interaction between the anaphase- promoting complex (APC) and Est1 (Ferguson et al. 2013). However, when steady levels of the Est1 protein, normalized to Est2, were monitored in strains in which these candidate APC recognition sites in Est1 were eliminated, we did not observe any change in Est1 protein levels in extracts prepared from either cells arrested in G1 or from asynchronous cultures (Figure 3.7B). Collectively, the above results challenge the premise that Est1 is a target of ubiquitination-dependent proteasomal degradation during the G1 phase of the cell cycle. We suggest instead that the almost threefold increase in Est1 protein during the cell cycle is the result of the previously observed almost threefold increase in Est1 mRNA levels between G1 and G2/M (Spellman et al. 1998; Osterhage et al. 2006).

## Discussion

In this study, we have generated a large panel of *sof*<sup>+</sup> mutations in *EST1*, which we show to define four biochemically distinct activities. Two of these activities mediate telomerase assembly; formation of the Est1-TLC1-Est2 preassembly complex relies on a novel RBD in the N-terminus of the Est1 protein, and subsequent formation of the telomerase quaternary complex requires Est3 interaction sites located in both the N- and C-terminal halves of the Est1 protein. A third activity promotes telomerase recruitment, through a direct interaction between Est1 and Cdc13. Finally, we describe a fourth newly discovered role for Est1, based on a cluster of mutations that do not affect either telomerase assembly or recruitment. Since at least one *sof*<sup>+</sup> mutation associated with each of these four activities confers critically short telomeres, this indicates that each of these four activities is indispensable for Est1's contributions to telomere length maintenance. The collection of *sof*<sup>+</sup> mutations analyzed in this study, along with their assigned biochemical activities, are summarized in Figure 3.8A.

### *Are there more than four Est1 activities?*

An obvious question raised by this analysis is whether our genetic strategy was in fact comprehensive, particularly since our mutagenesis was biased toward several amino acid categories. This question is addressed, at least in part, by a comparison with a prior ODN screen of another telomerase subunit (Est3) that relied on the same mutation bias. The resulting collection of *sof*<sup>+</sup> alleles of *EST3* defined two biochemically distinct activities (Lee et al. 2008; Lubin et al. 2013) that were subsequently shown to map to two clusters of residues on the Est3 protein surface, dubbed the TEL and TELR patches (Rao

et al. 2014). Once the Est3 structure became available, a structure-guided mutagenesis of the complete Est3 protein surface uncovered only two additional residues that conferred a strong telomere replication defect when mutated (in both LOF and ODN assays), which also mapped to the TEL and TELR patches (Rao et al. 2014). Thus, even with a bias toward charged residues, the ODN screen of *EST3* successfully identified the two functions performed by this telomerase subunit.

We also subjected *EST1* to a very high level of mutagenesis: 165 *est1<sup>-</sup>* missense mutations were screened for either ODN or LOF phenotypes, with 60% screened in both phenotypic assays; this represents an average coverage of one mutation for every four to five residues. Nevertheless, several regions of Est1 (amino acids 273–400 and 570–699) were dispensable for telomere length maintenance (Figure 3.2C), which potentially reveals omissions in our genetic strategy. Alternatively, this may reflect the fact that in *Saccharomyces cerevisiae*, there is a second gene, called *EBS1*, which is highly similar to *EST1*; these two paralogs arose as the result of the whole-genome duplication prior to the evolution of the *Saccharomyces* clade (Dujon 2010). In these species, Est1 and Ebs1 perform non-overlapping roles, as a subunit of telomerase (Tucey and Lundblad 2013) or as a component of the nonsense-mediated decay (NMD) pathway (Ford et al. 2006; Luke et al. 2007), respectively. In contrast, in most species (such as fission yeast), there is only a single protein that is homologous to the *EST1* and *EBS1* paralogs; in *Kluyveromyces lactis*, a deletion of this gene confers defects in both telomerase function and NMD (Hsu et al. 2012). This argues that, in *S. cerevisiae*, the Est1 and Ebs1 proteins presumably contain unique features that dictate their nonoverlapping *in vivo* roles. If so, this may account for why several regions of Est1 appear to be unnecessary for function (Figure



3.2C). We are testing this premise by conducting a comparable comprehensive mutagenesis of the *S. cerevisiae EBS1* gene.

Our collection of *sof* alleles does not include mutations in a number of residues that have been reported in prior publications (Evans and Lundblad 2002; Zhang et al. 2010; Sealey et al. 2011; Tong et al. 2011; Hawkins and Friedman 2014), either because we could not reproduce the original mutant phenotype (Figure 3.S3) or because our analysis argued that the mutant phenotype was due, at least in part, to protein destabilization (Figure 3.S1). This latter point might be attributed to the fact that several of these prior studies analyzed clusters of mutations (including mutant isolates from our laboratory; Evans and Lundblad 2002), which increases the possibility that one or more amino acids in a cluster might not be solvent-accessible.

#### *A working model for Est1*

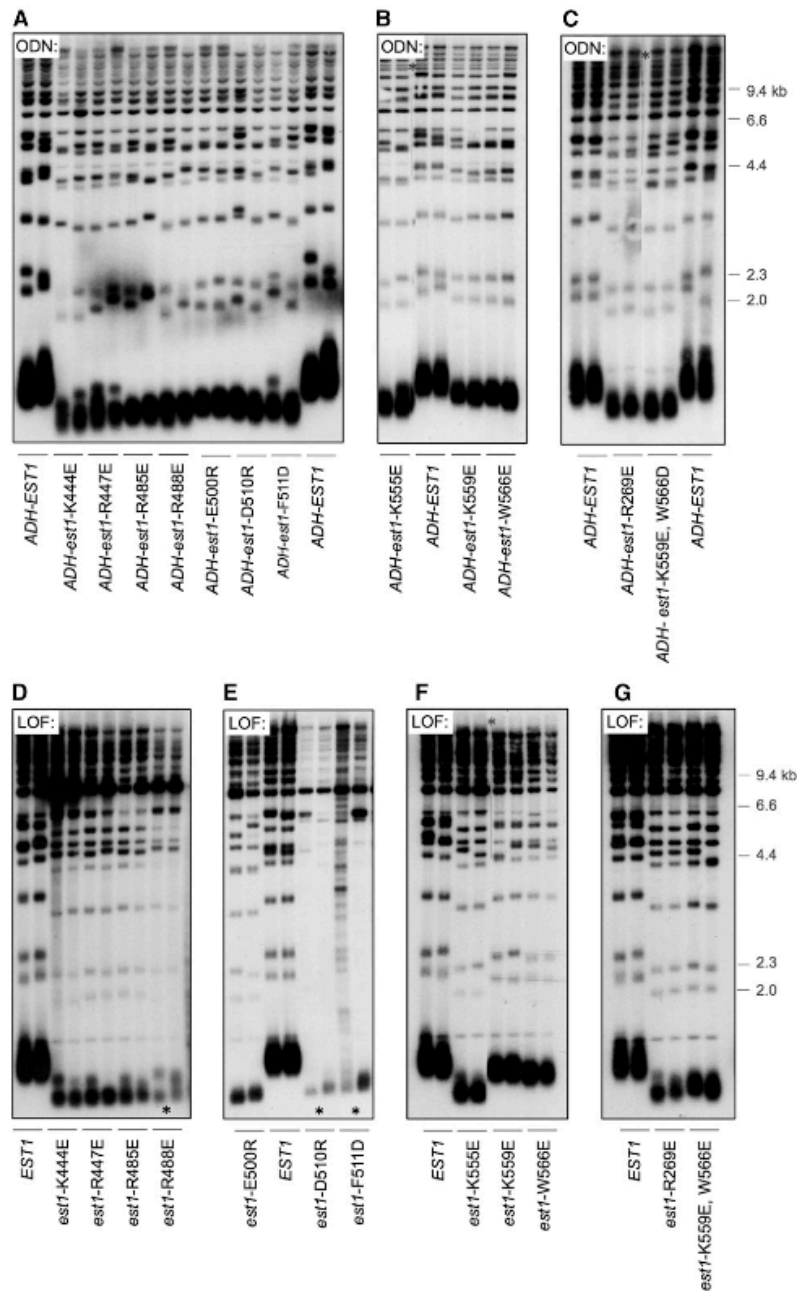
We propose a simple framework for the four Est1 activities (Figure 3.8B). Early in the cell cycle, Est1 employs its RBD to form an Est1-TLC1-Est2 subcomplex (Figure 3.3 and panel 1 in Figure 3.8B; Tucey and Lundblad 2013). This subcomplex subsequently binds the Est3 telomerase subunit to form the telomerase quaternary complex late in the cell cycle (Tucey and Lundblad 2014; panel 2 in Figure 3.8B). Est3 loading is a surprisingly complex step in the telomerase assembly pathway, as it involves two different sites on the N- and C-terminal domains of Est1 as well as the Ten domain of Est2 (Figure 3.4; Tucey and Lundblad 2014). We have previously suggested that association of Est3 might confer a conformational change in the telomerase complex; if so, this might explain why multiple surfaces on the preassembly complex are involved in

Est3 binding. Once the holoenzyme telomerase complex has been assembled, we propose that Est1 carries out two distinct functions as a subunit of telomerase (panels 3 and 4, Figure 3.8B). The first of these is the well-studied role in telomerase recruitment, whereby Est1 provides a bridge between the telomere-bound t-RPA complex and the catalytic core of telomerase, through a presumably direct interaction with Cdc13 (Pennock et al. 2001; Bianchi et al. 2004; Tucey and Lundblad 2013). Est1 also performs a newly discovered activity that is critical for telomere length maintenance, which does not appear to be mediated by previously characterized candidate telomerase interactors (Figure 3.6, B and C and Figure 3.S6). We speculate that the function of Est1 that is disrupted by mutations in Arg485 and Arg488E might be an interaction with an as-yet-undiscovered protein encoded by an essential gene (hypothetically dubbed “Est5” in Figure 3.8B), analogous to the interaction between Est1 and the product of the essential CDC13 gene (which was originally called EST4; Lendvay et al. 1996). The discovery of this fourth function also illustrates the efficiency and effectiveness of the ODN screening methodology, which was capable of discovering a new regulatory role even for a well-studied protein like Est1.

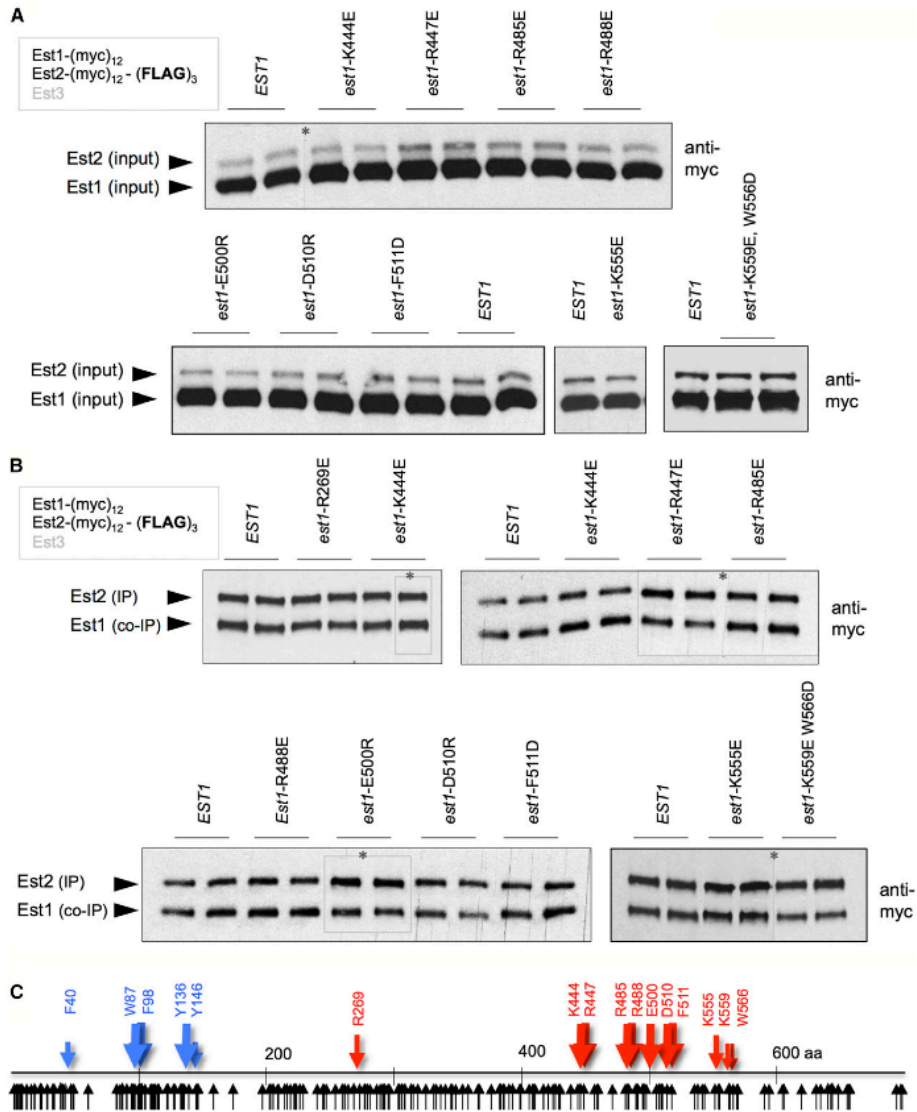
This analysis also highlights the potential limitations of using complete gene deletions for functional analysis, as an *est1-Δ* deletion simultaneously blocks assembly of the Est3 subunit into the complex, telomerase recruitment, and a newly identified regulatory function. Nevertheless, impairment of these distinct Est1 activities all result in a common phenotype: critically short telomeres (Figure 3.1, D–G and summarized in Figure 3.8A). This phenotypic similarity masks the pleiotropic consequences of many types of experiments, such as epistasis analysis, which monitors the consequences of

combining an *estI*- $\Delta$  null mutation with mutations in other genes. In future analyses, we suggest that the employment of a representative set of *sof*<sup>\*</sup> mutations has the potential to uncover genetic interactions that are specific for individual functions of a nonessential gene, thereby providing a far more nuanced view of the complex network of interactions that occur inside the cell.

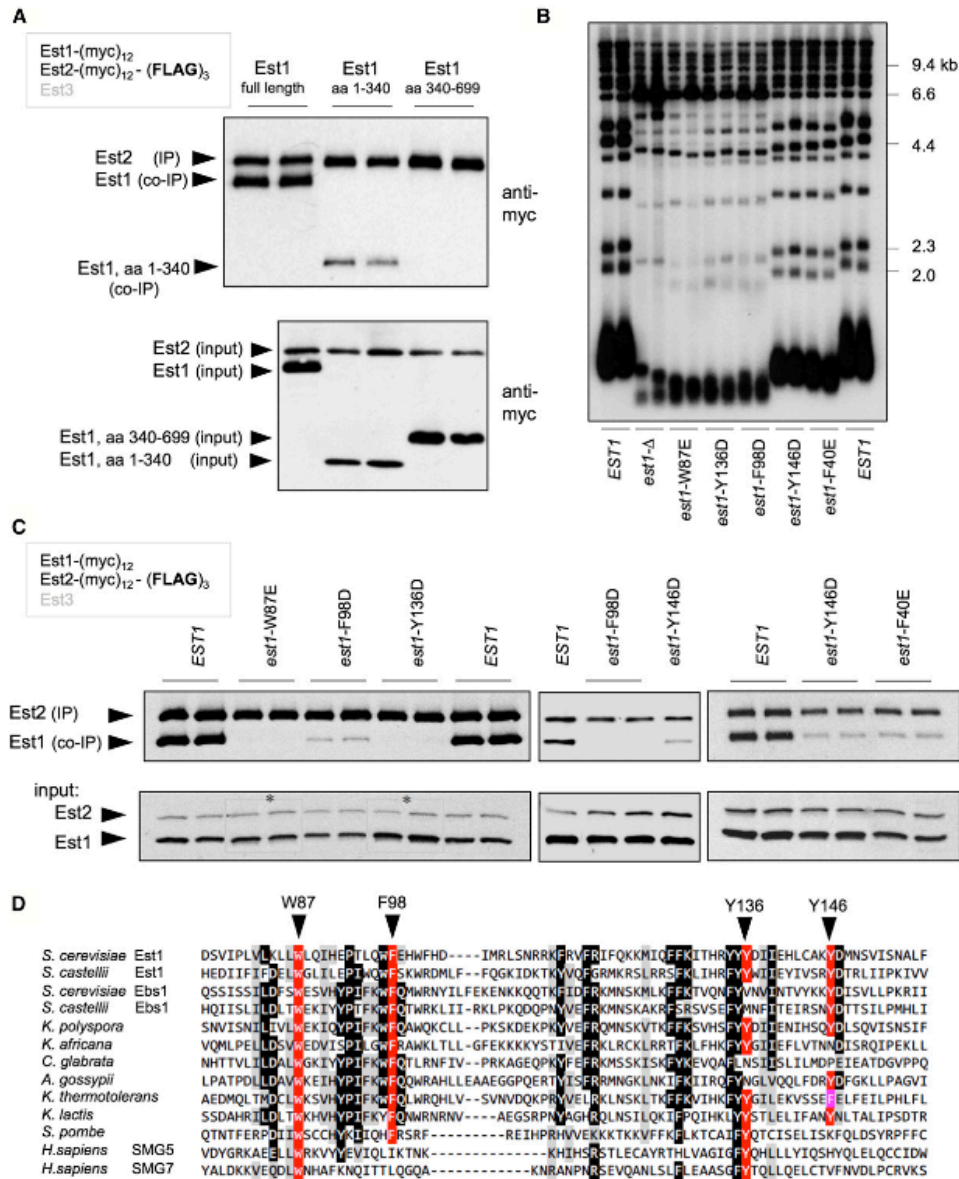
## Figures



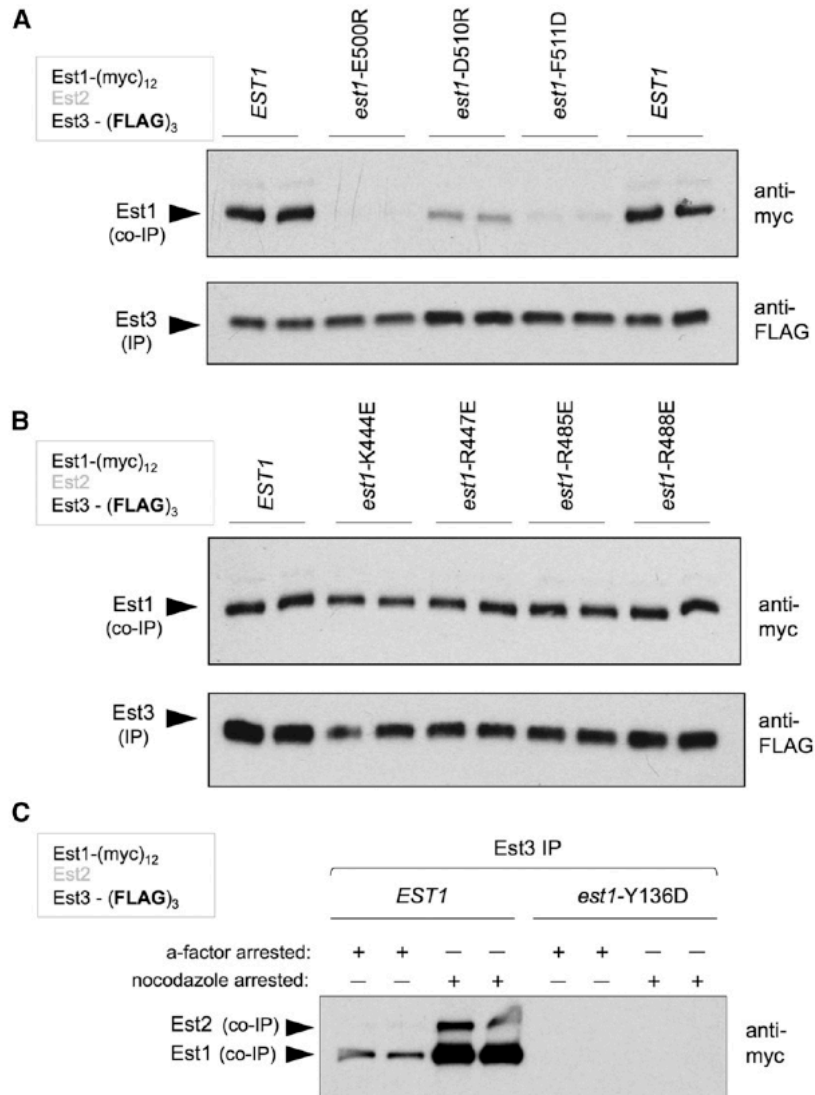
**Figure 3.1: ODN mutagenesis identifies 11 candidate separation-of-function mutations in *EST1*.** (A–C) Telomere length of wild yeast strains transformed with high-copy plasmids expressing either *EST1* or the indicated *est1*<sup>-</sup> mutations, under control of the ADH promoter, assessed after ~75 generations of growth. (D–G) Telomere length of *est1*-Δ strains transformed with single-copy plasmids with either *EST1* or the indicated *est1* mutations, expressed by the *EST1* promoter, determined after ~75 generations of growth following transformation of the *est1*-Δ strain; the exception was three mutant strains (indicated by asterisks) that were examined at 25 generations (at this time point, these three strains were senescent and indistinguishable from an *est1*-Δ null strain). Since *est1*-K559E and *est1*-W566E conferred very modest in vivo phenotypes, these two mutations were combined to facilitate subsequent biochemical analysis. LOF, loss-of-function; ODN, overexpression dominant negative.



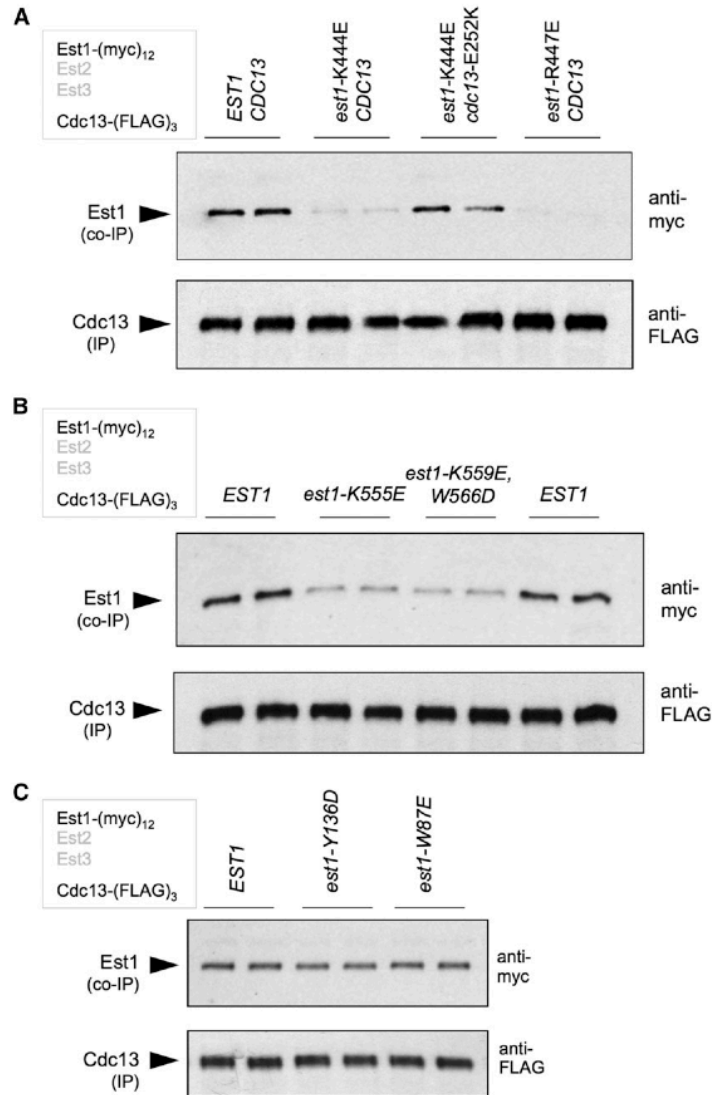
**Figure 3.2: Formation of the Est1-TLC1-Est2 subcomplex is unimpaired by 11 separation-of-function mutations in *EST1*.** (A and B) The relative levels of Est1 and Est2 proteins in extracts (A) and anti-Est2 IPs (B), as assessed by anti-myc westerns of anti-FLAG IPs prepared from strains with the indicated mutations, which were integrated into the genome in place of the wild-type *EST1* gene. Identical (myc)<sub>12</sub> epitopes are present on the C- and N-termini of Est1 and Est2, respectively, with an additional (FLAG)<sub>3</sub> epitope on Est2; different exposures were used (indicated by asterisks) in part (B), to ensure that the Est2 signal was the same for all of the images. (C) Schematic diagram of the Est1 protein, based on analysis shown in Figure 3.1 and Figure 3.3. The 11 *est1*<sup>-</sup> mutations identified by ODN mutagenesis are indicated as red arrows, and the five RNA-binding-defective mutations, identified in Figure 3.3, as blue arrows. The black arrows below the line correspond to each mutation that was analyzed for ODN and/or LOF phenotypes; see Figure 3.S1 for a higher resolution image of the position of each mutagenized amino acid in the 699-amino acid Est1 protein.



**Figure 3.3: Identification of a novel 60-amino acid RNA-binding domain in Est1.** (A) Co-IP of the N- (amino acids 1–340) or C-terminal (amino acids 340–699) domains of Est1 with Est2 was assessed by an anti-myc western of an anti-Est2 IP (top panel); no association between the C-terminal Est1 domain and Est2 was observed, even in a substantially darker exposure (Figure 3.S4), IP and extracts were resolved on 4–20% SDS-PAGE gradient gels. The reduced association of the N-terminal domain with Est2 compared to the full-length Est1 protein (top panel), was presumably due to reduced expression of this domain (bottom panel). (B) Telomere length of the five RNA-binding-defective *est1*<sup>-</sup> mutant strains, determined after 75 generations of growth following introduction of single-copy plasmids with either EST1 or the indicated mutations, expressed by the *EST1* promoter, into an *est1*-Δ strain. (C) The relative levels of Est1 and Est2 proteins in anti-Est2 IPs (top) and extracts (lower), assessed as in Figure 3.2. The slight increase in the levels of the Est1-Y136D protein in inputs, relative to Est2, was a reproducible observation; for the *est1*-W87E and *est1*-Y136D inputs, different exposures were used (as indicated by asterisks) to ensure that the Est2 signal was the same for each sample in this image. (D) The sequence of the RNA-binding domain from *S. cerevisiae* Est1 aligned with Est1 (or Ebs1) proteins from other yeasts, as well as the human SMG5 and SMG7 proteins; the alignment of the human proteins with yeast proteins is based on that in Fukuhara et al. (2005).

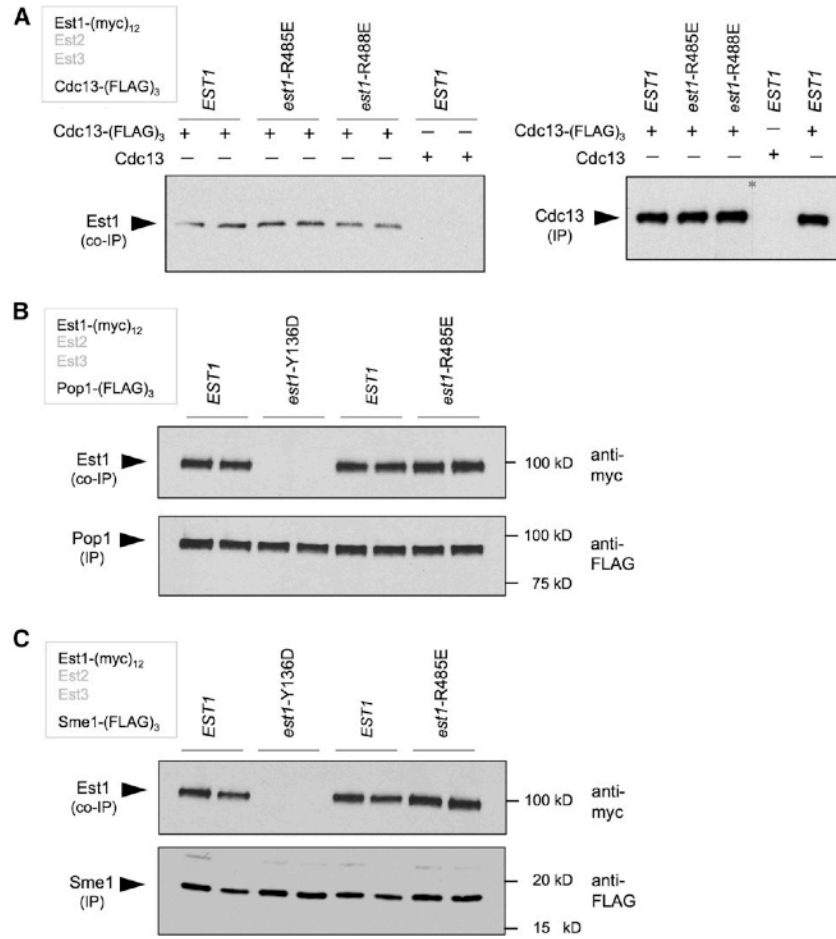


**Figure 3.4: A cluster of residues in the C-terminal domain of Est1 mediate the Est1-Est3 interaction.** (A and B) Association between Est1 and Est3, tagged with (myc)<sub>12</sub> and (FLAG)<sub>3</sub> epitopes, respectively, was monitored by anti-FLAG co-IP. A cluster of three mutations spanning an 11-amino acid region in the C-terminal region of Est1 substantially reduced the Est1-Est3 interaction (A), whereas other *sof* mutations in the C-terminal domain had no effect (B). (C) Est3 failed to associate with the RNA-binding-defective Est1-Y136D mutant protein, as assessed by Est1-Est3 co-IPs performed as in (A).

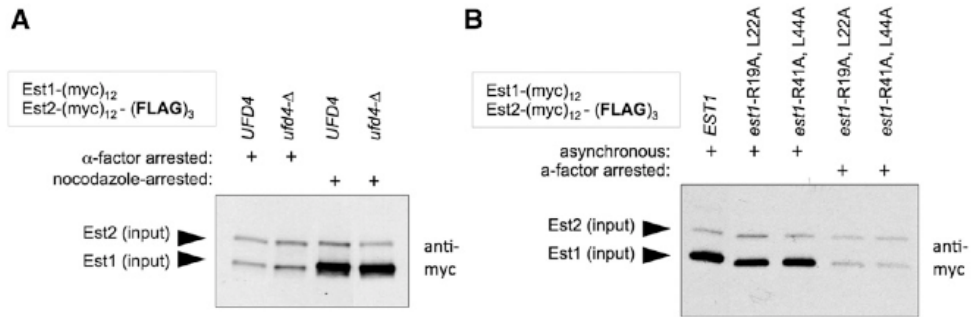


**Figure 3.5: An expanded interface on Est1 is required for binding to Cdc13.** (A) Association between Est1 and Cdc13, monitored by anti-FLAG IP, with Est1 and Cdc13 tagged with (myc)<sub>12</sub> and (FLAG)<sub>3</sub> epitopes, respectively, was abolished by mutations in adjacent residues (*est1-K444E* and *est1-R447E*). Consistent with prior observations (Tucey and Lundblad 2013), the *est1-K444E*-dependent loss of interaction with Cdc13 was restored when combined with the *cdc13-E252K* mutation (aka *cdc13-2*). (B) The Est1-Cdc13 association, assessed as in (A), was impaired by additional mutations in an ~10-amino acid span from 555 to 566 (since the *in vivo* defect displayed by the *est1-K559E* and *est1-W566D* single mutations was very modest, as shown in Figure 3.1F, these two mutations were combined). (C) The RNA-binding-defective Est1-W87E and Est1-Y136D proteins exhibited wild-type levels of association with Cdc13, as monitored by anti-FLAG IPs using the same protocol as in (A).

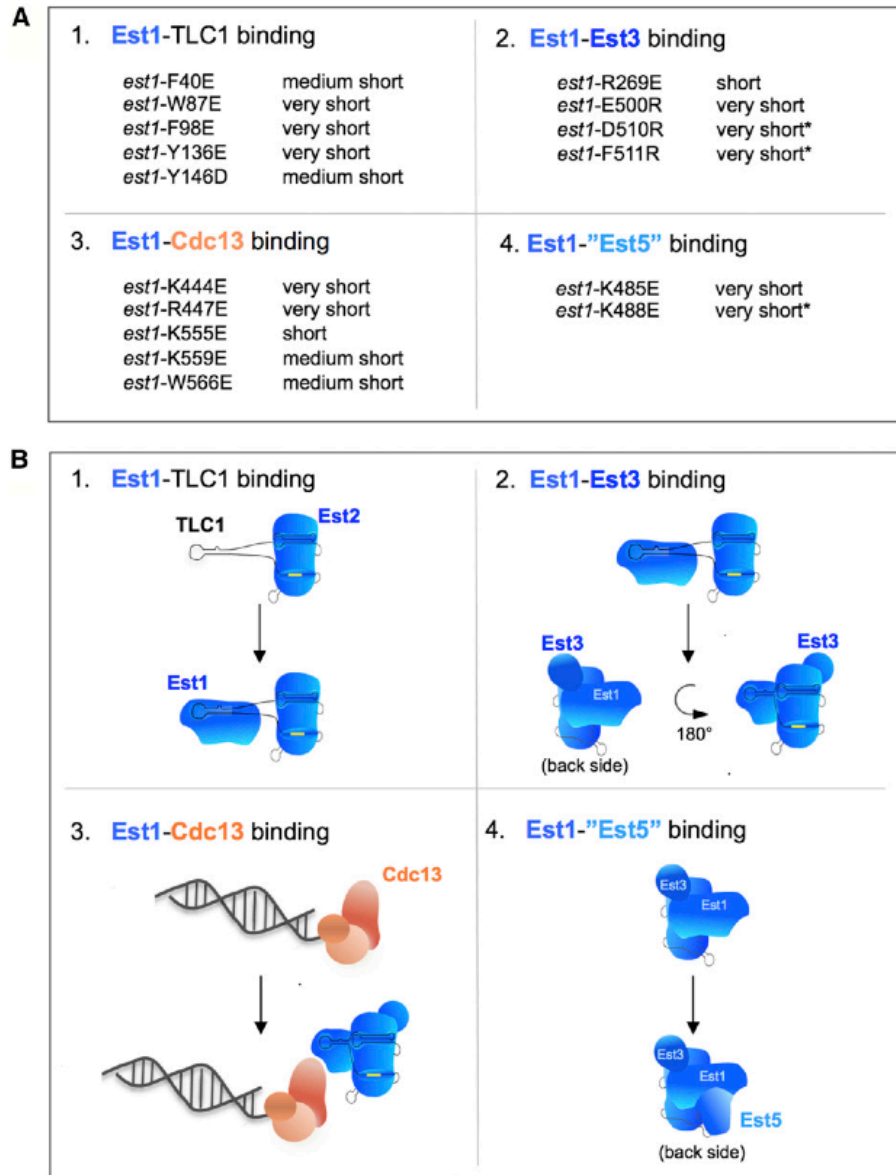




**Figure 3.6: Two mutations in the C-terminal domain of Est1 define a fourth novel function.** (A) The association between Est1 and Cdc13, monitored by anti-FLAG IP as in Figure 3.5A, is unaffected by the *est1-R485E* and *est1-R488E* mutations; an independent repeat of this experiment for *est1-R488E* is shown in Figure 3.S5. (B and C) Association between Est1 and Pop1 or Sme1 was monitored by anti-FLAG IP, with Est1 tagged with (myc)<sub>12</sub> and Pop1 or Sme1 tagged with (FLAG)<sub>3</sub> epitopes. Co-IP of Est1 with either the Pop complex (B) or the Sm complex (C) was abolished by the TLC1-binding-defective *est1-Y136D* mutation, but unaffected by the *est1-R485E* mutation.



**Figure 3.7: Reinvestigating the role of proteasomal degradation on Est1 protein levels.** (A) The steady-state levels of Est1 and Est2, from extracts of cells arrested either in G1 or G2/M and assayed by anti-myc westerns, are unaffected by the loss of UFD4, which has been proposed to target Est1 for degradation (Lin et al. 2015). (B) A similar analysis of Est1 and Est2 protein levels, assayed as in (A), does not reveal any changes in response to mutations in previously proposed Destruction boxes (Ferguson et al. 2013).



**Figure 3.8: A working model for Est1.** (A) A summary of the *sof<sup>-</sup>* mutations identified by either loss-of-function approaches (category 1) or overexpression dominant negative approaches (categories 2–4) and the effect of these mutations on telomere length and senescence (indicated by an asterisk). (B) A schematic depiction of the biochemical activity that is disrupted by each of the four categories of *sof<sup>-</sup>* mutations analyzed in this study. In panel 1, a simplified version of TLC1 is used to illustrate that Est1 and Est2 have independent binding sites on the telomerase RNA (Livengood et al. 2002); the template region of the RNA is indicated by a yellow box. The artistic rendition in panel 2 shows the association of Est3 with domains on both Est1 and Est2 to form the holoenzyme, accompanied by a proposed conformational change in the telomerase complex that is induced upon Est3 binding. Panels 3 and 4 show association of proteins encoded by known (*CDC13/EST4*) and proposed (*EST5*) essential genes; we currently have no information to assess whether the proposed fourth function in panel 4 occurs before (as shown) or after the telomerase recruitment depicted in panel 3.

## Supplemental Figures

**Figure 3.S1: Mutations in *EST1* that were examined for ODN and/or LOF phenotypes.** (A) Schematic representation of ODN and/or LOF phenotypes resulting from mutations in individual amino acids, as indicated on the Est1 protein sequence. Examples of ODN phenotypes are shown in Figure 3.1A – 1C and Supplemental Figure 3.S1C, 3.S1D and 3.S2, and examples of LOF phenotypes are shown in Figure 3.1D – 1G and Supplemental Figure 3.S1D and 3.S3. Mutations that failed to show a phenotype are indicated by a black arrow; mutations that conferred a phenotype are indicated by arrows in a range of sizes to indicate the severity of the phenotype. Brown arrows highlight those allele where the LOF phenotype was more severe than the ODN phenotype (see also Supplemental Figure 3.S1B and 3.S1C); blue arrows correspond to the five mutations that are impaired for binding to TLC1. (B) Assessment of Est1 protein levels, for mutant Est1 proteins that exhibited LOF phenotypes that were more severe than the corresponding ODN phenotypes (ODN and LOF data for these alleles are shown in Supplemental Figure 3.S1C, 3.S1D and 3.S3K). Mutant Est1 protein levels were reduced to ~25 to 30%, relative to wild type Est1, for the Est1-R291E and Est1-F408D proteins, and 2-fold for Est1-W442D; protein levels were assayed in strains in which each mutation was integrated into the genome, to avoid plasmid-dependent variations in Est1 protein levels, and the anti-myc signal for Est1- myc<sub>12</sub>, was normalized to myc<sub>12</sub>-Est2. The Est1-42 mutant protein, with amino acid changes (D287A, E290A, R291A, R292A) that partially overlapped with Est1-R291E, also showed a 4-fold reduction in protein levels. Genetic analysis of the *est1-42* mutation was previously used to argue that this mutation was specifically impaired for the so-called “second function” of Est1 (Evans and Lundblad 2002); however, the results shown here argue that this “second function” phenotype was instead most likely due to reduced protein stability, rather than loss of a specific biochemical activity. A similar caveat applies to the interpretation of the in vivo role of Arg291 from a different study (Hawkins and Friedman 2014). (C) Examples of mutations that exhibit weak ODN phenotypes in the *yku80-Δ* synthetic lethal assay (relative to the magnitude of the corresponding LOF phenotype). A *yku80-Δ* / p *CEN URA3 YKU80* strain was transformed with 2 μ plasmids containing the indicated *est1*<sup>-</sup> mutation, which was expressed by the constitutive ADH promoter; serial dilutions of two independent transformants for each mutation were examined for viability on media that selected for the presence or loss of the *YKU80* plasmid. The temperature- dependence of this synthetic growth phenotype provides a sensitive assay for detecting a broad range of ODN phenotypes, as previously described (Lee *et al.* 2008) and as illustrated by the *est1*-D513R mutation; this mutation confers an LOF phenotype that was indistinguishable from that conferred by *est1*-D510R and *est1*-F511D (Figure 3.1E and data not shown), but an ODN phenotype that was reproducibly less pronounced, relative to that of *est1*-D510R and *est1*-F511D. (D) Telomere length analysis in ODN and LOF assays, for six mutations that exhibit an attenuated ODN phenotype when compared with the corresponding LOF phenotype; *est1*-K444E and *est1*-R488E, which exhibit comparably strong ODN and LOF phenotypes, were included for comparison. ODN or LOF effects on telomere length (the top three panels and the bottom three panels, respectively) were assayed as described in Figure 3.1.

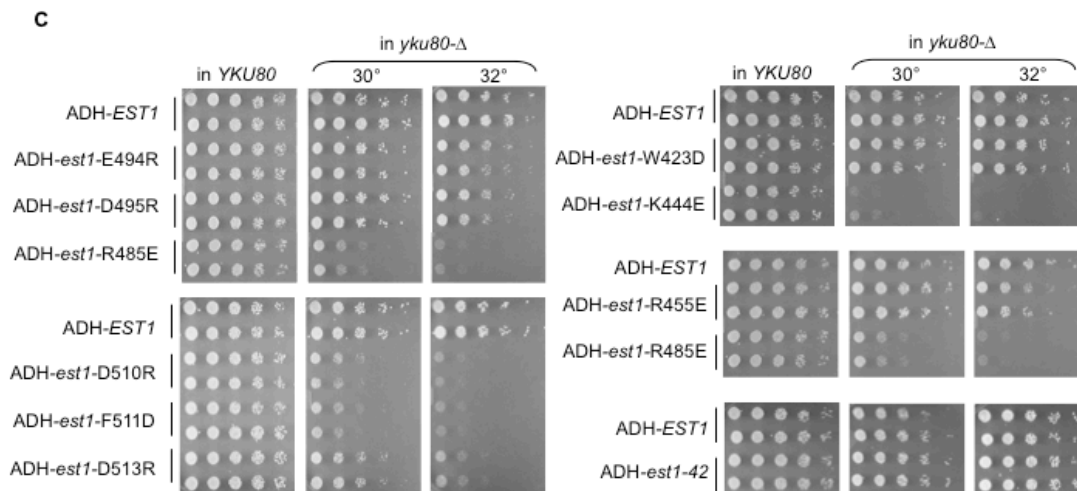
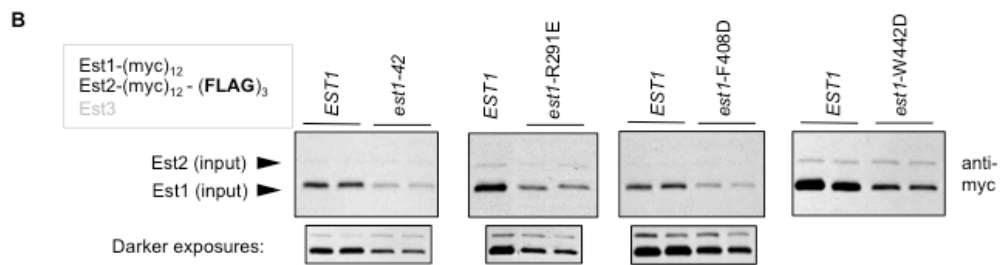


**A (continued)** Lubin et al.

ODN: 541 ECVLRIRSI I FSGMKFLEKN DTGVIWNASK YKFDLISPNI KIKRQIALSE ISSKINVKTQ  
 LOF: ↑ ↑ ↑ ↑ ↑ ↑ ↑ ↑ ↑ ↑

ODN: 601 QERVVSSRKV EAKRDEQQRK RAGKIAVTEL EKQFANVVRT KKLSPLEPKD GVSSELVKHA  
 LOF: ↑ ↑ ↑ ↑ ↑ ↑ ↑ ↑ ↑ ↑

ODN: 661 ASRGRKTITG PLSSDFLSYP DEAIDAEDEI TVQVPDTPT  
 LOF: ↑ ↑ ↑ ↑



**Figure 3.S1: Mutations in *EST1* that were examined for ODN and/or LOF phenotypes (continued).**

D

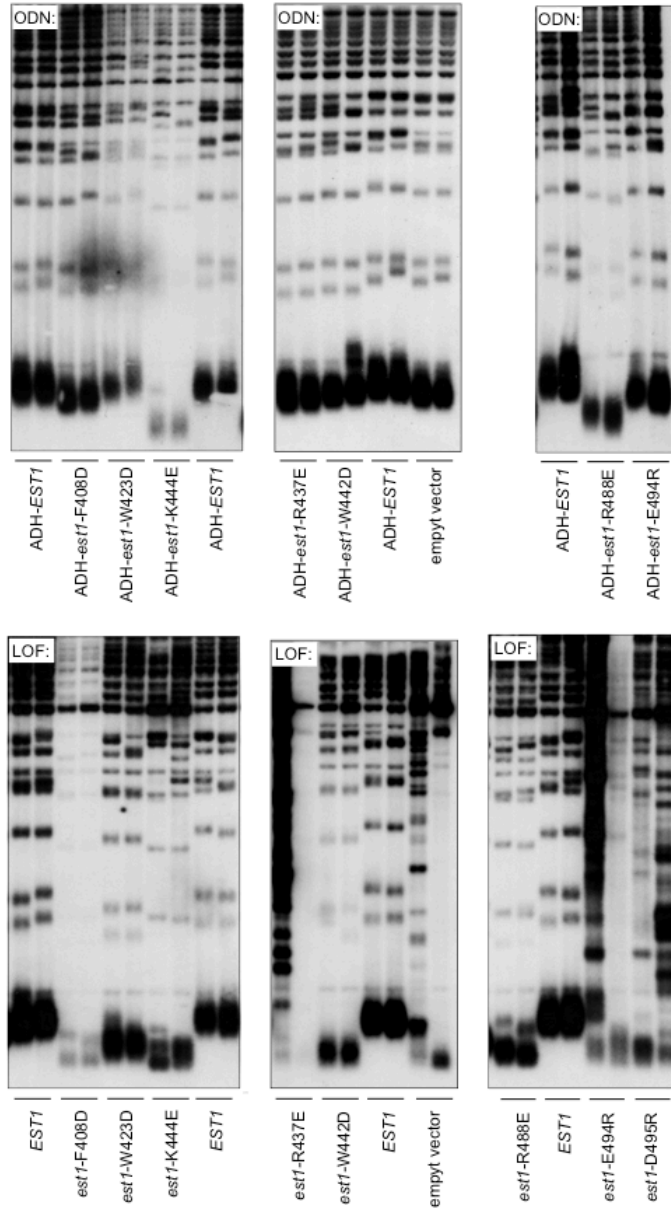
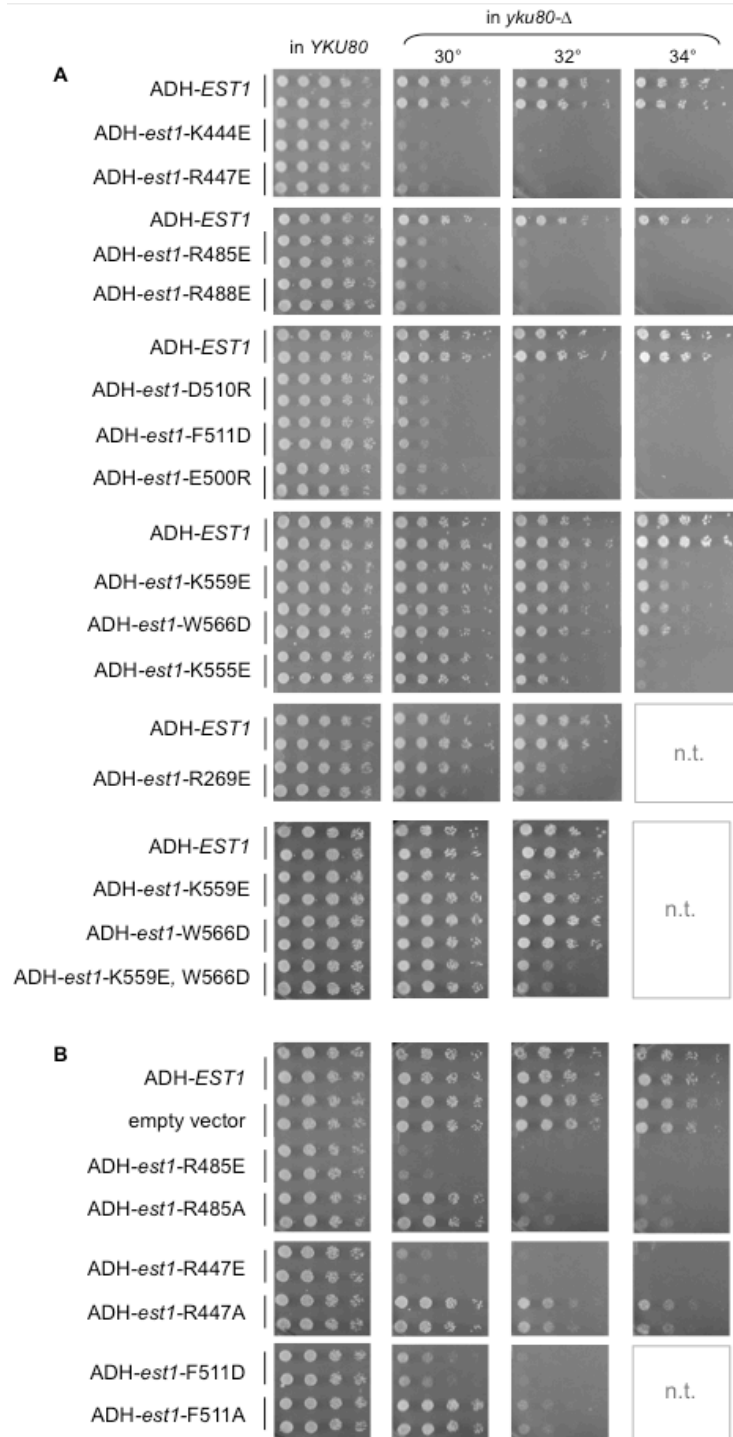


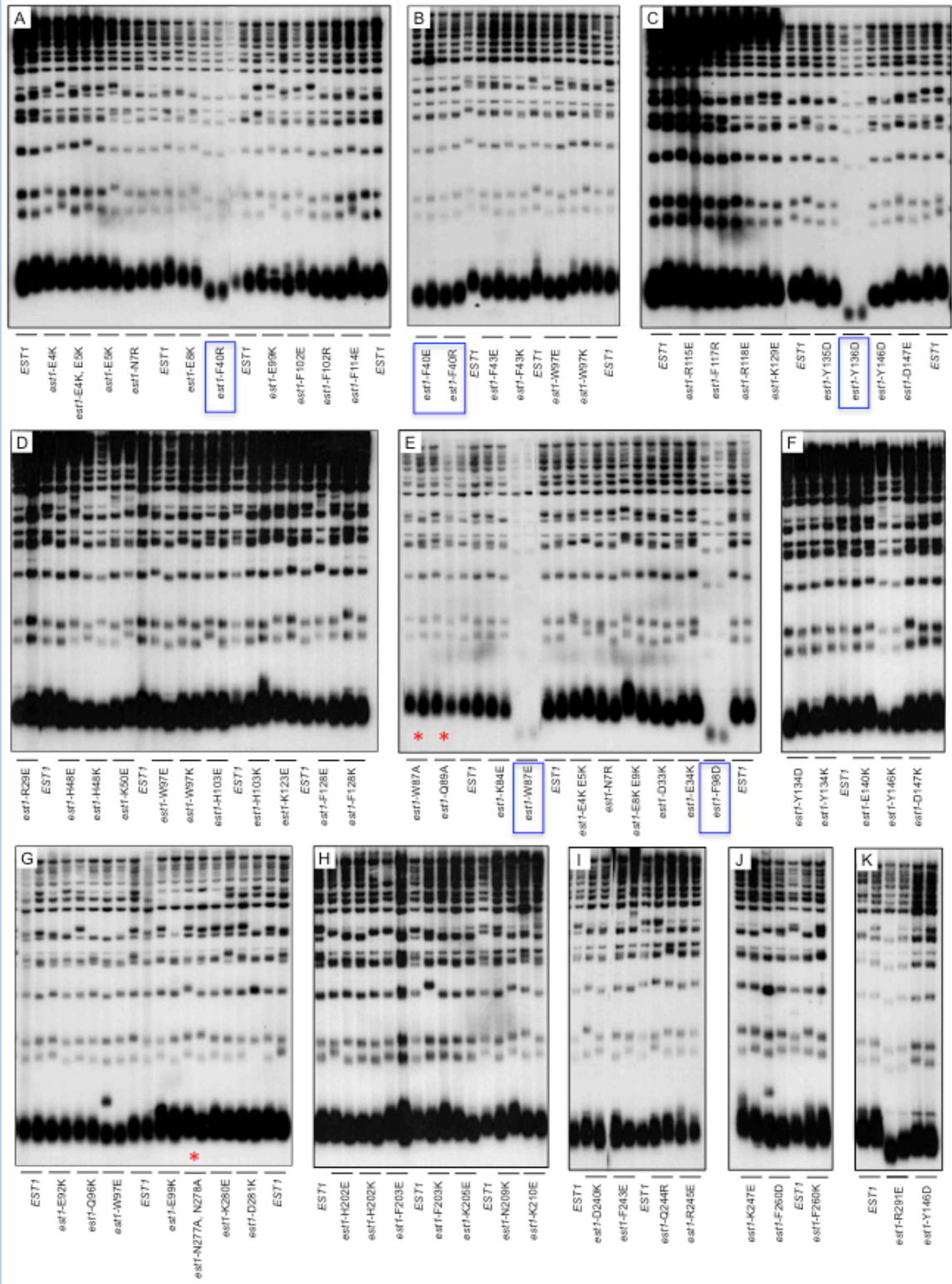
Figure 3.S1: Mutations in *EST1* that were examined for ODN and/or LOF phenotypes (continued).



**Figure 3.S2: ODN phenotypes of 11 separation-of-function mutations in *EST1*.** (A) ODN phenotypes in a *yku80*- $\Delta$  strain of the 11 separation-of-function *est1*<sup>-</sup> mutations shown in Figure 3.1, assayed as described in Supplemental Figure 3.S1C. (B) Examples of three Est1 amino acids (Arg447, Arg485 or Phe511) that exhibited a pronounced ODN phenotype when mutated to a charged residue, but a much less severe ODN phenotype when mutated to alanine, consistent with our prior observations (Lubin et al. 2013).



**Figure 3.S3: Loss-of-function analysis of telomere length for an extensive panel of *est1*<sup>-</sup> mutations.** Telomere length of *est1*-Δ strains transformed with single copy plasmids with the indicated *est1*<sup>-</sup> mutations, expressed by the *EST1* promoter, determined after ~75 generations of growth following transformation of the *est1*-Δ strain. Mutations that are boxed (panels A – E) are defective for RNA binding, as shown in Fig. 3.3. Mutations indicated by a red asterisk (panels E, G, P and Q) conferred a wild type telomere length phenotype, in contrast to what was observed in previous reports (Zhang *et al.* 2010; Tong *et al.* 2011; Sealey *et al.* 2011). Mutations with a blue asterisk (panel P) correspond to a cluster of residues proposed to mediate nuclear localization (Hawkins and Friedman 2014); we propose instead that the mutant phenotype more likely due to protein destabilization, based on the very weak ODN phenotype of *est1*-K455E (see Supplemental Figure 3.S1C), relative to the more pronounced LOF phenotype for this mutation.



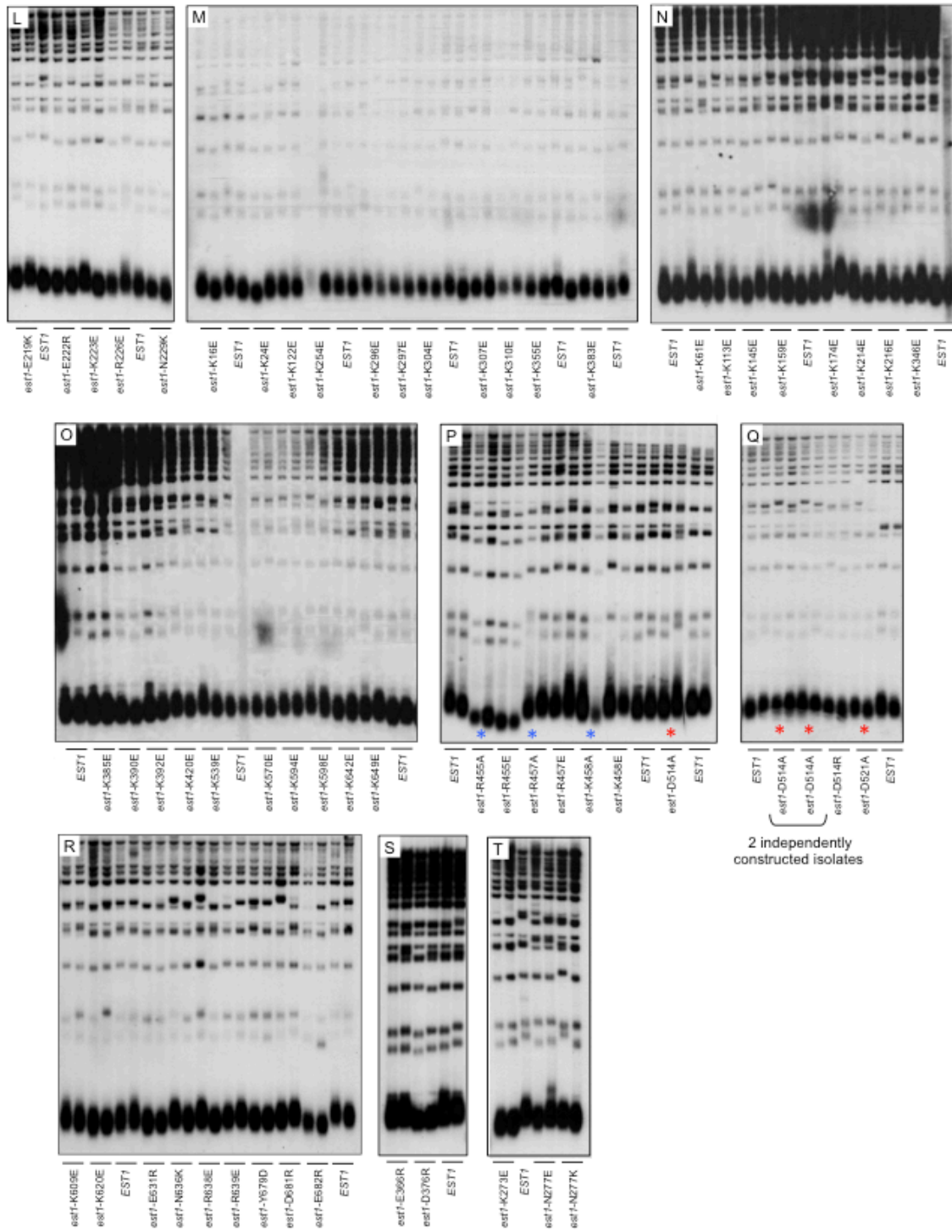
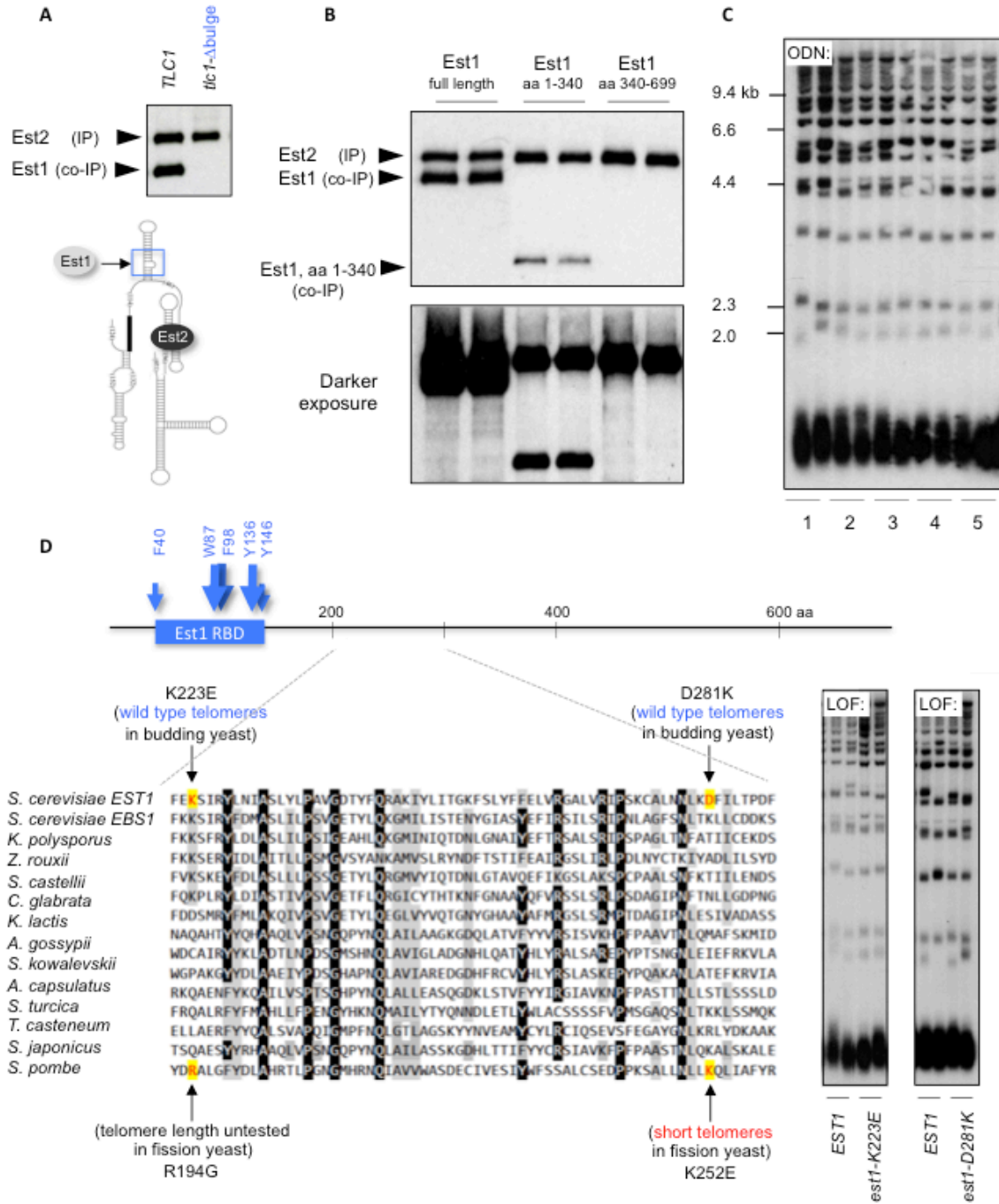
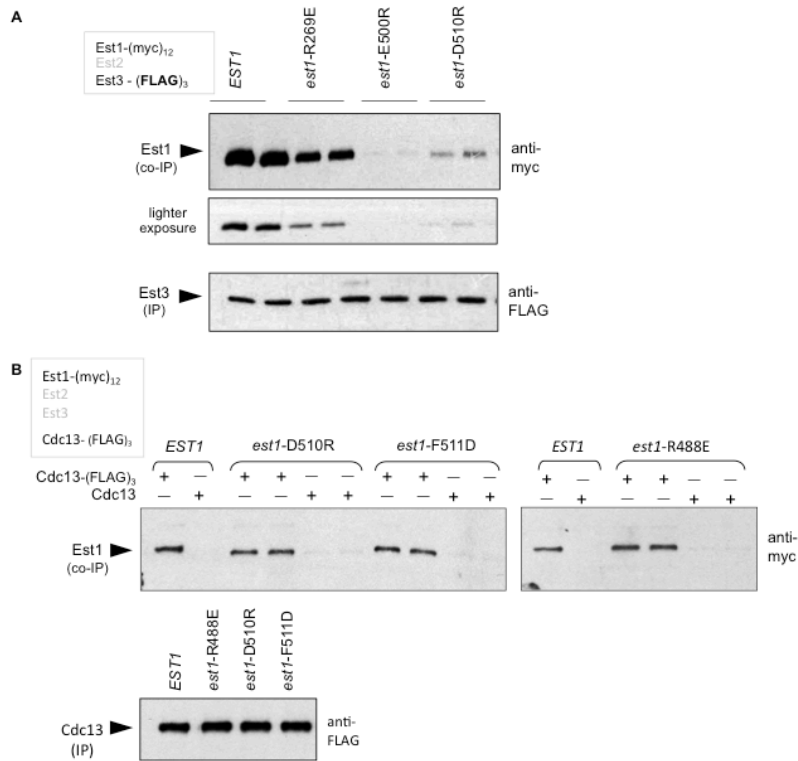


Figure 3.S3: Loss-of-function analysis of telomere length for an extensive panel of *est1*<sup>-</sup> mutations (continued).

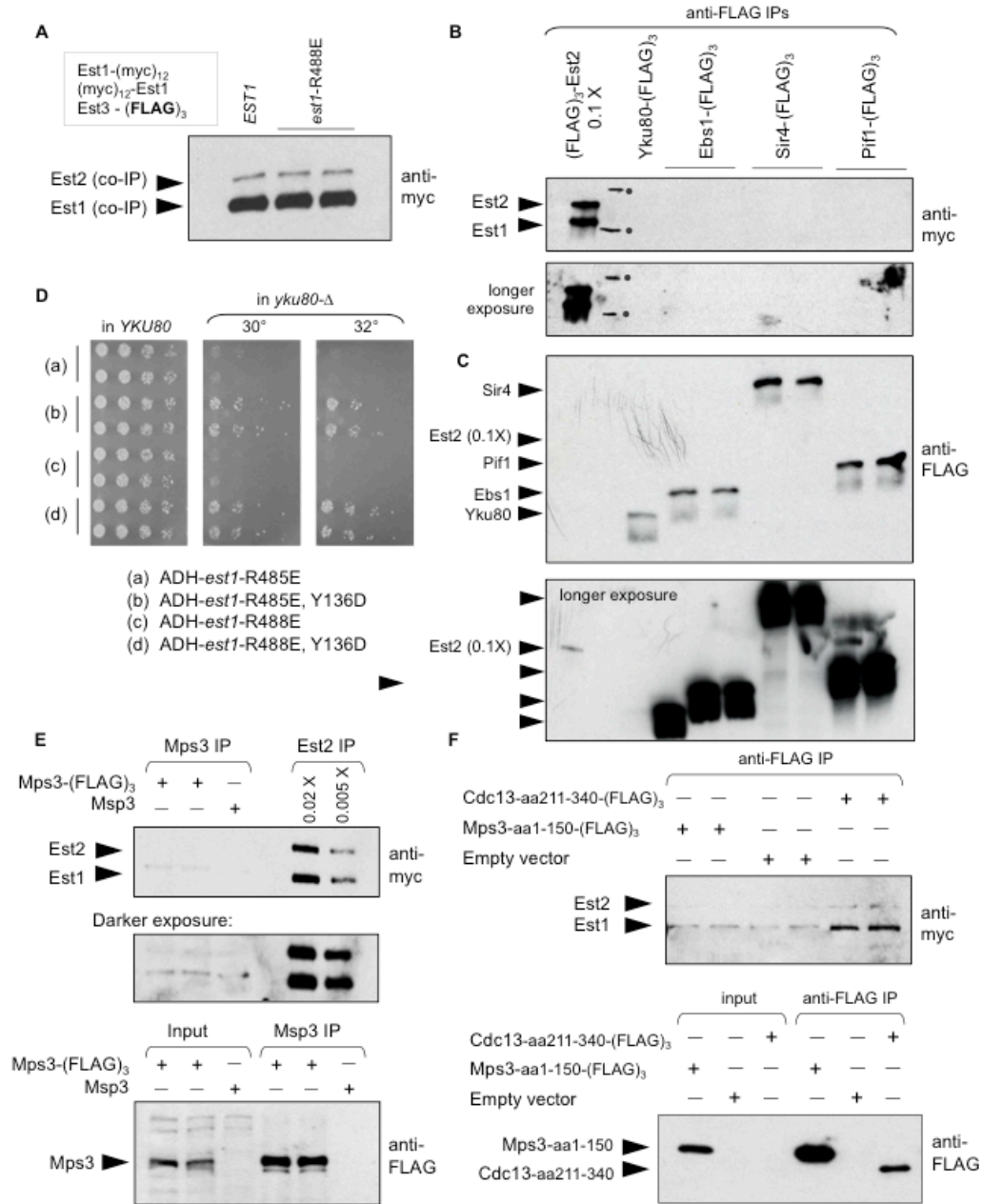
**Figure 3.S4: Additional analysis of the RNA binding domain of Est1.** (A) Est1 fails to co-IP with Est2 in a strain bearing a mutation in the 5-nucleotide bulge of TLC1 (indicated by the blue box in the cartoon image), which has been previously shown to be required for the Est1-TLC1 interaction (Seto *et al.* 2002). (B) A darker exposure of the image shown in Figure 3.3A, providing further support for the inability of the C-terminal domain of Est1 to form a complex with TLC1 and Est2. (C) Over-expression of RNA-binding-defective *est1* mutations in a wild type yeast strain did not confer an ODN phenotype on telomere length, assayed as described in Figure 3.1. Lanes 1-2, *ADH-EST1*; lanes 3-4, *ADH-est1-W87E*; lanes 5-6, *ADH-est1-Y136D*; lanes 7-8, *ADH-est1-F98D*; lanes 9-10, *ADH-est1-Y146D*. The *est1-F40E* mutation (not included here) failed to show an ODN phenotype in the *yku80-Δ* strain (data not shown). (D) The position of the Est1 RBD identified in this study (indicated by a blue box on the schematic figure of Est1) contradicts a previous report, which relied on a three-hybrid approach to identify a different region of the fission yeast Est1 protein that bound the telomerase RNA (Webb and Zakian 2012. Two of the fission yeast residues implicated in this previously proposed fission yeast RNA binding activity (R194 and K252, highlighted in yellow) are poorly conserved, as shown by an alignment of Est1 proteins from budding and fission yeasts from this region. In addition, mutations in the equivalent residues (K223 and D281) in *S. cerevisiae* resulted in a wild type telomere length (right hand panel), further suggesting that these fission yeast residues do not define a conserved function. A third fission yeast residue (L48) identified in this prior study was in a region of the fission yeast Est1 protein with very limited sequence conservation, which precluded identification of the comparable residue for *in vivo* analysis in *S. cerevisiae*. In contrast, key residues in the Est1 RBD identified in this study are highly conserved from budding yeast to fission yeast (Fig. 3.3D).





**Figure 3.S5: Additional analysis of Est3-binding-defective alleles of *EST1*.** (A) Comparing the effect of three mutations on the association between Est1 and Est3, tagged with (myc)<sub>12</sub> and (FLAG)<sub>3</sub> epitopes, respectively, following anti-FLAG immunoprecipitation. (B) Association between Est1 and Cdc13 (monitored by anti-FLAG immunoprecipitation with Est1 and Cdc13 tagged with (myc)<sub>12</sub> and (FLAG)<sub>3</sub> epitopes, respectively) was unaffected by *est1*-D510R, *est1*-F111D or *est1*-R488E mutations.

**Figure 3.S6: Additional analysis of the fourth function of Est1.** (A) Anti-FLAG IPs, with the (FLAG)<sub>3</sub> epitope on Est3, reveals an altered Est1:Est2 ratio, which we have previously argued is due to a telomerase disassembly complex (Tucey and Lundblad 2014); this ratio is not disrupted in IPs from the *est1*-R488E strain, demonstrating that the disassembly pathway is not altered by this mutation. (B and C) Anti-FLAG IPs from strains with (FLAG)<sub>3</sub> epitopes on Est2, Yku80, Ebs1, Sir4 or Pif1; Est1 and Est2 were tagged with (myc)<sub>12</sub> in all five strains. The amount of anti- Est2 IP was 0.1X of the amount loaded in the other lanes. (B) Est1 association with Est2 was clearly detected in the anti-Est2 IP lane, whereas following anti-FLAG IP of Yku80, Ebs1, Sir4 or Pif1, no association of these four proteins with either Est1 or Est2 could be detected, even in a substantially darker exposure of the anti-myc western. The hand-drawn marks on the anti-myc westerns (indicated by dots) correspond to pre-stained 100 and 150 kDa size markers (visualized on the membrane after transfer). (C) Anti-FLAG westerns show that the (FLAG)<sub>3</sub>-tagged versions of Yku80, Ebs1, Sir4 or Pif1 were readily detectable in the anti-FLAG IPs, relative to the 10-fold reduction Est2 signal. (D) The ODN phenotypes of *est1*-R485E and *est1*-R488E, as assayed by the *yku80*-Δ synthetic lethal assay, were reversed by the presence of the TLC1-binding-defective *est1*-Y136D mutation. (E) A re-examination of the previously proposed interaction between Mps3 and Est1 (Antoniacci *et al.* 2007; Schober *et al.* 2009); anti-FLAG IP were performed as described for part (C), above, with a strain containing a (FLAG)<sub>3</sub> epitope on Mps3 and (myc)<sub>12</sub> epitopes on Est1 and Est2. As a control, 0.02X and 0.005X amounts of an anti-FLAG IP from a strain with the (FLAG)<sub>3</sub> epitope was on Est2 were included. (F) Because Mps3 is a nuclear envelope integral protein (and thus potentially difficult to assay in immunoprecipitations), we examined the interaction between Est1 and the soluble N-terminal domain of Mps3 (aa 1-150) (Bupp *et al.* 2007), which was tagged with (FLAG)<sub>3</sub> and over-expressed by the ADH promoter on a high copy plasmid. Even though the Mps3 N-terminal domain was efficiently expressed, an Est1-Mps3 interaction could not be detected in anti-FLAG IPs. In contrast, association between Est1 and the 130 amino acid recruitment domain of Cdc13 could be readily detected. Based on the results in parts (D) and (E), we conclude that Mps3 does not exhibit a detectable interaction with either Est1 or Est2.





**Table 3.1: Yeast Strains used in this chapter.**

<b>Strain</b>	<b>Genotype</b>
YVL2967	<i>MATa ura3-52 lys2-801 trp1-Δ1 hist3-Δ200 leu2-Δ1</i>
YVL3814	<i>MATa est1-Δ / p CEN URA3 EST1 ura3-52 lys2-801 trp1-Δ1 hist3-Δ200 leu2-Δ1</i>
YVL3142	<i>MATa yku80-Δ / p CEN URA3 YKU80 ura3-52 lys2-801 trp1-Δ1 hist3-Δ200 leu2-Δ1</i>
YVL3528*	<i>MATa EST1-(Gly)6-(myc)12 (FLAG)3-(myc)12-(Gly)6-EST2</i>
YVL3692*	<i>MATa est1-(aa 1-340)-(Gly)6-(myc)12 (FLAG)3-(myc)12-(Gly)6-EST2</i>
YVL3830*	<i>MATa est1-(aa 340-699)-(Gly)6-(myc)12 (FLAG)3-(myc)12-(Gly)6-EST2</i>
YVL4311*	<i>MATa est1-F40R-(Gly)6-(myc)12 (FLAG)3-(myc)12-(Gly)6-EST2</i>
YVL4222*	<i>MATa est1-W87E-(Gly)6-(myc)12 (FLAG)3-(myc)12-(Gly)6-EST2</i>
YVL4132*	<i>MATa est1-F98D-(Gly)6-(myc)12 (FLAG)3-(myc)12-(Gly)6-EST2</i>
YVL3896*	<i>MATa est1-Y136D-(Gly)6-(myc)12 CDC13-(FLAG)3</i>
YVL3898*	<i>MATa est1-Y146D-(Gly)6-(myc)12 CDC13-(FLAG)3</i>
YVL3979*	<i>MATa EST1-(Gly)6-(myc)12 CDC13-(FLAG)3</i>
YVL4553*	<i>MATa est1-W87E-(Gly)6-(myc)12 CDC13-(FLAG)3</i>
YVL4551*	<i>MATa est1-Y136D-(Gly)6-(myc)12 CDC13-(FLAG)3</i>
YVL4348*	<i>MATa EST1-(Gly)6-(myc)12 EST3-(FLAG)3</i>
YVL3813*	<i>MATa EST1-(Gly)6-(myc)12 (myc)12-(Gly)6-EST2 EST3-(FLAG)3</i>
YVL4025*	<i>MATa est1-Y136D-(Gly)6-(myc)12 (myc)12-(Gly)6-EST2 EST3-(FLAG)3</i>
YVL3803*	<i>MATa EST1-(Gly)6-(myc)12 (myc)12-(Gly)6-EST2</i>
YVL3903*	<i>MATa EST1-(Gly)6-(myc)12 (myc)12-(Gly)6-EST2</i>
YVL3904*	<i>MATa EST1-(Gly)6-(myc)12 (myc)12-(Gly)6-EST2</i>
YVL3905*	<i>MATa EST1-(Gly)6-(myc)12 (myc)12-(Gly)6-EST2</i>
YVL3906*	<i>MATa EST1-(Gly)6-(myc)12 (myc)12-(Gly)6-EST2</i>
YVL4026*	<i>MATa EST1-(Gly)6-(myc)12 (myc)12-(Gly)6-EST2</i>
YVL5518*	<i>MATa EST1-(Gly)6-(myc)12 POPI-(FLAG)3</i>
YVL5529*	<i>MATa est1-Y136D-(Gly)6-(myc)12 POPI-(FLAG)3</i>
YVL5520*	<i>MATa est1-R485E-(Gly)6-(myc)12 POPI-(FLAG)3</i>
YVL5519*	<i>MATa EST1-(Gly)6-(myc)12 SME1-(FLAG)3</i>
YVL5531*	<i>MATa est1-Y136D-(Gly)6-(myc)12 POPI-(FLAG)3</i>
YVL5521*	<i>MATa est1-R485E-(Gly)6-(myc)12 POPI-(FLAG)3</i>

\* *leu2 trp1 ura3-52 prb<sup>-</sup> prc<sup>-</sup> pep4-3 bar1-Δ::KAN*

**Table 3.1: Yeast Strains used in this chapter (continued).**

<b>wild type parent:</b>	<b>YVL3528</b>	<b>YVL3979</b>	<b>YVL4348</b>
<i>estl</i> -K444E	YVL4745	YVL4301	n.a.
<i>estl</i> -R447E	YVL4747	YVL4340	n.a.
<i>estl</i> -R485E	YVL4396	YVL4303	YVL4382
<i>estl</i> -R488E	YVL4398	YVL4325	YVL4384
<i>estl</i> -E500R	YVL4749	YVL4305	YVL5039
<i>estl</i> -D510R	YVL4402	YVL4307	YVL4974
<i>estl</i> -F511D	YVL4404	YVL4344	YVL4975
<i>estl</i> -R269E	YVL4394	n.a.	YVL4555
<i>estl</i> -K555E	YVL5480	YVL4309	n.a.
<i>estl</i> -K559E, W566D	YVL5477	YVL4342	n.a.

**Table 3.2: Plasmids used in this chapter.**

<b>Plasmid</b>	<b>Description</b>	<b>Vector backbone</b>
pVL367	<i>CEN URA3 EST1</i>	YCplac 33
pVL809	2 $\mu$ <i>HIS3 ADH-EST1</i>	pRS423
pVL5187	<i>URA3 EST1</i> -(Gly)6-(myc)12	YIplac211
pVL6685	2 $\mu$ <i>TRP1 ADH-CDC13</i> -aa211-340-(FLAG)3	YEplac112
pVL6732	2 $\mu$ <i>TRP1 ADH-MPS3</i> -aa1-150-(FLAG)3	YEplac112

<b>wild type parent:</b>	<b>pVL367</b>	<b>pVL809</b>	<b>pVL5187</b>
<i>est1</i> -F40E	pVL7343	pVL7759	pVL6889
<i>est1</i> -W87E	pVL6793	pVL7399	pVL6636
<i>est1</i> -F98D	pVL6794	pVL4681	pVL6071
<i>est1</i> -Y136D	pVL6803	pVL7356	pVL6072
<i>est1</i> -Y146D	pVL6804	pVL4688	pVL6073
<i>est1</i> -K444E	pVL6478	pVL4534	pVL5236
<i>est1</i> -R447E	pVL6479	pVL4512	pVL6686
<i>est1</i> -R485E	pVL6481	pVL4517	pVL6687
<i>est1</i> -R488E	pVL6482	pVL4519	pVL6688
<i>est1</i> -E500R	pVL6485	pVL4826	pVL6689
<i>est1</i> -D510R	pVL6486	pVL4525	pVL6691
<i>est1</i> -F511D	pVL6487	pVL6473	pVL6690
<i>est1</i> -R269E	pVL6820	pVL4607	pVL6882
<i>est1</i> -K555E	pVL6490	pVL4612	pVL6692
<i>est1</i> -K559E, W566D	pVL7761	pVL4695	pVL6807

## Materials and Methods

### *Genetic analysis*

The full list of strains and plasmids used in this study are described in Supplemental Material, Tables 3.1 and 3.2, respectively. Standard genetic and molecular methods were used to introduce plasmids into yeast, introduce missense mutations into the *EST1* gene, and assess synthetic lethality in the *yku80-Δ* strain, as previously described (Lendvay et al. 1996; Lee et al. 2008; Lubin et al. 2013). Telomere length was assessed from two independent single colonies that were propagated for ~75 generations, following transformation into either a wild-type yeast strain (for ODN assays) or an *est1-Δ* strain freshly generated by shuffling off a covering plasmid (for LOF assays).

### *Biochemical analysis*

For all of the biochemical experiments described in this study, mutations were integrated into the genome in place of the wild-type gene, as previously described (Paschini et al. 2012; Tucey and Lundblad 2014). This eliminates the possibility that effects on immunoprecipitation (IP) efficiency were due to incomplete gene expression by plasmid-borne alleles (as a consequence of either variations in plasmid copy number and/or incomplete promoters). Strains expressing integrated copies of both the wild-type *EST1* gene and mutant *est1 sof<sup>+</sup>* alleles exhibited a healthy (i.e., nonsenescent) growth phenotype; PCR analysis was used to confirm that each mutant allele was integrated without unanticipated genomic rearrangements. Subsequent isolates that had lost the wild-type *EST1* gene and retained only the mutant *est1<sup>-</sup>* allele (following propagation on 5-FOA) were confirmed by molecular analysis (by sequencing across the integrated

mutant allele), as well as phenotypic analysis (telomere length and/or senescence), for every constructed strain. Whole- cell extracts were prepared from two independent 250 ml cultures (OD 0.8–0.9) for each genotype and processed in parallel. Cells were pelleted, washed in TMG200 (10 mM Tris-HCl pH 8, 1 mM MgCl<sub>2</sub>, 5% glycerol, and 200 mM NaCl<sub>2</sub>) + protease inhibitors + 0.1% Tween20, and resuspended in 1 ml of the same buffer. Extracts were prepared by grinding this 1-ml suspension in a mortar in the presence of liquid N<sub>2</sub> until the suspension formed a fine powder. Extracts were clarified by three 10 min spins at 4 at 25,000 3 g, and supernatants were immediately subjected to IP by incubation with anti-Flag M2 affinity gel (Sigma [Sigma Chemical], St. Louis, MO), in TMG200 + protease inhibitors + 0.1% Tween20 for 2 hr at 4, with gentle rocking. Beads were washed 3X in the same buffer, and eluted for 4 min at 95 with TMG200 + 0.1% Tween20 equilibrated with SDS loading buffer + 0.7% β-mercaptoethanol. Immunoprecipitated proteins were resolved on 6% (for detection of Est1, Est2, or Pop1) or 12% (for detection of Est3 or Sme1) SDS-PAGE and probed with anti-myc 2272 (Cell Signaling Technology) at 1:1000 or anti-Flag F7425 (Sigma) at 1:10,000 dilution, followed by anti-rabbit IgG HRP conjugate (Promega, Madison, WI) at 1:10,000, and subsequent enhanced chemiluminescence (ECL) detection using preflashed film. ECL was used rather than alternative options (such as Li-cor Odyssey) due to substantially less background and a significantly higher signal-to-noise ratio; we previously demonstrated that this protocol can detect as little as twofold differences with high reproducibility over a 10-fold detection range (Tucey and Lundblad 2013).

### *Data availability*

The authors state that all data necessary for confirming the conclusions presented in the article are represented fully within the article.

### **Acknowledgments**

We thank members of the Lundblad laboratory, both past and present, for many useful suggestions during the course of this study. This work was supported by National Institutes of Health grants R01 AG-11728 (to V.L.), T32 GM-007240 (to T.M.T. and J.W.L.), and P30 CA-014195 (to the Salk Institute Cancer Center), a Rose Hills Foundation Fellowship (to T.M.T.), a Graduate Fellowship from the Glenn Center for Aging Research at the Salk Institute (to J.W.L.), and a National Science Foundation Graduate Research Fellowship DGE-1650112 (to J.W.L.).

Chapter 3 is a formatted reprint of the material as it appears in Lubin, J.W., Tucey, T.M., Lundblad, V. Using separation-of-function mutagenesis to define the full spectrum of activities performed by the Est1 telomerase subunit *in Vivo*. *Genetics* 208: 97-110 (2018). The dissertation author was the co-primary investigator and author of this paper.

## **CHAPTER FOUR:**

Over-expression dominant negative site-directed mutagenesis identifies a fifth *EST* gene

The over-expression dominant negative assay (ODN) proved extremely valuable in identifying the functionally important residues on the surface of telomerase, but I wanted to determine if ODN could also be useful if applied to other protein complexes, specifically essential genes involved in DNA replication and repair. Under my supervision, a group of undergraduate students mutagenized a large panel of essential genes (~15) involved in various aspects of DNA metabolism. They screened these mutations in a set of strains sensitized to defects in DNA replication, as well as for defects in telomere length maintenance. Identification of this gene marks the discovery of the fifth *EST* gene (*CDC13* being the fourth), potentially providing an alternative therapeutic pathway not previously considered for telomere related diseases. This chapter reports on the analysis of *EST5*.

Chapter 4 contains unpublished material. Margherita Paschini contributed Figure 4.2B. The dissertation author was the primary investigator and author of this chapter.



## Introduction

### *Discovery of the EST genes*

The Est (ever-shorter telomeres) phenotype is characterized by mutations in the telomerase pathway that give rise to progressively shorter telomeres upon cellular propagation, which eventually leads to senescence. *EST1* was first identified thirty years ago (Lundblad and Szostak 1989) by whole-genome mutagenesis screening, and a subsequent forward mutagenesis screen uncovered three additional *EST* genes – *EST2*, *EST3*, and *EST4* (which turned out to be the mutation in *CDC13* that abolished the Est1-Cdc13 interaction; (Lendvay et al. 1996). Several years later, a screen of the 4200 non-essential yeast gene deletion set revealed that the only genes with an Est phenotype were *EST1*, *EST2*, and *EST3* (Askree et al. 2004). However, the possibility still remained that there were additional essential genes, like *CDC13*, that contain *EST* alleles. Identifying those alleles will provide a great understanding of telomerase regulation, just as the discovery of *EST4* (by identification of *cdc13-2*) led to the discovery of telomerase recruitment through the Cdc13-Est1 interaction.

By targeting conserved, charged residues of essential genes, using over-expression dominant negative (ODN) mutagenesis, we were able to identify *EST5*, the first discovery of an *EST* gene in over two decades, and a novel regulatory pathway of telomerase.

## Results

### *ODN mutagenesis identifies residues on the surface of an essential DNA replication gene involved in telomere length regulation*

To identify residues on the surface of essential proteins involved in DNA replication, recombination, and repair that may also contribute to telomere length regulation, we employed an over-expression dominant negative (ODN) strategy previously shown to be able to identify mutations on the surface of properly folded proteins (Lubin et al. 2013; Rao et al. 2014). In this assay, mutations were screened for their ability to disrupt telomere length regulation, when over-expressed, in the presence of wild-type copy of the gene. Under my supervision, Jocelyn Ramirez, a summer student, introduced 111 missense mutations by reverse mutagenesis into essential genes that encode a protein complex. The mutations were expressed on high-copy plasmids with a constitutive ADH promoter and were chosen based on conservation among 14 different yeast species, with an emphasis placed on charged and aromatic residues, as previously described (Lubin et al. 2013; Chapter 3). Each mutant plasmid was transformed into a *yku80-Δ / p CEN URA3 YKU80* strain and assessed for cellular growth following the loss of the *YKU80* plasmid. We have previously demonstrated that increasing expression of telomerase mutations in this strain causes a loss of viability comparable to the telomere length defect (i.e. the greater the loss of viability, the shorter the telomeres) (Lee et al. 2008; Lubin et al. 2013; Chapter 3). However, because over-expression of *CDC13* is lethal to the cell, we have only been able to observe this phenotypic correlation with mutations on the surface of telomerase itself. Surprisingly, though, this process identified three mutations in one subunit of a protein complex

(subsequently referred to as *EST5*) that, when over-expressed in a *yku80-Δ* strain, had reduced viability at increased temperature (Figure 5.1a) when compared to either wild-type *EST5* or plasmid lacking a gene.

This severe reduction in growth at 32°C is the same phenotype observed in *est*<sup>-</sup> mutations, so I next wanted to verify the telomere length of these *est5*<sup>-</sup> mutations. To do so, I transformed the three over-expression mutant plasmids into wild-type yeast, propagated for ~75 generations, and assessed telomere length by southern blot analysis (Figure 5.1b). When compared to the over-expression of the wild-type copy of the gene, these mutations displayed a significant reduction in telomere length. One mutation, *est5-1*, showed remarkably short telomeres, comparable to that observed in the most severe telomerase mutants (i.e. *est1-60*).

Interestingly, all three of the *EST5* ODN mutations cluster within a 14 amino acid region. Additionally, all of the mutations are highly conserved within the yeast species we compared, and the most severe mutant, *est5-1*, is conserved all the way to *H. sapiens* (data not shown).

#### *EST5 is in the telomerase pathway*

We next wanted to observe the phenotypic consequence of the *est5*<sup>-</sup> mutations when integrated into the genome of wild-type yeast (rather than over-expressed on a plasmid). After integrating *est5-1* into the genome of a wild yeast strain, I transformed the strain with a high-copy plasmid bearing either wild-type *EST5* or an empty vector and propagated to observe cellular growth. By ~50 generations, the strain containing the empty vector plasmid showed signs of senescence (Figure 5.2a), a phenotype previously

only observed in mutations in telomerase (*EST1*, *EST2*, *EST3*), or in the telomerase pathway (*cdc13-2/EST4*).

In order to further demonstrate *EST5* is, in fact, in the telomerase pathway, Margherita Paschini (a former graduate student in the Lundblad lab) performed a senescence assay on each of the *EST5* mutations. This assay has previously been used for epistasis analysis of the telomerase pathway for genes implicated in telomere length regulation (Ballew and Lundblad 2013). The rate of senescence was compared for a strain bearing the *est5-1* mutation, a telomerase deletion (*tlc1-Δ*), and the double mutant (*est5-1 tlc1-Δ*). The combination of *est5-1* to *tlc1-Δ* had no effect on the rate of senescence compared to either single mutant (Figure 5.2b), placing *EST5* directly in the telomerase pathway.

#### *Identifying an external binding partner of Est5*

The next question to ask was if Est5 regulates telomerase through an interaction with an external binding factor. I took several genetic and biochemical approaches to attempt to identify an interactor of *est5-1*.

I first tried to identify a mutation that would suppress the senescence phenotype of *est5-1*. If such a co-suppressing mutation existed, it would argue for a direct interaction between it and *EST5*, as was shown to be the case for *est1-60* and *cdc13-2* (Pennock et al. 2001). Discovery of this interaction could further lead to an understanding of how this interaction regulates telomerase. In brief, I chose several candidate genes, expressed on high-copy plasmids, and subjected them to random mutagenesis using the *E. coli* mutator strain XL1 Red. I then transformed the mutant

libraries into a strain containing the *est5-1* mutation and looked for cells that survived following several generations of propagation. Additionally, I took a whole-genome mutagenesis approach in which I subjected the *est5-1* strain to ethyl methanesulfonate (EMS) mutagenesis to generate random mutations throughout the genome, plated cells, and looked for viable cells following propagation.

I also attempted to find a gene that, when over-expressed, was able to suppress the senescence phenotype of *est5-1*, as over-expression of *EST1* is capable of suppressing senescence of *cdc13-2* (Evans and Lundblad 1999). After transforming high-copy plasmids, containing candidate genes under control of the ADH promoter, into the *est5-1* strain, I propagated for ~75 generations and looked for alleviation of senescence. Additionally, I transformed a library containing each yeast gene on a high-copy plasmid (Engebrecht et al. 1990) into the *est5-1* strain and looked for viable colonies following propagation.

Unfortunately, none of these genetic experiments were successful in identifying a suppressor of the *est5-1* allele. A more detailed Results and Discussion section on these experiments is included in Appendix A of this dissertation.

In combination with the genetic approaches, I also used biochemical assays in an attempt to identify an Est5 interactor. I created a yeast strain with a (FLAG)<sub>3</sub> epitope on the C-terminus of Est5, as well as a strain containing a (FLAG)<sub>3</sub> epitope on the C-terminus of Est5-1. Following an anti-FLAG immunoprecipitation (IP) of Est5, Est5-1, and an untagged control, samples were sent to the Mass Spectrometry core at Salk Institute for analysis. By comparing the resulting spectra for each sample I was able to observe several proteins that were present in the pull-down of Est5, but absent (or

reduced) in the pull-down of Est5-1. Figure 5.3a shows a curated list of proteins that were selected from the raw dataset, as they were most likely to be real candidates based on their proposed roles in chromosome maintenance or DNA replication, as well as being essential genes. Corrine Moeller, a graduate student in the Lundblad lab, is pursuing the most promising candidates further.

Mec1 and Lcd1, part of the ATR-ATRIP protein kinase complex, became the top candidates from the list because of their role in the cellular response to DNA replication stress (Zho and Elledge 2012). To further validate the interaction between this complex and Est5, I integrated the (FLAG)<sub>3</sub> epitope at the C-terminus of Est5 into a strain containing a (myc)<sub>12</sub> epitope on the C-terminus of Mec1. Following an anti-FLAG IP of Est5, I observed Mec1 co-IP on an anti-myc western blot (Figure 5.3b). This Mec1 signal was not observed when the anti-FLAG IP was done with an untagged version of Est5. Unfortunately, I was unable to introduce *est5-1-(FLAG)<sub>3</sub>* into the strain containing a (myc)<sub>12</sub> epitope on Mec1 to verify the Est5-Mec1 interaction was lost upon introduction of the *est5-1* mutation.

#### *The interaction between Est5 and telomerase*

I also wanted to explore the idea of a direct interaction between Est5 and telomerase. To do so, I first created a strain containing a (FLAG)<sub>3</sub> epitope on Est5 and a (myc)<sub>12</sub> epitope on both Est1 and Est2. Following an anti-FLAG IP, I assessed the interaction by co-IP western blotting (Figure 5.4a). While Est1 and Est2 expressed in extracts as expected from prior studies (Lubin et al. 2012; Tucey and Lundblad 2013), there did not appear to be an observable interaction between Est5 and Est1 or Est2.

However, it is possible for Est5 to interact with Est3 without interacting with Est1 or Est2, since Est3 binds to telomerase late in the cell cycle (Tucey and Lundblad 2014), so I repeated the anti-FLAG IP of Est5 in a strain bearing a (myc)<sub>12</sub> epitope on Est3. Yet again, no interaction was observed by co-IP western blotting (Figure 5.4b).

Tagging Est3 has been shown to cause slight impairment to telomerase (Tucey and Lundblad 2014) so to ensure the tag was not affecting the Est5-Est3 interaction, I performed the reciprocal anti-FLAG IP – with the (FLAG)<sub>3</sub> epitope on Est3 and the (myc)<sub>12</sub> epitope on Est5 (Figure 5.4c). While Est5-(myc)<sub>12</sub> was observed on the anti-myc western, the signal was not above that of the untagged Est3 control, meaning the co-IP was non-specific.

The interaction between Est1 and Cdc13 was first observed genetically (Nugent et al. 1996), long before it could be seen biochemically (Tucey and Lundblad 2013), so I surmised that I could perhaps detect a direct genetic interaction between Est5 and telomerase despite not seeing this interaction biochemically. From previous studies, our lab had a collection of mutations in each subunit of telomerase that cause severe telomere length defects, yet these residues are not responsible for interacting with any known binding partners (Chapter 2; Chapter 3; unpublished data). If any of these mutations were capable of suppressing any of the *est5*<sup>-</sup> mutant phenotypes, this would argue for a direct interaction between the two proteins. Because previous genetic attempts at suppressing *est5-1* were unsuccessful, I decided to look for co-suppressing mutations of *est5-3*, which is located very close to *est5-1*, has an extremely short telomere phenotype, yet does not confer senescence (Figure 5.1). After integrating *est5-3* into the genome at its genomic locus, and expressed by its native promoter, I transformed the strain with

various *est3*<sup>-</sup> mutations, express on high-copy plasmids under control of the ADH promoter, and propagated ~50 generations by performing successive streak-outs on selective media (Figure 5.5a). Surprisingly, some *est3*<sup>-</sup> mutations seemed to have an additive affect, leading to cellular senescence (*est3-1*, *est3-4*, *est3-5*), while others did not (*est3-2*). Interestingly, *est3-5* has a more severe phenotype than *est3-3* (Lubin et al. 2013), so the fact *est3-5* appeared healthier than *est3-3* in the presence of *est5-3* suggested there might be a direct interaction between *est3-3* and *est5-3*.

To explore this interaction further, I assessed the telomere length of these cells by southern blotting after ~75 generations (Figure 5.5b), which revealed telomere length is restored in the *est5-3* strain when *est3-3* is over-expressed. Notably, however, the telomere length of *est3-3* appears to be slightly longer than the telomere length of over-expressed *EST3*. Over-expression of wild-type *EST3* causes a slight reduction in telomere length when compared to the over-expression of an empty vector, suggesting that perhaps *est3-3* is displaying the phenotype of an empty vector, rather than of restored Est5-Est3 interaction. However, this premise was not supported by western blot analysis, as protein expression levels appeared to be unchanged (data not shown).

If, *est5-3 est3-3* does indeed restore an Est5-Est3 interaction, then one would expect the over-expression of *est5-3* in a strain with *est3-3* integrated into the genome would produce the same suppression result as *est3-3* over-expressed in the *est5-3* strain. However, this was not the case. Integration of *est3-3* resulted in a senescent strain. This senescence was not attenuated in the presence of a high-copy plasmid containing *est5-3* under control of the ADH promoter (data not shown).



### *The role of EST5 in telomerase assembly*

One way in which telomerase is regulated is through the assembly of the holoenzyme (Tucey and Lundblad 2013; Tucey and Lundblad 2014). To determine if *est5-1* affects how telomerase was assembled, I introduced the *est5-1* mutation into a strain bearing a (myc)<sub>12</sub> epitope on Est1, as well as a (myc)<sub>12</sub> and (FLAG)<sub>3</sub> epitope on Est2. Following an anti-FLAG IP, I compared the co-IP of Est1 on an anti-myc western blot between an *EST5* and *est5-1* strain. The 1:1 ratio of Est1:Est2 previously observed in this strain background (Tucey and Lundblad 2013; Tucey and Lundblad 2014) was unaltered in the presence of *est5-1* (Figure 5.6) indicating *EST5* does not affect the telomerase pre-assembly complex.

### **Discussion**

The results presented in this chapter demonstrate the ODN strategy is more broadly applicable for identifying functional residues on the surface of proteins other than telomerase. More importantly, ODN identified the first *EST* gene found in over twenty years, in a protein complex not previously shown to act in the telomerase pathway.

While the exact mechanism is unknown, it is clear *EST5* is regulating telomerase. This regulation may be occurring through its interaction with an unknown factor, an interaction with telomerase itself, and/or the formation of the RPA complex, which may affect replication forks, the preferred substrate for telomerase. Just as the discovery of *EST4* (*cdc13-2*) ultimately led to the telomerase recruitment model, this discovery of *EST5* will certainly lead to a better understanding of telomerase regulation. The identification of *EST5* also potentially provides an alternative therapeutic target for

treating cancer or telomerase-mediated genetic diseases.

### *The role of EST5 in regulating telomerase*

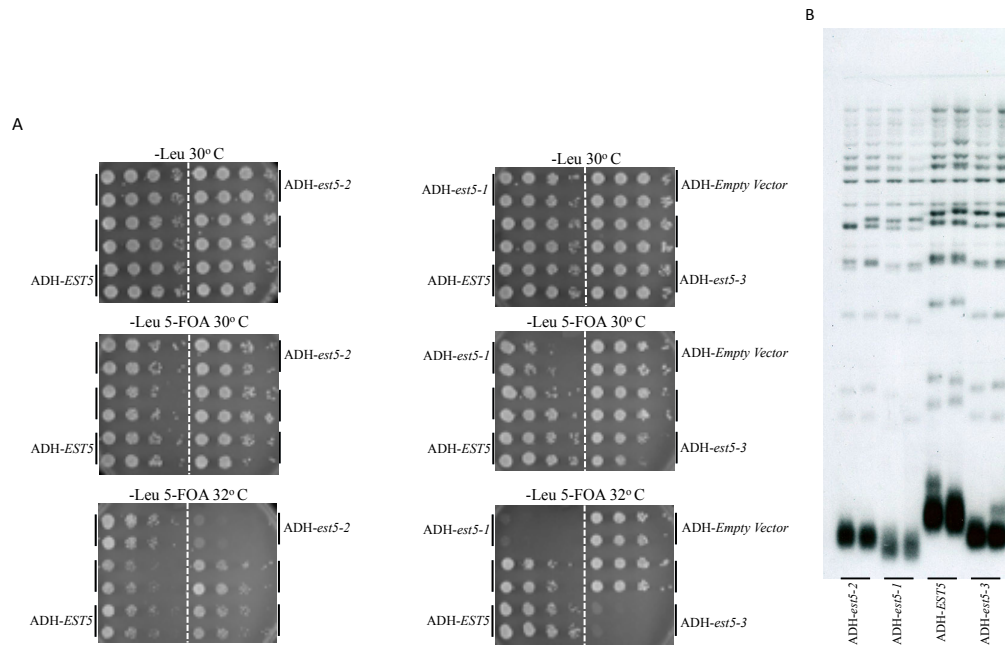
*EST5* could be regulating telomerase in three ways – holoenzyme formation, telomerase recruitment, and enzyme activity. While I have shown that *EST5* is not regulating the telomerase pre-assembly complex, I have not ruled out the possibility that *EST5* affects the interaction of Est3 with the holoenzyme. Further biochemical work is needed to conclude holoenzyme formation is not affected by *est5<sup>-</sup>* mutations.

My studies have also not determined whether or not *EST5* is regulating the recruitment of telomerase to the telomere. For instance, if *EST5* regulates how or when Cdc13 binds telomeric DNA, this would affect the recruitment of telomerase to the telomere. A series of papers from the Matsuura lab (Takata et al. 2004, 2005) describe a complex association of proteins at telomeres. Their findings suggest that Cdc13 association with telomeric DNA is dependent on Mec1 association. If *est5<sup>-</sup>* mutations do affect an Est5-Mec1 interaction, perhaps this is limiting the ability of Cdc13 to associate with telomeres, and therefore affecting recruitment of telomerase.

Finally, *EST5* may play a role in telomerase activity. A recent working model (Greider 2016) suggests that telomerase travels with the replication fork as it moves through telomeric DNA. If telomerase passively travels with the replication fork as an inactive enzyme, it may be *EST5* that receives and/or sends some regulatory signal resulting in telomerase activity. Examining enzyme activity of telomerase biochemically in the presence or absence of *est5<sup>-</sup>* mutations would be a valuable experiment in determining the role of Est5 on its activity. The Lundblad lab now has an assay capable

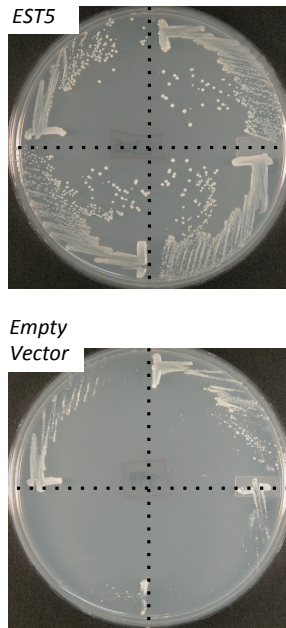
of determining telomerase activity *in vivo*, which is discussed in Appendix B.

## Figures

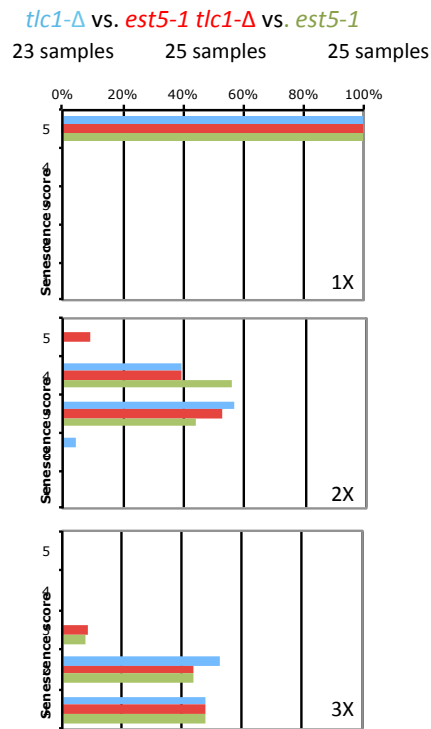


**Figure 4.1: ODN mutagenesis identifies residues on the surface of an essential DNA replication protein involved in telomere length regulation.** (A) ODN phenotypes of the *est5*<sup>-</sup> mutations in the *yku80*- $\Delta$  synthetic lethal assay versus wild type, empty vector, and mutations conferring no phenotype. A *yku80*- $\Delta$  / p *CEN URA3 YKU80* strain was transformed with 2 $\mu$  plasmids containing the indicated *est5*<sup>-</sup> mutation, which was expressed by the constitutive ADH promoter; serial dilutions of two independent transformants for each mutation were examined for viability on media that selected for the presence or loss of the *YKU80* plasmid. The temperature-dependence of this synthetic growth phenotype provides a sensitive assay for detecting a broad range of ODN phenotypes, as previously described (Lee *et al.* 2008). (B) Telomere length of wild yeast strains transformed with high-copy plasmids expressing either *EST5* or the indicated *est5*<sup>-</sup> mutations, under control of the ADH promoter, assessed after  $\sim$ 75 generations of growth.

A



B

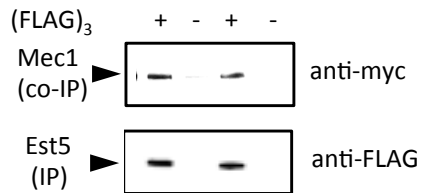


**Figure 4.2: *EST5* is in the telomerase pathway.** (A) Growth of the *est5-1* allele at ~50 generations when integrated into the genome of a wild-type yeast strain. Four separate isolates were propagated following transformation of a high-copy plasmid containing either *EST5* or an empty vector. *EST5* was capable of rescuing the senescent *est5-1* phenotype, while the empty vector was not. (B) An example of one of two senescence assays performed by Margherita Paschini. The senescence score of *est5-1 tlc1-Δ* is neither accelerated nor perturbed compared to the single mutants, indicating *EST5* is in the telomerase pathway.

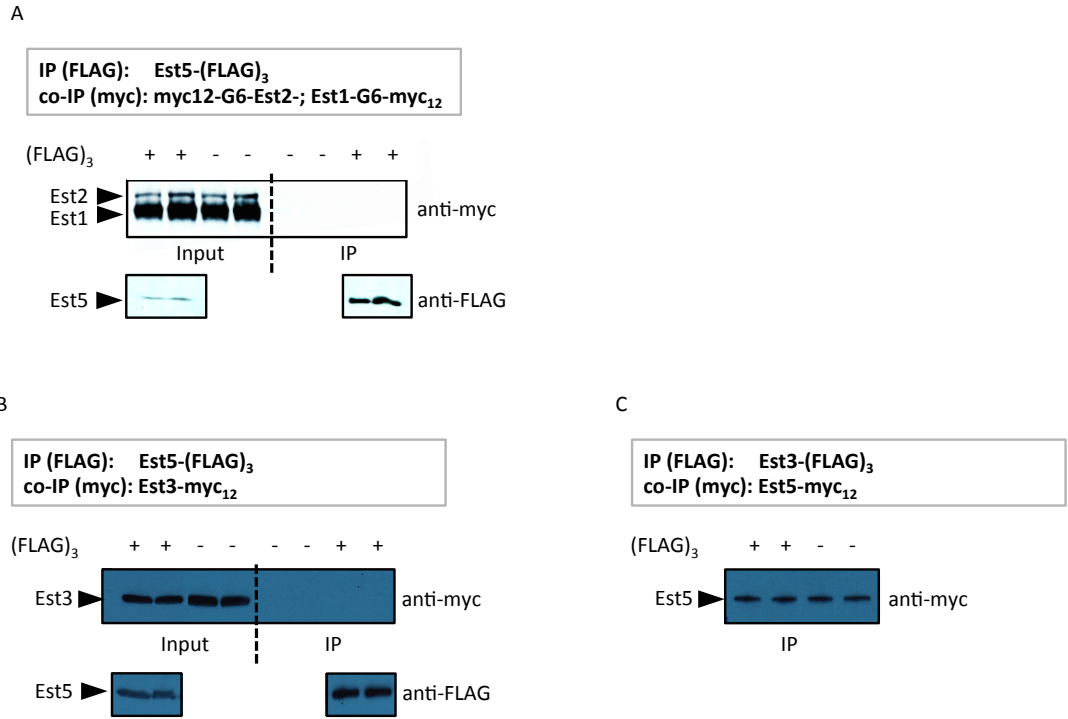
A

	Untagged		Est5-(FLAG) <sub>3</sub>			est5-1-(FLAG) <sub>3</sub>			
	A	B	A	B	average	A	fold change	B	fold change
EST5	1	0	397	554	475.5	555	1.2	176	0.4
RIM1	0	0	205	94	149.5	46	down 4-fold	18	down 3-fold
MEC1	11	0	96	75	85.5	22	down 4.5-fold	8	down 4-fold
LCD1	1	0	10	12	11	4	down 3-fold	0	down > 4-fold
MSH2	0	0	28	25	26.5	5	down 6-fold	0	down > 10-fold
MSH6	0	0	13	10	11.5	0	down > 10-fold	0	down > 5-fold
MSH3	0	0	4	3	3.5	0	down > 3-fold	0	down > 3-fold
RAD52	0	0	15	16	15.5	5	down 4-fold	1	down 5-fold
DNA2	0	0	27	69		54		18	
MGM101	0	0	21	22		24		22	
VPS1	0	0	24	17		9		0	
MPH1	0	0	23	20		17		3	
KAP95	0	0	23	47		1		0	

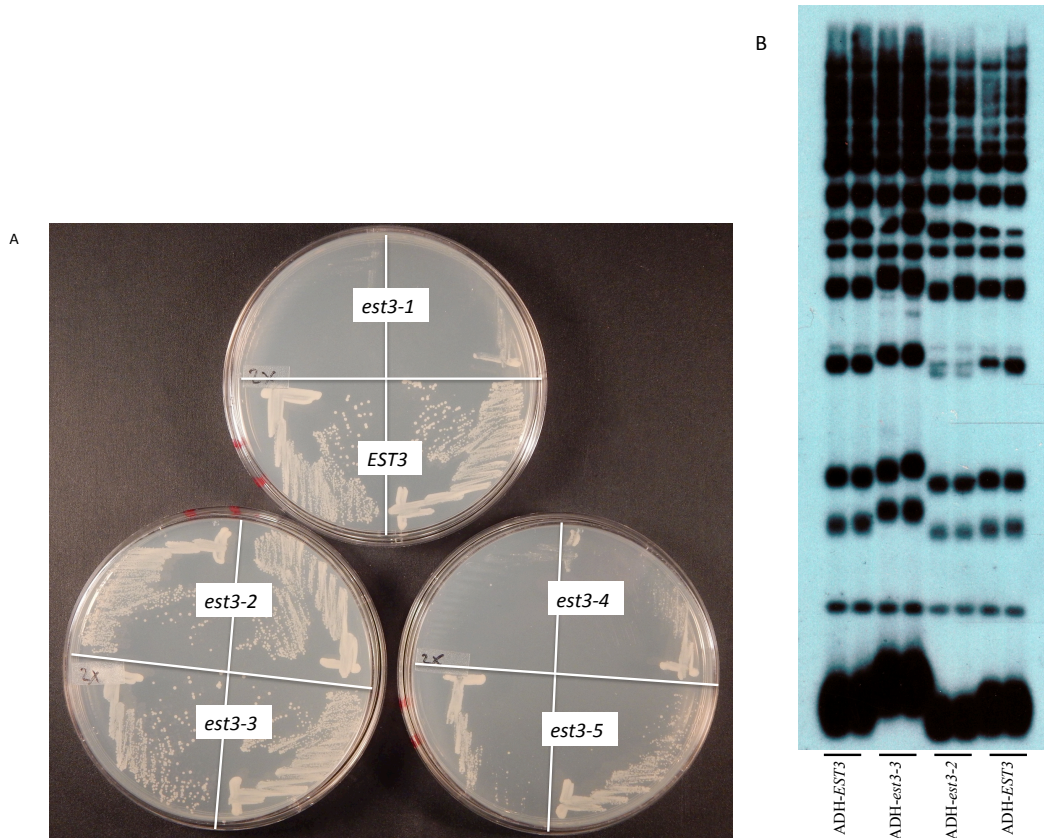
B



**Figure 4.3: Identifying an external binding partner of Est5.** (A) Selected mass spectrometry results. Two samples of each – untagged control, Est5-(FLAG)<sub>3</sub>, and est5-1-(FLAG)<sub>3</sub> – were analyzed by mass spectrometry following anti-FLAG IP. The number of peptides counted from each protein in the sample is displayed in the chart. (B) Western blot analysis of the Est5-Mec1 interaction. Anti-FLAG IP of tagged or untagged Est5, followed by anti-myc and anti-FLAG western blotting shows Mec1 co-IP with Est5.

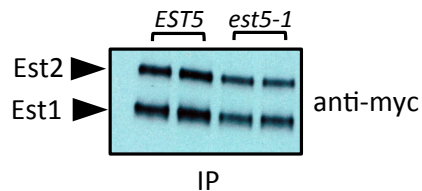


**Figure 4.4: Biochemical analysis of the interaction between Est5 and telomerase.** (A) Western blot analysis of the Est5-Est1/Est2 interaction. Anti-FLAG IP of tagged or untagged Est5, followed by anti-myc and anti-FLAG western blotting shows neither Est1 nor Est2 co-IP with Est5. (B) Western blot analysis of the Est5-Est3 interaction. Anti-FLAG IP of tagged or untagged Est5, followed by anti-myc and anti-FLAG western blotting shows Est3 does not co-IP with Est5. (C) The reciprocal IP shown in (B), western blot analysis of the Est5-Est3 interaction. Anti-FLAG IP of tagged or untagged Est3, followed by anti-myc and anti-FLAG western blotting shows the Est5 co-IP with Est3 is not specific.



**Figure 4.5: Genetic analysis of the interaction between Est5 and telomerase.** (A) 2X (~50 generations) streak-outs of an *est5-3* strain transformed with over-expressed *EST3* or *est3<sup>-</sup>*. Three *est3<sup>-</sup>* mutations lead to senescence (*est3-1*, *est3-4*, *est3-5*), while two appeared healthy like wild-type *EST3* (*est3-2*, *est3-3*). In *EST5* cells, *est3-3* has a more severe phenotype than *est3-5*. (B) Telomere length of an *est5-3* yeast strain transformed with high-copy plasmids expressing either *EST3* or the indicated *est3<sup>-</sup>* mutation, under control of the ADH promoter, assessed after ~75 generations of growth. The telomere length of cells bearing ADH-*est3-3* was restored to levels slightly above ADH-*EST3*.

IP (FLAG): (FLAG)<sub>3</sub>-(myc)<sub>13</sub>-Est2  
co-IP (myc): Est1-(myc)<sub>12</sub>



**Figure 4.6: Biochemical analysis of the effect of *EST5* on telomerase assembly.** Western blot analysis of the Est2-Est1 interaction in the presence of the *est5-1* mutation. Anti-FLAG IP of Est2, followed by anti-myc western blotting shows the Est1-Est2 interaction is unaffected.



**Table 4.1: Strains used in this chapter.**

STRAIN	GENOTYPE
YVL3142	<i>MATa ura3-52 lys2-801 trp-Δ1 his3-Δ200 leu2-Δ1 yku80-Δ::kanMX</i>
YVL3477	<i>MATa leu2 trp1 ura3-52 GAL+ prb- prc- pep43 MEC1-myc13::KanR</i>
YVL3528	<i>MATa leu2 trp1 ura3-52 GAL+ prb- prc- pep43 Est1-G6-myc12 (FLAG)3-myc12-G6-Est2 bar1-Δ::KAN</i>
YVL3584	<i>MAT a/alpha ura3-52/ura3-52 lys2-801/lys2-801 trp-Δ1/trp1-Δ1 his3-Δ200/his3-Δ200 leu2-Δ1/leu2-Δ1 TLC1/tlc1Δ::HIS</i>
YVL4250	<i>MAT a ura3-52 lys2-801 trp-Δ1 his3-Δ200 leu2-Δ1 est5-1</i>
YVL4261	<i>MAT a/alpha ura3-52/ura3-52 lys2-801/lys2-801 trp-Δ1/trp1-Δ1 his3-Δ200/his3-Δ200 leu2-Δ1/leu2-Δ1 tlc1-Δ/TLC1 est5-1/EST5</i>
YVL4939	<i>MATa leu2 trp1 ura3-52 GAL+ prb- prc- pep43 Est1-G6-myc12 (FLAG)3-myc12-G6-Est2 bar1-Δ::KAN est5-1</i>
YVL5031	<i>MATa leu2 trp1 ura3-52 GAL+ prb- prc- pep43 Est1-G6-myc12 myc12-G6-Est2 EST5-(FLAG)3 bar1-Δ::NAT</i>
YVL5066	<i>MATa leu2 trp1 ura3-52 GAL+ prb- prc- pep43 EST5-(FLAG)3</i>
YVL5077	<i>MATa leu2 trp1 ura3-52 GAL+ prb- prc- pep43 est5-1-(FLAG)3</i>
YVL5155	<i>MATa leu2 trp1 ura3-52 GAL+ prb- prc- pep43 MEC1-myc13::KanR EST5-(FLAG)3</i>
YVL5506	<i>ura3-52 lys2-801 trp-Δ1 his3-Δ200 leu2-Δ1 est5-3</i>
YVL5589	<i>MATa leu2 trp1 ura3-52 GAL+ prb- prc- pep43 Est3-(FLAG)3 ; bar1-Δ::NAT; EST5-myc13::KAN</i>
YVL5630	<i>MATa leu2 trp1 ura3-52 GAL+ prb- prc- pep43 Est3-G6-myc12 EST5-(FLAG)3</i>

**Table 4.2: Plasmids used in this chapter.**

Plasmid Name	Gene	Type	Marker	Promoter
pVL6305	<i>EST5</i>	2μ	<i>LEU2</i>	ADH
pVL6958	<i>est5-1</i>	2μ	<i>LEU2</i>	ADH
pVL7840	<i>est5-3</i>	2μ	<i>LEU2</i>	ADH

## Materials and Methods

### *Genetic analysis*

Standard genetic and molecular methods were used to introduce plasmids into yeast, introduce missense mutations into the *EST5* gene, and assess synthetic lethality in the yku80- $\Delta$  strain, as previously described (Lendvay et al. 1996; Lee et al. 2008; Lubin et al. 2013). Telomere length was assessed from two independent single colonies that were propagated for ~75 generations, following transformation into a wild-type yeast strain.

### *Biochemical analysis*

Mutations were integrated into the genome in place of the wild-type gene, as previously described (Paschini et al. 2012; Tucey and Lundblad 2014). PCR analysis was used to confirm that each mutant allele was integrated without unanticipated genomic rearrangements. Subsequent isolates that had lost the wild-type *EST5* gene and retained only the mutant *est5<sup>-</sup>* allele (following propagation on 5-FOA) were confirmed by molecular analysis (by sequencing across the integrated mutant allele), as well as phenotypic analysis (telomere length and/or senescence), for every constructed strain. Whole-cell extracts were prepared from two independent 250 ml cultures (OD 0.8–0.9) for each genotype and processed in parallel. Cells were pelleted, washed in 1% NP-40 Buffer (20 mM Tris-HCl pH 8, 10% glycerol, 100 mM NaCl<sub>2</sub>, and 1% Nonidet P-40) + protease inhibitors, and resuspended in 1 ml of the same buffer. Extracts were prepared by grinding this 1-ml suspension in a mortar in the presence of liquid N<sub>2</sub> until the suspension formed a fine powder. Extracts were clarified by three 10 min spins at 4 at 25,000 3 g, and supernatants were immediately subjected to IP by incubation with anti-

Flag M2 affinity gel (Sigma [Sigma Chemical], St. Louis, MO), in 1% NP-40 Buffer + protease inhibitors for 2 hr at 4, with gentle rocking. Beads were washed 3X in 20mM Tris-HCl pH 8 + 0.5% Tween20, and eluted for 4 min at 95 with 20mM Tris-HCl pH 8 + 0.5% Tween20 equilibrated with SDS loading buffer + 0.7% b-mercaptoethanol. Immunoprecipitated proteins were resolved on 6% (for detection of Est1, Est2, or Mec1) or 14% (for detection of Est3 or Est5) SDS-PAGE and probed with anti-myc 2272 (Cell Signaling Technology) at 1:1000 or anti-Flag F7425 (Sigma) at 1:10,000 dilution, followed by anti-rabbit IgG HRP conjugate (Promega, Madison, WI) at 1:10,000, and subsequent enhanced chemiluminescence (ECL) detection using preflashed film. ECL was used rather than alternative options (such as Li-cor Odyssey) due to substantially less background and a significantly higher signal-to-noise ratio; we previously demonstrated that this protocol can detect as little as twofold differences with high reproducibility over a 10-fold detection range (Tucey and Lundblad 2013).

Samples analyzed by mass spectrometry were sent to the Salk Institute Mass Spectrometry core facility.

### **Acknowledgments**

Thank you to Jocelyn Ramirez for her hard work during her summer internship, and to Margherita Paschini for guidance and thought-provoking discussions.

This work was supported by the Mass Spectrometry Core of the Salk Institute with funding from NIH-NCI CCSG: P30 014195 and the Helmsley Center for Genomic Medicine. I thank J. Moresco, J. Diedrich and W. Low for technical support.

Chapter 4 contains unpublished material. Margherita Paschini contributed Figure 4.2B. The dissertation author was the sole investigator and author of this chapter.

## **CHAPTER FIVE:**

Conclusion

For many years, the telomerase field struggled to overcome the challenges imposed by the lack of structural data in order to define the functional surface of telomerase and identify key regulatory processes. By using over-expression dominant negative phenotypes, I was developed the ODN assay to forgo the need for protein structures to be able to define the functional surface of telomerase. After demonstrating the usefulness of ODN using *EST3* (Lubin et al. 2013; Rao et al. 2014), the strategy was then successfully applied to *EST1* (Lubin et al. 2018) and *EST2* (Nguyen 2013; unpublished). ODN has enabled us to identify the distinct functionally important surfaces on telomerase, including two novel patches involved in telomerase regulation for which roles have not yet been identified.

All of the ODN mutagenesis was done prior to, and without the use of, any structural data. Once the structure of Est3 and Est1 were solved (Rao et al. 2014; Chen et al. 2018), it allowed me to map the ODN mutations on the protein structure and verify the residues were indeed on the surface, and that the biochemically distinct categories of mutations clustered.

To determine if the ODN would be more broadly applicable than only to telomerase, I supervised several undergraduate students and summer interns to mutagenize a large number of essential genes involved in DNA replication and repair. This exploratory endeavor not only showed ODN can be used on a wide range of protein complex in different genetic strain background, but also led to the remarkable discovery of a fifth *EST* gene, a finding which as not been accomplished in over two decades.

### *Separation-of-function mutations in EST1, EST2, and EST3*

Using ODN mutagenesis, I was able to identify 16 amino acids of *EST3* that define two discrete functions and thus constitute two different sets of *sof* alleles, as summarized in Figure 5.1A and Table 5.1. One set of residues (V75, Y78, E114, N117, D166, and V168) promotes the association of the Est3 protein with the telomerase complex, whereas a second group (K71, L171) performs at least one other activity that is not required for either interaction with telomerase or enzyme activity (Lee et al. 2008, 2010; Lubin et al 2013; Rao et al. 2014).

ODN mutagenesis allowed me to identify 11 *sof* candidates in *EST1* after screening 134 missense mutations (~25% of the protein) (Figure 5.1B and Table 5.1). Similar to the analysis of *EST3*, we were able to categorize these mutations based on their biochemical functions. Four residues (R269, E500, D510, F511) are responsible for the interaction between Est1 and Est3. In addition to the previously known *est1-60* allele, we identified four other amino acids (R447, K555, K559, W566) that affect the Est1-Cdc13 interaction. And most notably, we found two mutations (K485E, K488E) that, despite conferring a severe telomere length defect and senescence, did not affect the interaction with any known binding partners of Est1.

Finally, work done by a former Master's student in the Lundblad lab, Lisa Nguyen (Nguyen 2012), as well as some of my own work, identified 27 ODN mutations in *EST2*, the catalytic subunit of telomerase (Figure 5.1C). Several of these mutations abolish the interaction of Est2 with telomerase, and presumably, many of them interfere with catalysis of the telomerase enzyme. Interestingly, while some mutations in *EST2* result in shortened telomeres, there are other mutations that give rise to very elongated

telomeres (data not shown; Nguyen 2013). These results demonstrate the ODN assay was not only effective in identifying residues involved in protein-protein interaction, but also in identifying residues involved in enzyme catalysis, further expanding the usefulness of the protocol.

### *Structural validations*

A major assumption of the ODN assay was that mutants with an observable phenotype not only encode structurally stable proteins, but also reside on the surface of the protein. Fortunately, our collaborators in the Wuttke lab (Rao et al. 2014) were able to solve the NMR structure of the Est3 protein, and the Lei lab solved the structure of Est1 in *K. lactis*, a closely related yeast species (Chen et al. 2018). These structures allowed me to map our ODN mutations and confirm that indeed, all of them were on the surface. I was also able to perform two additional analyses – (i) how effective we were in identifying the functionally important residues by focusing on charged, conserved residues, and (ii) if mutations with different biochemical classifications mapped to discrete patches.

Using the Est3 structure as a guide, I mutated the entire surface of the protein to identify additional functionally important residues not found in the initial ODN screen. Amazingly, prior to the Est3 structure, the ODN strategy identified 11 out of the 16 (~70%) residues in *EST3* important for telomere length homeostasis showing how effective and efficient ODN mutagenesis is.

The Est1 and Est3 structures also allowed me to map the ODN mutations and determine if amino acids with similar biochemical properties clustered to discrete

patches. Indeed, residues on Est3 responsible for binding telomerase form a contiguous surface (TEL patch), while other residues not involved in telomerase interaction form another distinct surface (TELR patch). Similarly, ODN mutations in Est1 clustered on the surface based on their biochemical properties (Figure 5.1B).

#### *Alanine versus charge swap mutagenesis*

In the Lubin et al. 2013 paper, we argued the importance of making amino acid changes to the opposite charge rather than simply to alanine. My mutagenesis of *EST1* provides further evidence to support this claim. Most notably, the R269E mutation, which disrupts the interaction with Est3, does not show a growth defect when mutated to alanine. Similarly, *est1-R291E* has a phenotype, while the alanine substitution does not (Figure 5.2).

Not surprisingly, this phenomenon is not unique to yeast. Zhou et al. 1998 showed in *C. elegans*, the choice of amino acid substitution had a significant effect on the observable phenotype. Mutations at residue D289 in the FliG gene and at R90 in the MotA gene both cause mobility impairment, even when the substitution is made to alanine. Worms with the double mutation show increased impairment when the mutants are made to alanine, however, if both mutations are made as charge-swaps, the immobility phenotype is rescued. This rescue does not occur to the same extent if one residue is mutated to alanine, and the other to the opposite charge, again highlighting how charge-swap mutagenesis can reveal insights that might be missed with alanine substitutions.

The phenotypic relationship between charge-swap mutations versus those made to



alanine may be indicative of the type of interaction occurring at the specific residue. For instance, a surface residue that interacts with another protein surface via a salt bridge interaction may have a stronger phenotype when a charge-swap mutation is made, rather than a substitution to alanine. If however, the surface residue helps to create a specific protein conformation, pocket, or hinge, the amino acid substitution may not matter. Understanding how different amino acid substitutions affect different protein interactions may help guide the approach a researcher should take in identifying the interacting partner. Obviously more work needs to be done to test this hypothesis, but if correct, this could lead to much faster discoveries of interacting partners following the identification of ODN mutations.

#### *Applying ODN mutagenesis to other genes and pathways*

In the Lundblad lab, the ODN approach has also been effective in identifying *sof*<sup>+</sup> mutations in genes other than telomerase, specifically essential genes involved in DNA replication and recombination, suggesting that this protocol is widely applicable (Lubin, J. W., Meunier, M.A., Moeller, C.A., and Lundblad, V., unpublished data). This method obviously will not be comprehensive in identifying every functional residue on the surface of a protein, especially if only conserved charge residues are targeted, and it is not applicable to proteins that confer lethality when overexpressed; however, even a limited subset of new *sof*<sup>+</sup> mutations, especially in essential genes, could be highly instructive, as this class of genetic reagents has a long history of uncovering previously unanticipated functions of proteins.

ODN mutagenesis led to the remarkable discovery of a fifth *EST* gene,

implicating an essential DNA replication complex in the telomerase pathway. To date, only two genome-wide mutagenesis screens, and now ODN, have been able to uncover such a class of genes.

In collaboration with many other lab members, I have also been able to expand the ODN strategy to probe outside of the telomerase pathway. By utilizing different “sensitized” yeast strains, other than *yku80-Δ*, we have been able to identify functionally important residues on the surfaces of several protein complexes involved in various pathways of DNA replication, recombination, and repair. Over-expressing mutations in strains with either specific genes deleted, temperature sensitive alleles introduced, or with exposure to common stressors (i.e. hydroxyurea, ultra violet light, methyl methanesulfonate) has provided us with novel insights and useful reagents for further exploration of these complexes.

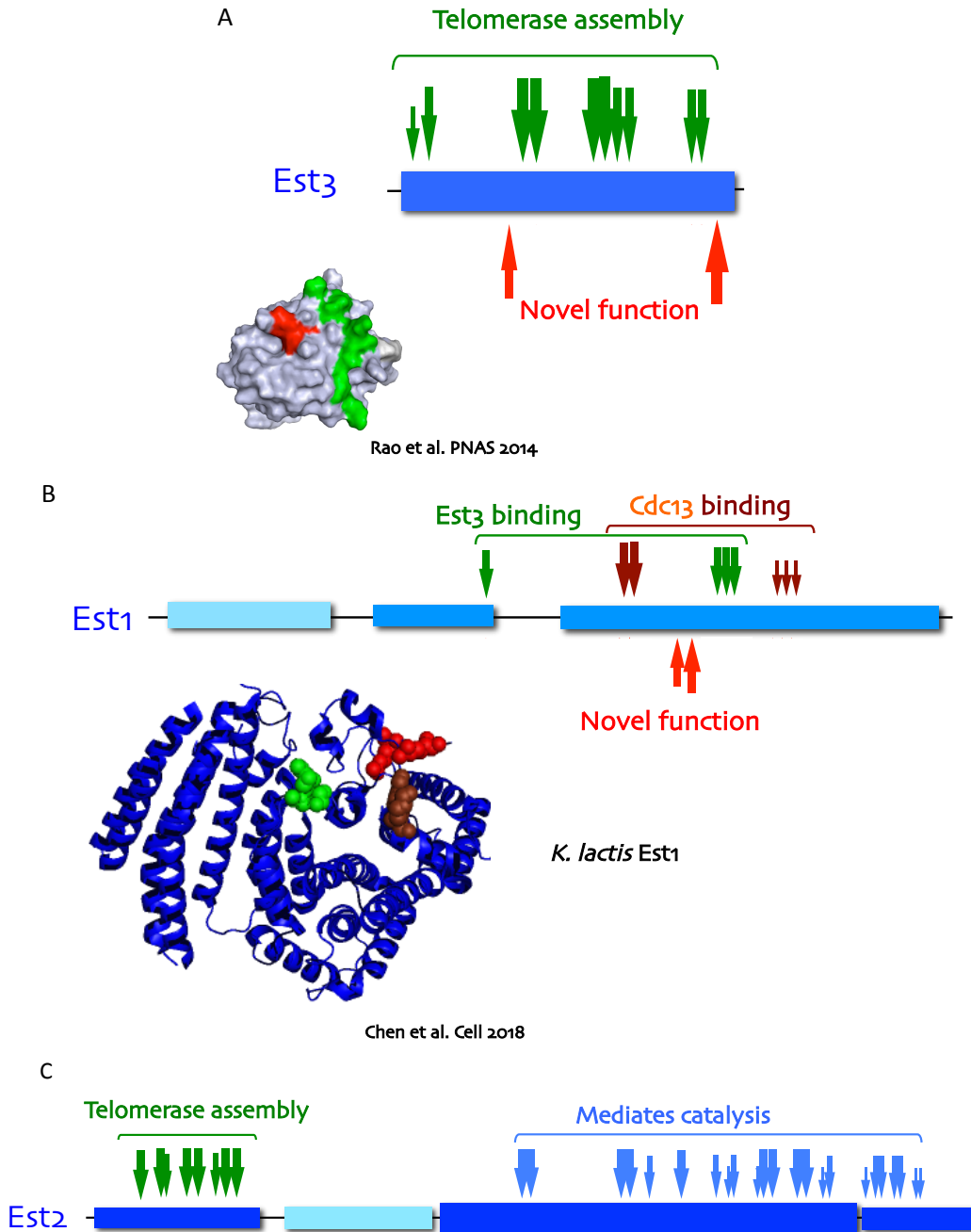
I was also able to show, using the *RAD51* gene (Appendix C), that ODN not only can identify the functionally important residues on the surface of a protein, but can also help in distinguishing different classes of *sof* alleles. By over-expressing the same mutations in various strain backgrounds, with perturbations in different pathways (i.e. DNA replication or replication fork stability), I was able to classify which residues were necessary for that protein’s function in the specific pathway. Other members in the lab have also achieved similar success in other protein complexes.

#### *Future directions*

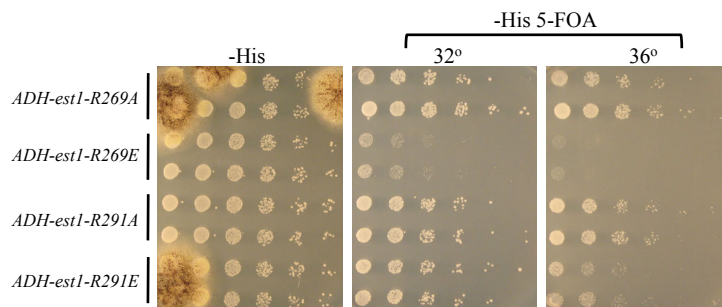
ODN has proven to be extremely useful in targeting the functionally important residues, but it is the starting point for inquiry of a protein, not the end. However, the

library of reagents generated by ODN can be used for much faster discovery of a protein's biochemical and regulatory function. By integrating the ODN mutations I found in telomerase into the genome, we were able to characterize each of them and discover that both Est1 and Est3 have novel regulatory sites their surfaces. Not only do we know these sites exist, but we also know the exact amino acids that are responsible for playing this role. Knowledge of these alleles will provide incredibly useful tools for furthering the field's understand of telomerase.

**FIGURES**



**Figure 5.1: ODN mutations identified in telomerase.** Mutations with an ODN phenotype are indicated by arrows, with the size of the arrow indicating severity. (A) Mutations identified in *EST3*. Locations of the mutations are indicated on the surface of the protein structure. (B) Mutations identified in *EST1*. Locations of the mutations are indicated on the surface of the *K. lactis* protein structure. (C) Mutations identified in *EST2* (Nguyen 2013)



**Figure 5.2: Examples of ODN phenotypes in *EST1* that depend on amino acid substitution.** An alternative assay for ODN phenotypes, based on synthetic lethality in the presence of a *yku80*- $\Delta$  mutation, as previously described (Evans and Lundblad 2001; Lee et al. 2008). Growth of *YKU80* or *yku80*- $\Delta$  strains (generated by plating on media that selects either for or against a *YKU80 URA3* plasmid) which also contain high copy plasmids expressing the indicated mutations in *EST1*, under control of the ADH promoter.

**Table 5.1: ODN mutations identified in telomerase.** A summary of the ODN mutations identified in each telomerase protein subunit and the function of each, as determined by integration of the mutation, followed by biochemical analysis.

Protein	Association			Catalytic Activity (not tested)
	Telomerase	Cdc13	Unknown	
Est1	R269 E500 D510 F511	K444 R447 K555 K559 W566	K485 K488	
Est3	V75 Y78 E114 N117 D166 V168		K71 L171	
Est2	H61 N80 Y86 N96 N104 K111 N133 N150 N153 H156			K443 R450 D530 D592 D670 D671 K667 N701 K704 K734 F753 L756 F760 R763 N774 Q782 F798

## **Appendix A:**

Genetic approaches to reveal the *EST5* binding partner

The discovery of *EST5* (discussed in Chapter Five) can have profound impacts on our understanding of telomere biology, just as the discovery of *EST4 (CDC13)* led to an understanding of the telomerase recruitment pathway. The interaction between Est1 Cdc13 was first observed genetically through the identification of co-suppressing mutations (Nugent et al. 1996), and then later observed biochemically (Tucey and Lundblad 2013). With the hope of achieving similar success, I sought to find the interactor of *EST5* by identifying a co-suppressing mutation in another gene. I used several genetic screening techniques to try to accomplish this goal – i) random mutagenesis of candidate genes, ii) random genome-wide mutagenesis, iii) suppression by over-expression – but was, unfortunately, unsuccessful. This appendix presents the the genetic screens I attempted, which may help guide future efforts.

### **Co-suppression by mutagenesis**

#### *Candidate genes*

Several genes seemed like reasonable candidates for the potential *EST5* interacting partner, including members of telomerase and the t-RPA complex. From prior experiments in the lab, we had collections of mutations in these genes, which allowed for a site-directed approach to look for a suppressor of *est5-1*.

I narrowed down the list of mutant candidates to those that displayed a telomere length defect and were in amino acids of an opposite charge as *est5-1*. I then transformed the over-expression plasmid of the candidate mutant into an *est5-1* strain, picked single colonies, and propagated for ~50-75 generations and looked for restored viability. This analysis included 6 mutations in *EST1*, 6 mutations in *EST2*, 5 mutations in *EST3*, and 7



mutations in *MECI* (chosen based on slight growth phenotypes observed in the *yku80-Δ* strain). None of these mutations were capable of suppressing the phenotype of *est5-1* and the strains were senescent by the second or third streak-out (~50-75 generations) (data not shown). There were also two mutations in *CDC13* that fit the candidate criteria, however, over-expression of *CDC13* is lethal, so I transformed the *cdc13*<sup>-</sup> mutations into a *cdc13-Δ* strains containing either ADH-*est5-1* or an empty vector. Single colonies were propagated for ~50 generations and telomere length was assessed by southern blotting. Neither of the *cdc13*<sup>-</sup> mutations rescued the telomere length defect of over-expression of *est5-1*, and in fact had a negative additive effect on telomere length (Figure A.1).

In addition to a site-directed approach, I chose to randomly mutagenize *EST2*, *STN1*, and *TEN1* by passaging over-expression plasmids containing each gene through the *E. coli* mutator strain, XL1 Red to create a mutant library. To see if any mutations were capable of suppressing the senescence phenotype of *est5-1*, I transformed each library into a freshly dissected haploid *est5-1 rad52-Δ* strain and plated for single colonies on 30 plates containing media to select for the plasmid. Growth on the plates was lower than expect, at ~150,000 colonies for *STN1*, ~30,000 colonies for *EST2*, and ~105,000 colonies for *TEN1*. The colonies were then scraped from the plates, pooled in 10 batches for each gene containing ~1/10 of the total colonies, and dilutions were re-plated on selective media. If growth was observed after the re-plating, that plate was replica plated onto selective media. Following these successive rounds of propagation, only two colonies survived, both from the *STN1* mutagenized library transformation. I picked each single colony and streaked for single colonies on selective media.

Unfortunately, the plate became contaminated with mold and was unrecoverable. The experiment was not repeated.

### *Genome-wide mutagenesis*

Because the interactor of *EST5* could in fact be *EST6* (i.e. an additional essential gene not yet known to regulate telomerase), I also took a genome-wide approach to finding a mutant suppressor of *est5-1*. I subjected an *est5-1 rad52-Δ/p CEN URA3 EST5 RAD52* strain to ethyl methanesulfonate (EMS), to induce random mutations throughout the genome, and plated on 45 CM 5-FOA plates to select against the covering plasmid. ~7,000 colonies formed per plate and cells were scraped into pools of 8 plates. The pools were diluted, re-plated on CM 5-FOA, scraped again and diluted for re-plating. Viable colonies were then streaked on plates containing YPAD media. Only one colony was viable following propagation, but upon further investigation, the *RAD52* covering plasmid was found to be present in this colony, meaning the viability was likely due to the survivor pathway, rather than a co-suppressing mutation of *est5-1*.

### **Suppression by over-expression**

#### *Candidate genes*

Over-expression of *EST1* is capable of suppressing the phenotype of *cdc13-2* (*EST4*) (Evans and Lundblad 1999), so I wanted to see if there is a gene that, when over-expressed, suppresses the *est5-1* phenotype. The Lundblad lab has a collection of genes cloned into a high-copy plasmid vector, under the control of the ADH promoter. I transformed each of these plasmids into a strain bearing the *est5-1* mutation and

propagated ~50 generations to look for strains with alleviated senescence. A list of the transformed genes can be found in Table A.1. Mostly all of the strains were inviable after the 2X streak-out, but over-expression of a few genes appeared to alleviate senescence, particularly *RIF2* (Figure A.2). Prior work has shown that certain genes are capable of increasing or slowing the rate of senescence in yeast (Ballew and Lundblad 2013), so I wanted to see if the *RIF2* rescue was specific to *est5-1*, or if it was a more general suppression of senescence. I transformed the high-copy plasmid containing *RIF2* into an *est1-Δ* strain and propagated single colonies on selective media. After ~50 generations, the cells over-expressing *RIF2* were viable, while the cells containing a high-copy empty vector plasmid had reached senescence (Figure A.3), indicating the *RIF2* rescue was not specific to *est5-1*.

#### *High-copy genome library*

Because of the likelihood the gene needed to suppress the *est5-1* phenotype was not in the limited number of over-expression plasmids in the Lundblad lab, I also transformed the *est5-1* strain with a high-copy genomic library (J. Hirsch), which contains fragments from the entire yeast genome cloned into a high-copy plasmid backbone (Engelbrecht et al. 1990).

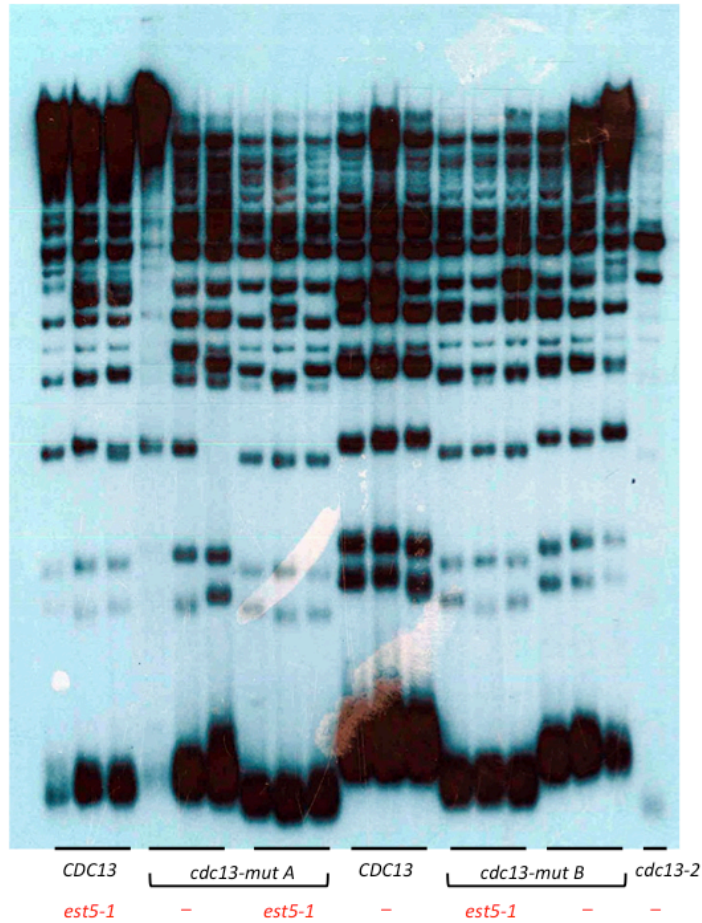
I transformed the library into a freshly dissected haploid *est5-1 rad52-Δ* strain and plated for single colonies. Roughly 175,000 colonies formed, which were then scraped from the plates, pooled in 10 batches for each gene containing ~1/10 of the total colonies, and dilutions were re-plated on selective media. 37 candidates were picked and plasmids were recovered from surviving colonies by rescue through *E.coli*. The plasmids were

transformed into a *yku80*- $\Delta$  strain containing *ADH-est5-1* and serial dilutions of two independent transformants for each were examined for viability (Figure A.4). The genomic inserts were then analyzed by restriction mapping and sequencing. Inserts included empty vector, *est5-1*, Chr. XIII b.p. 772739-773617, Chr. XV b.p. 644999-645837, Chr. XI b.p. 112450-113412, Chr. XIV b.p. 546722-547610, Chr. XIII b.p. 810486-8111313 (Table A.2). However, upon re-transformation into an *est5-1* strain, none of these inserts were capable of suppressing the senescence phenotype.

## **Conclusion**

I used several different genetic approaches in an attempt to identify a suppressor of the *est5-1* phenotype and find its interacting partner; however, these attempts were not exhaustive and repeating these experiments at higher volume may have led to success. It is also possible, though, the *est5-1* residue does not interact via a salt bridge interaction, so these methods will not be useful in finding a reciprocal co-suppressing mutation.

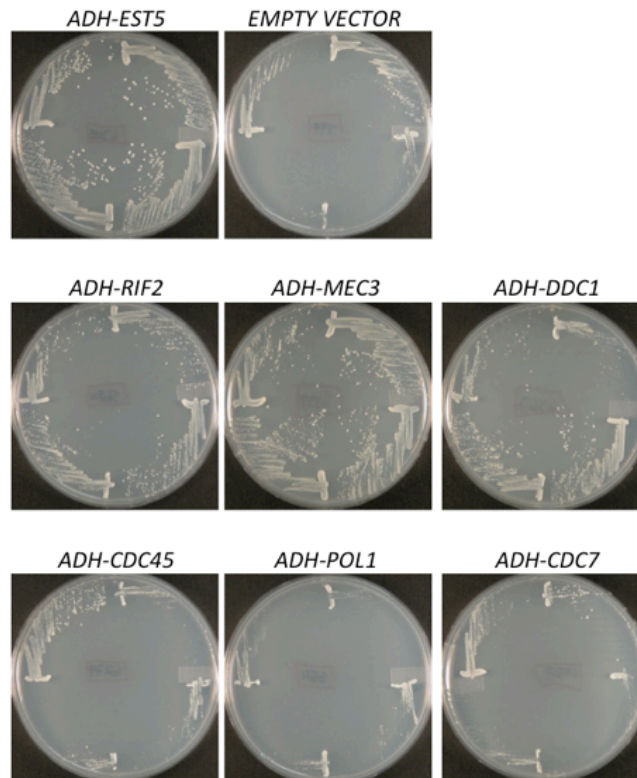
## Figures



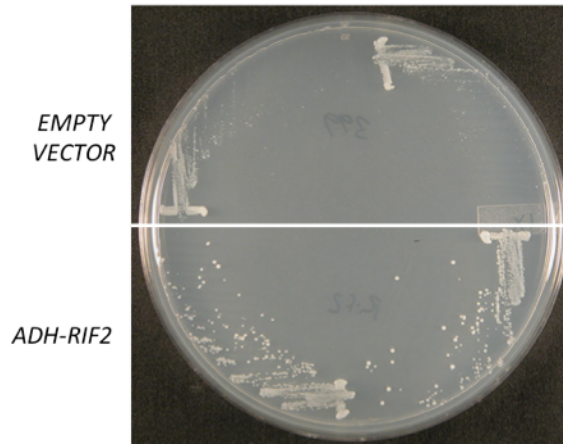
**Figure A.1: *cdc13* mutations are not capable of suppressing the telomere length defect of *est5-1*.** A southern blot showing telomere length of *cdc13* mutations on plasmids transformed into a *cdc13-Δ* strain along with either *ADH-est5-1* or an empty vector. Single colonies were propagated for ~50 generations before analysis.

**Table A.1: Genes over-expressed in an *est5-1* strain.** High-copy plasmids containing each gene under control of the ADH promoter were transformed into an *est5-1* strain and propagated for ~50 generations to assess viability.

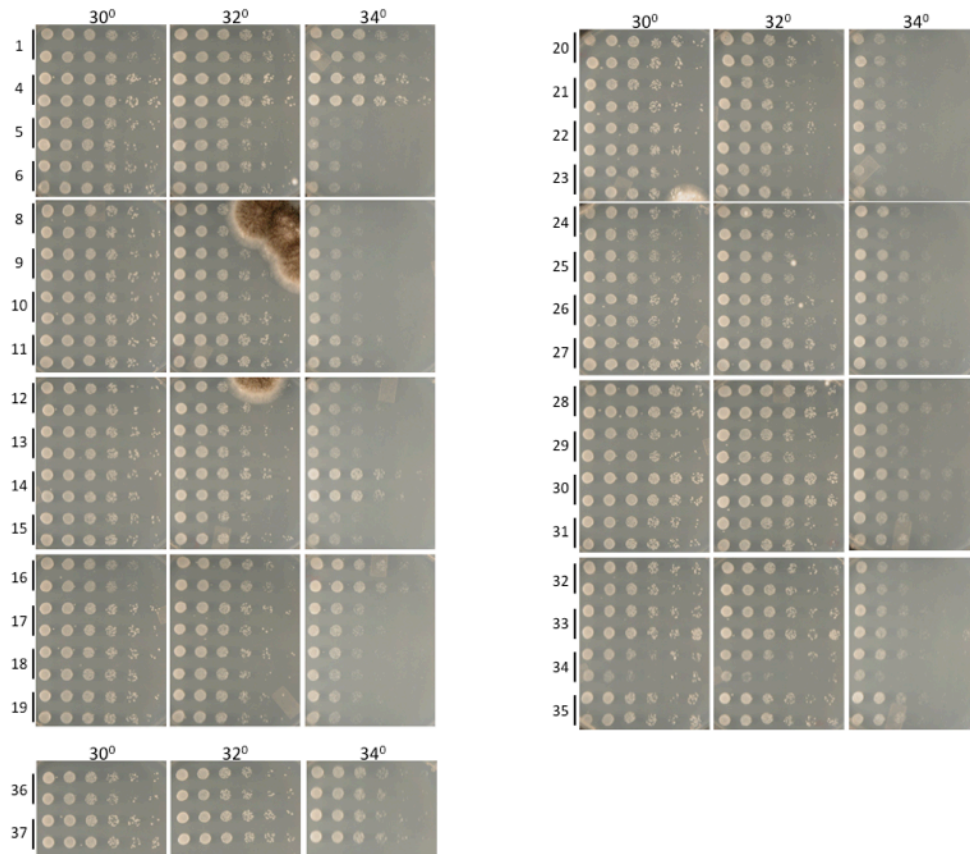
GENE	VIABILITY
<i>EST5</i>	+++
<i>CDC45</i>	-
<i>CDC7</i>	-
<i>CDC9</i>	-
<i>CSM2</i>	-
<i>DDC1</i>	+
<i>EST1</i>	-
<i>EST2</i>	-
<i>EST3</i>	-
<i>MEC1</i>	-
<i>MEC3</i>	+
<i>POL1</i>	-
<i>POL12</i>	-
<i>POL30</i>	-
<i>POL32</i>	-
<i>PRI1</i>	-
<i>PRI2</i>	-
<i>PSY3</i>	-
<i>RAD17</i>	-
<i>RAD27</i>	-
<i>RFC1</i>	-
<i>RFC2</i>	-
<i>RFC3</i>	-
<i>RFC4</i>	-
<i>RIF1</i>	-
<i>RIF2</i>	-
<i>RPA</i>	++
<i>SHU2</i>	-
<i>STN1</i>	-
<i>TEN1</i>	-



**Figure A.2: Selected pictures of growth of genes over-expressed in an *est5-1* strain.** High-copy plasmids containing each gene under the control of the ADH promoter were transformed into an *est5-1* strain and propagated for ~50 generations to assess viability. ADH-*EST5* rescues the senescence phenotype of *est5-1*, while Empty Vector and other genes do not. Some genes appear to have some alleviated senescence.



**Figure A.3: Over-expression of *RIF2* alleviates senescence.** A high-copy plasmid containing *RIF2* under the control of the ADH promoter was transformed into an *est1*- $\Delta$  strain and propagated for  $\sim$ 50 generations to assess viability.



**Figure A.4: Candidate plasmids from the 2 $\mu$  library retransformed into a *yku80*- $\Delta$  strain containing ADH-*est5-1*.** Plasmids were rescued from survivors of the 2 $\mu$  library screen and transformed into a *yku80*- $\Delta$  strain containing ADH-*est5-1* and plated on -Leu-Trp to select for both plasmids. After re-streaking on selective media, colonies were picked into 2ml selective media and serially diluted 1:5 and gridded on selective media at 30 $^{\circ}$ C, 32 $^{\circ}$ C, and 34 $^{\circ}$ C. Pictures were taken after 3 days of growth.

**Table A.2: Genomic inserts of candidate plasmids from 2 $\mu$  library.** Candidate plasmid inserts were analyzed by restriction mapping and sequencing. Sequencing from both ends of plasmid cloning sites identified the genomic region present in each plasmid.

Candidate	Genomic Insert
1	Ch. XIII bp772739-773617
4	<i>est5-1</i>
5	empty vector
6	<i>est5-1</i>
8	Ch. XV bp644999-645837 (DDP1, GET4)
9	<i>est5-1</i>
10	Ch. XV bp644999-645837 (DDP1, GET4)
11	Ch. XV bp644999-645837 (DDP1, GET4)
12	Ch. XV bp644999-645837 (DDP1, GET4)
13	Ch. XV bp644999-645837 (DDP1, GET4)
14	Ch. XI bp112450-113412
15	Ch. XV bp644999-645837 (DDP1, GET4)
16	empty vector
17	Ch. XV bp644999-645837 (DDP1, GET4)
18	Ch. XV bp644999-645837 (DDP1, GET4)
19	Ch. XV bp644999-645837 (DDP1, GET4)
20	Ch. XV bp644999-645837 (DDP1, GET4)
21	<i>est5-1</i>
22	Ch. XV bp644999-645837 (DDP1, GET4)
23	<i>est5-1</i>
24	<i>est5-1</i>
25	empty vector
26	Ch. XV bp644999-645837 (DDP1, GET4)
27	<i>est5-1</i>
28	<i>est5-1</i>
29	<i>est5-1</i>
30	<i>est5-1</i>
31	Ch. XV bp644999-645837 (DDP1, GET4)
32	Ch. XV bp644999-645837 (DDP1, GET4)
33	<i>est5-1</i>
34	<i>est5-1</i>
35	Ch. XIV bp546722-547610
36	Ch. XIII bp 810486-811313
37	empty vector



**APPENDIX B:**

Developing an assay to examine the effect of *EST5* on telomerase activity at collapsed replication forks

The Lundblad lab has recently shown that a collapsed replication fork, as it moves through telomeric DNA sequence, is a preferred substrate for telomerase (Paschini et al. submitted). Margherita Paschini, a former graduate student, developed an assay that can monitor telomerase activity in a single cell division by sequencing the DNA at this substrate (Paschini 2015). She placed the DNA sequence of a native telomere ~25 Kbps from the natural chromosome terminus and ~ 7 Kbps downstream of a strong origin of replication (ARS922). The portion of the chromosome downstream of the inserted sequence is non-essential, meaning that loss of this region would not result in lethality. Additionally, the gene *ADE2* was moved from its genomic locus and inserted downstream of the telomeric sequence. Yeast strains that lose the *ADE2* gene accumulate a red pigment, allowing for a visual readout of when a fork collapse occurred during replication through this region. If the fork collapse occurred in the first cell division, it will give rise to a colony that is half white and half red. A schematic of this strain is shown in Figure B.1A. It is possible to sequence the DNA from the red portion of this colony by PCR amplification of the region, followed by cloning of the PCR product into a TA cloning vector. By aligning the DNA sequences retrieved from these clones with the sequence of the interstitial telomere tract, one can see where the fork collapsed occurred and where telomerase acted by observing the divergence in DNA sequence (Figure B.1B). In yeast, telomerase adds degenerative repeats, meaning it does not utilize the full template each time it add nucleotides, so sequence added by telomerase, after replication, diverges from inherited DNA sequences. Therefore, DNA sequence that diverges from the parental sequence (internal telomeric tract), yet is homologous to all clones, is indicative of nucleotides added by telomerase in the first cell division (Figure

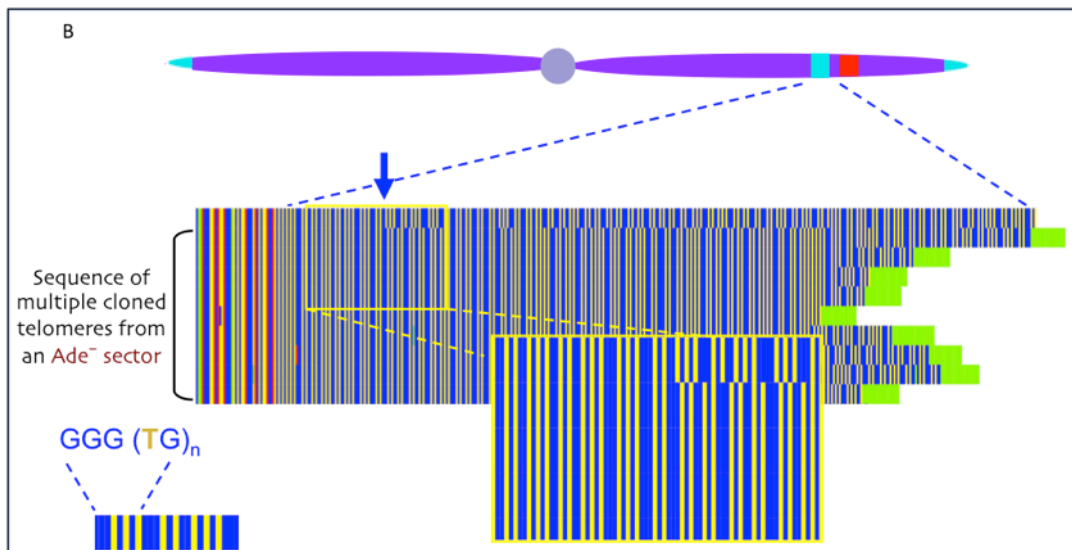
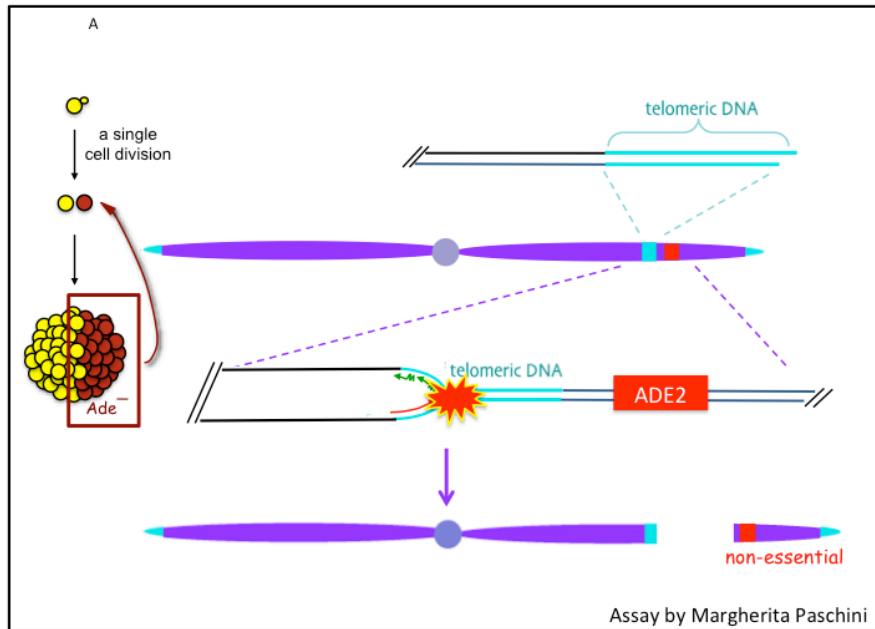
B.1C). By exploiting this property of yeast telomerase in this replication fork assay (RepFC), one can observe the extent and frequency of elongation events in one cell division. Aligning the sequences of ~10-12 clones from a single half-sector provides enough data to draw conclusions about how telomerase acted during the fork collapse that occurred in the first cell division (i.e. did it act, and if so, how many nucleotides did it add). Generating this data for 30-40 half-sectors allows for conclusions to be drawn regarding how frequently telomerase acts at a collapsed replication fork in a telomere. Comparing the RepFC data from a wild-type strain to an *est5*<sup>-</sup> mutant strain should provide insights about how *EST5* affects telomerase activity.

The challenge in implementing the RepFC assay to examine telomerase activity in a senescent strain background (i.e. *est5-1*) is that as the cells propagate, telomeres continue to shorten, eliminating the nucleotide sequences necessary to retrieve useful data. To overcome this, I developed a strategy to express the mutant gene, yet maintain telomere length after the fork collapse and first cell division occur. I transformed the appropriate RepFC strain with a high-copy plasmid containing the mutant gene, expressed by a galactose inducible promoter. Growing this strain in the presence of galactose over-expresses the mutant gene, ensuring the mutant protein out-competes the wild-type protein. The cells are then plated for single colonies on rich media containing glucose and lacking galactose, effectively turning off expression of the mutant gene yet ensuring the mutant protein was present during the first cell division. As the cells continue to divide, only the wild-type protein is expressed, allowing the cell to maintain its telomere length. During the first cell division, telomerase is acting in the presence of the mutant protein and the sequence it adds is inherited in subsequent cell divisions when

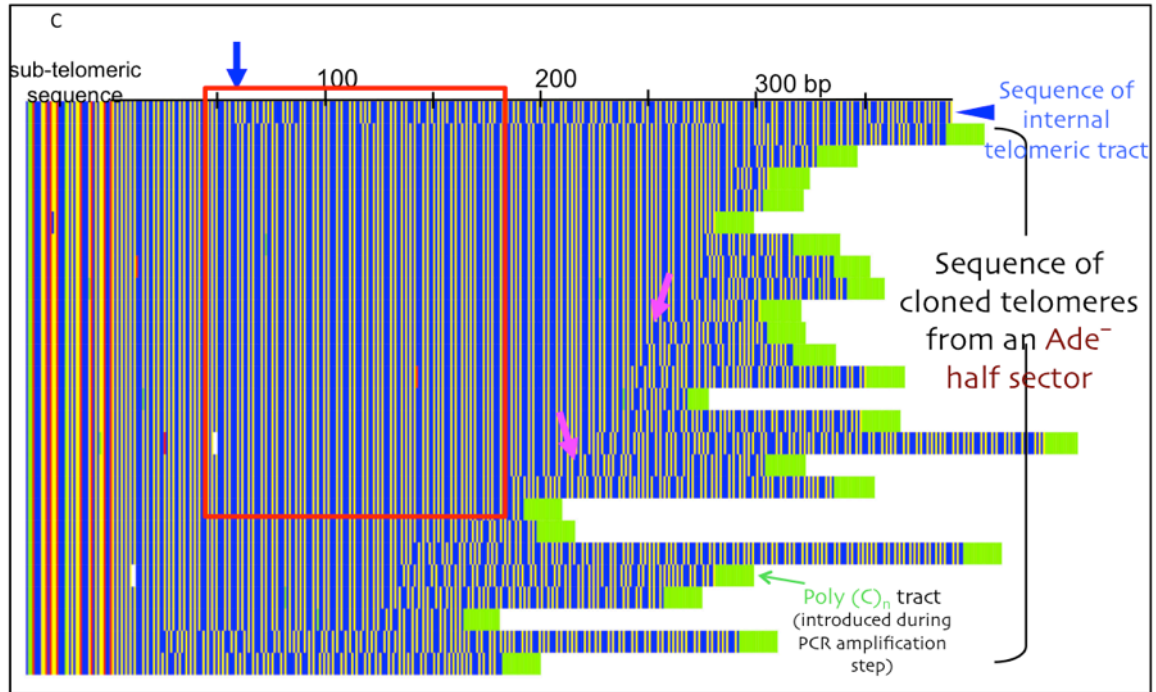
telomerase is acting in a wild-type situation. Because the newly formed telomere is maintained with each cell division, the inherited sequence can be observed.

While preliminary data (not shown) suggests this strategy will be effective, I also have an alternative approach. The concept is the same, but in this situation, the mutant gene is integrated into the genome and the strain is transformed with a high-copy plasmid containing the wild-type gene expressed by an inducible galactose promoter. The strain is grown to repress the expression of the wild-type gene and then plated on media containing galactose. Again, during the first cell division, the mutant protein is present, but subsequent cell divisions occur in the presence of the wild-type protein. This alternative approach does have the advantage of the mutant being expressed at native levels, rather than over-expressed; however, this approach requires the replication fork collapse occurs on selective galactose media, which could potentially have an effect on the cells. Additionally, the galactose promoter does cause a basal level of expression, even in the absence of galactose, which means some low level of wild-type protein may be present in the cell during the first cell division.

## Figures



**Figure B.1: The RepFC assay captures telomerase activity in a single cell division.** (A) A schematic of the RepFC strain. An internal telomeric tract was placed ~25 Kbps from the natural terminus, down-stream of an efficient origin of replication. The *ADE2* gene was placed down-stream, such that a fork collapse event would give rise to viable, red colonies. (B) Nucleotides added by telomerase following a fork collapse leads to a divergence in sequence from the parental strain. The top row of sequence comes from the internal telomeric tract. The divergence in sequence of the clones below the parental sequence indicate where telomerase acted, rather than sequence inherited through DNA replication. (C) Sequence that diverges from the parent, yet is homologous to each clone, indicates sequence added by telomerase in the first cell division when the replication fork collapse occurred (indicated by the red box).



**Figure B.1: The RepFC assay captures telomerase activity in a single cell division (continued).**

## **Appendix C:**

Applying ODN to another gene: *RAD51*

The ODN strategy was extremely successful in identifying *sof* mutations in telomerase, so to determine if ODN could be applied more broadly we decided to mutagenize other genes involved in DNA replication and repair. Among those genes was *RAD51*, which encodes a protein involved in DNA recombination, replication, and repair (Ha et al. 2012). By over-expressing *RAD51* mutations in different strain backgrounds, I was able to identify *sof* mutations in more than one pathway. Some of the ODN mutations confirmed previously published results, and others identify new functionally important surface residues.

## Results

Along with an undergraduate summer intern, Catherine Shir, we made 138 missense mutations in *RAD51* in an over-expression plasmid. The mutations were first chosen based on conservation from a protein sequence alignment of 16 yeast strains and *H. sapiens* (data not shown), targeting charged residues as well as Phe, Tyr, Asn, and Gln., then mapped on the structure of Rad51 to ensure they were on the surface of the protein. Charged amino acids were mutated to the opposite charge, Asn and Gln were mutated to both Glu and Lys, and Phe and Tyr mutated to Glu.

The goal was to identify mutations in *RAD51* that affect replication fork progression, so I chose to over-express the mutations in strains that had temperature-sensitive mutations in DNA replication genes and expose the strains to non-permissive temperatures and observe growth. I also subjected mutants to replication stress with the use of hydroxyurea.



*A DNA polymerase delta temperature sensitive strain reveals ODN and ODP mutations*

I transformed the collection of *RAD51* over-expression mutant plasmids into a strain bearing a temperature sensitive mutation in the catalytic subunit of polymerase delta (*cdc2-2*). Over-expression of *RAD51* in this strain does not show any growth defect at permissive temperatures, but growth becomes impaired at non-permissive temperatures (~31°C) (Figure C.1A; Table C.1). Mutations that, when over-expressed, interfere with the activity of wild type Rad51 display a growth defect even at permissive temperatures. 33 mutations were unable to grow at the permissive temperature of 28°C. Seven of those mutants were so severe their growth was reduced even at 25°C.

Interestingly, two mutations (D117K, D130K) actually enhanced the growth of the strain at non-permissive temperatures (Figure C.1B; Table C.1). Despite over-expression of *RAD51* displaying reduced growth at 31°C, these over-expression dominant positive (ODP) mutations grew almost as well at non-permissive temperatures as they did at lower temperatures, suggesting *RAD51* might play both a positive and negative regulatory role in DNA replication.

Many of these mutations were also transformed into another temperature sensitive strain (*cdc9-1*), defective in the DNA replication pathway, and as expected, the resulting phenotypes were the same as observed in the *cdc2-2* strain (data not shown).

*A lethal replication fork stability strain (sgs1-Δ mus81-Δ) is rescued by selected rad51 missense mutations*

Deletion of two genes involved in replication fork stability (*SGS1* and *MUS81*) results in lethality, however, deletion of *RAD51* in this strain restores viability.

Therefore, I was able to use a *sgs1-Δ mus81-Δ* strain to screen for *rad51*<sup>-</sup> mutations that, when over-expressed, could rescue the lethal phenotype. Because wild type *RAD51* was still present, this argued that a mutation that resulted in viable growth was affecting a specific biochemical activity of Rad51. I identified 43 *RAD51* mutations that rescued the viability of the *sgs1-Δ mus81-Δ* strain, 5 of which improved growth significantly (Figure C.2; Table C.1).

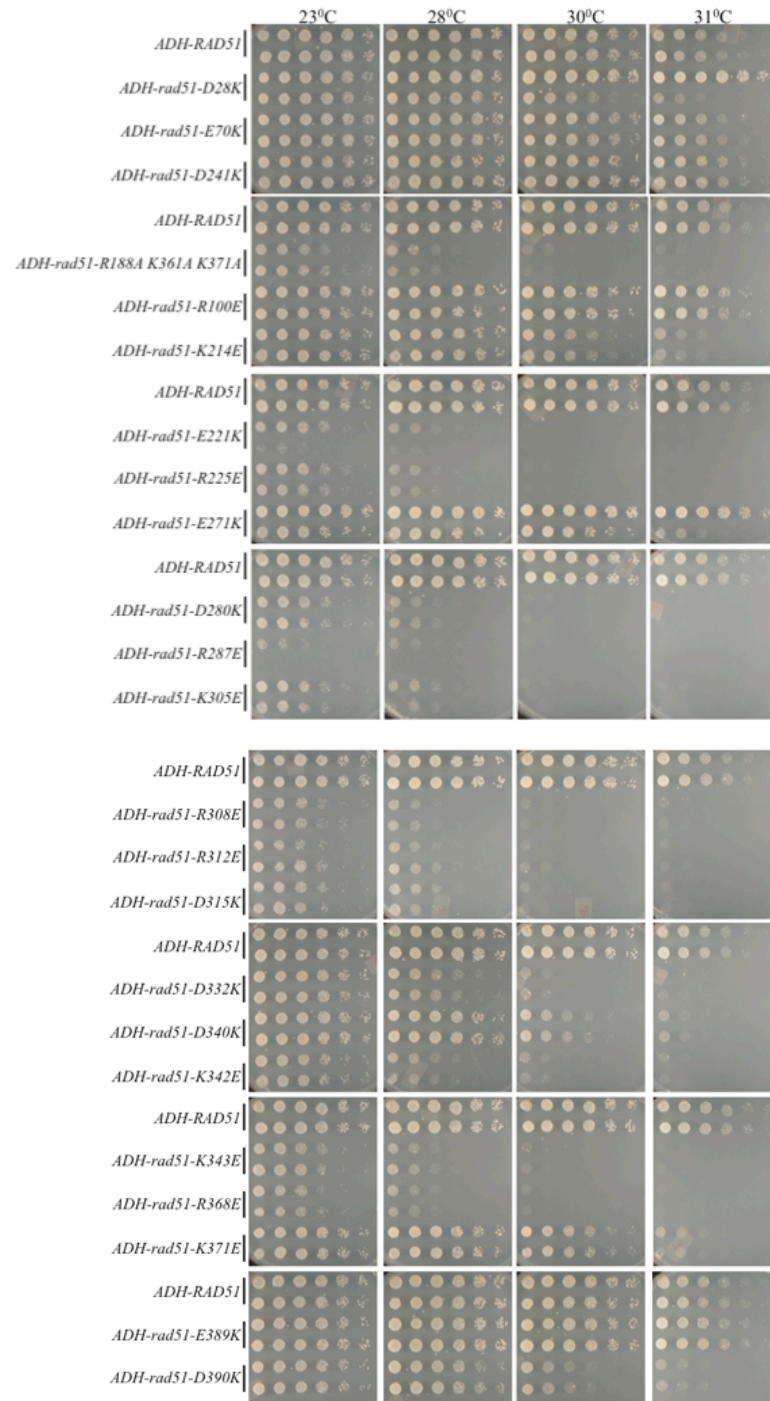
Interestingly, 3 mutations (K128E, R273E, H302) showed a growth defect in the *cdc2-2* strain at non-permissive temperatures but did not display a phenotype in the *sgs1-Δ mus81-Δ* strain. Conversely, there were 4 other mutations (N325E, N325K, H352A, R357E) that displayed a mutant phenotype in the *sgs1-Δ mus81-Δ* strain, yet behaved like wild type in the *cdc2-2* strain (Table C.1). Together, these data suggest I was able to identify *sof* alleles in *RAD51* that behave in distinct pathways.

#### *Growth of ODN mutations exposed to hydroxyurea correlates with the other growth assays*

I also transformed the *RAD51* mutant collection into a *rad51-Δ* strain and exposed the cells to hydroxyurea (HU), which depletes dNTP pools and causes replication stress (Koç et al. 2004). The mutations that showed growth phenotypes in this assay correlated with those that had phenotypes in the other growth assays (Table C.1), further confirming these residues are important for the role Rad51 plays in DNA replication.

## Figures

A



**Figure C.1: Over-expression of *rad51* mutations in a *cdc2-2* strain.** High-copy plasmids containing *rad51* mutations under the control of the ADH promoter were transformed into a *cdc2-2* temperature-sensitive strain and assessed for viability. (A) Pictures taken after 2 days. (B) Pictures taken after 3 days. (C) Pictures taken after 4 days.

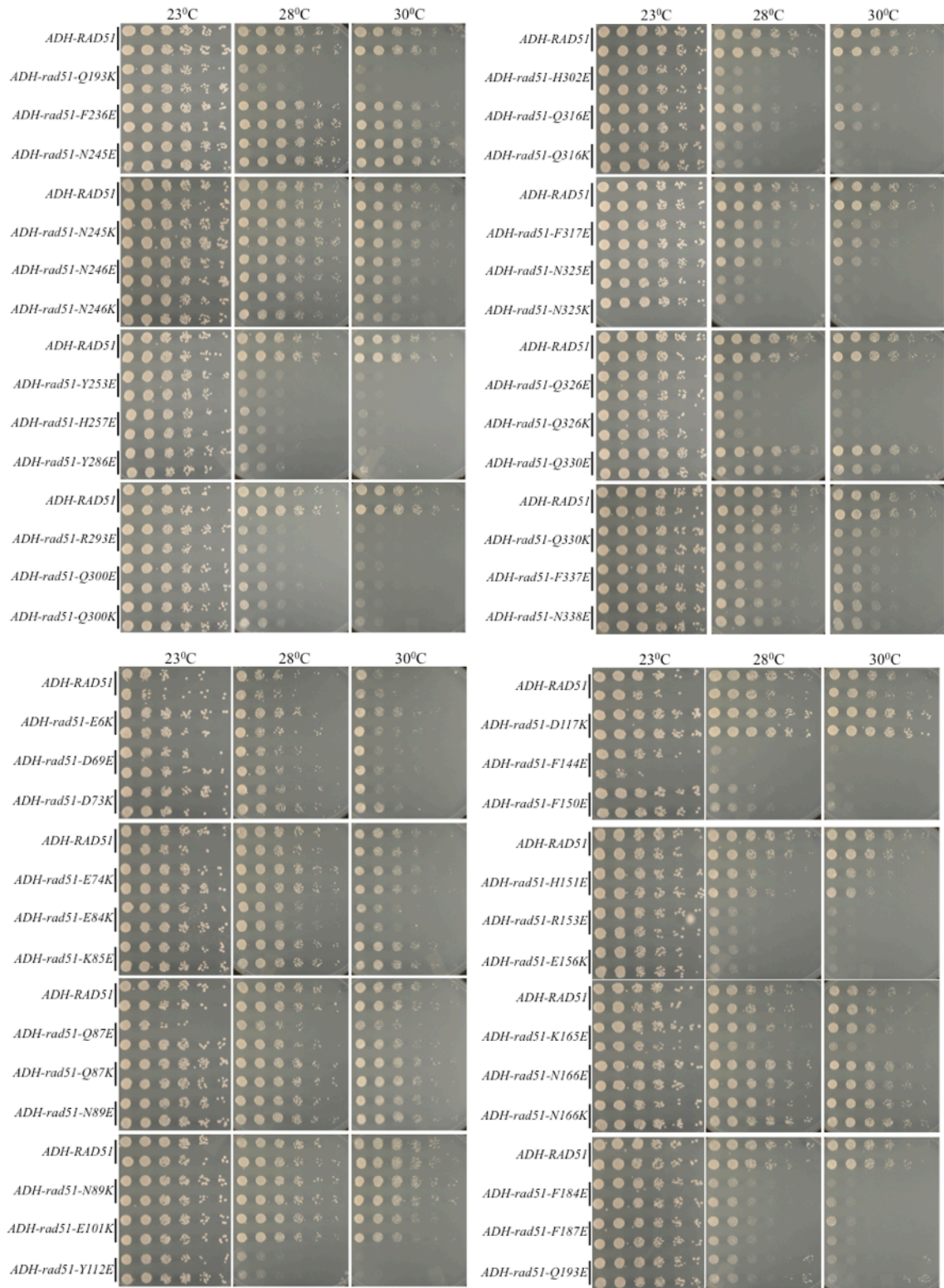


Figure C.1: Over-expression of *rad51* mutations in a *cdc2-2* strain (continued).

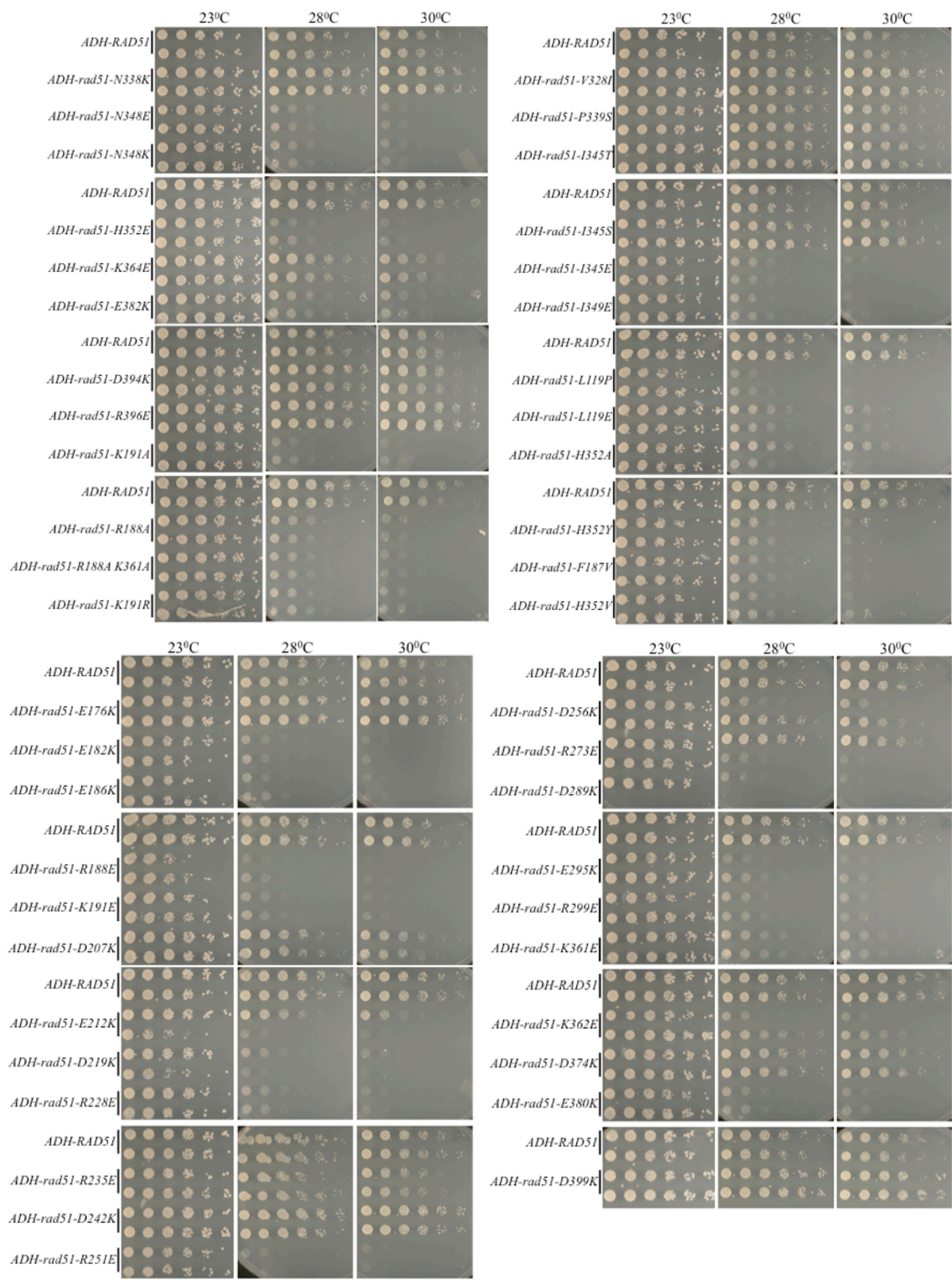


Figure C.1: Over-expression of *rad51* mutations in a *cdc2-2* strain (continued).

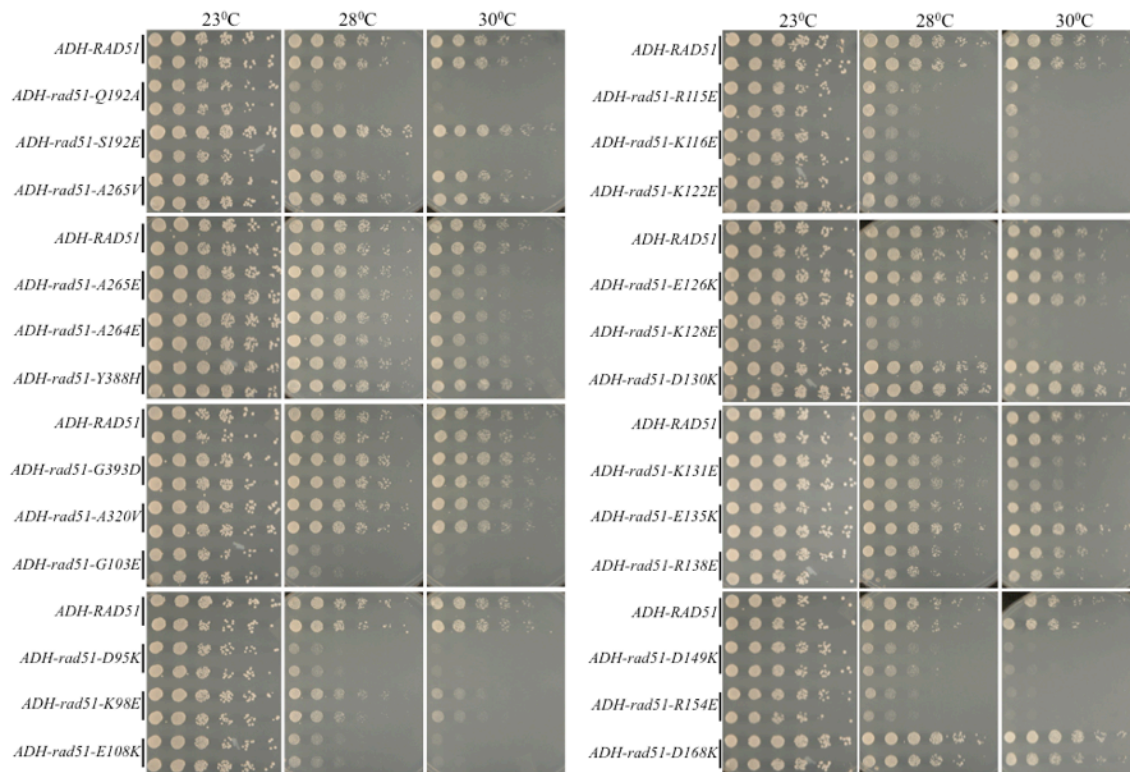


Figure C.1: Over-expression of *rad51* mutations in a *cdc2-2* strain (continued).

B

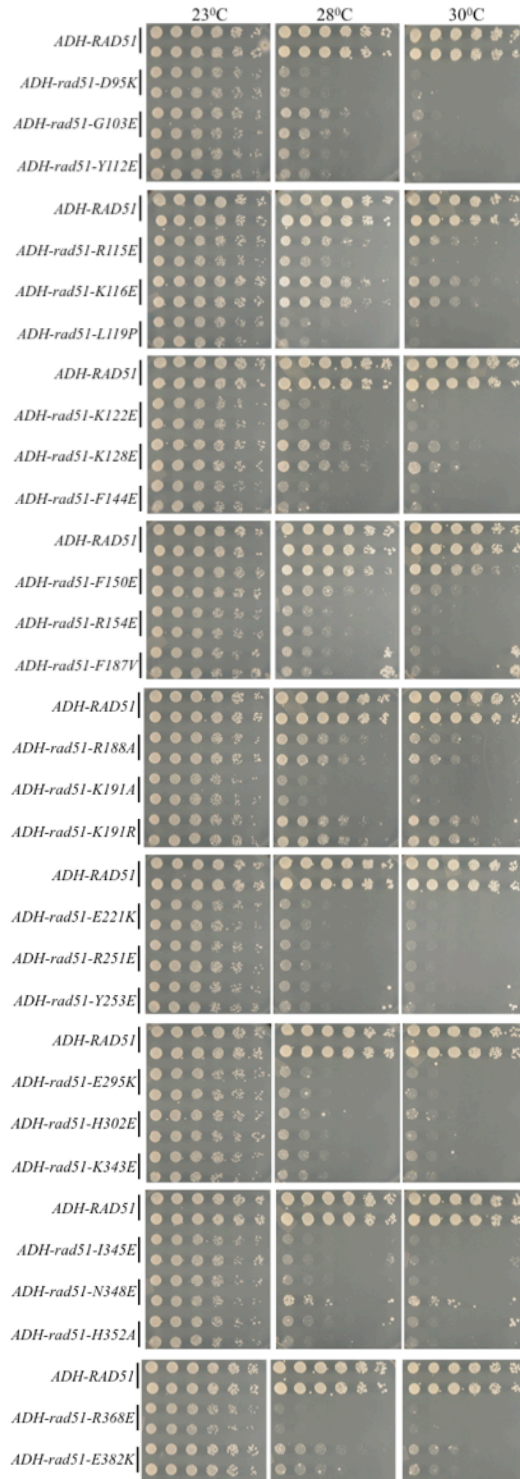


Figure C.1: Over-expression of *rad51T* mutations in a *cdc2-2* strain (continued).

C

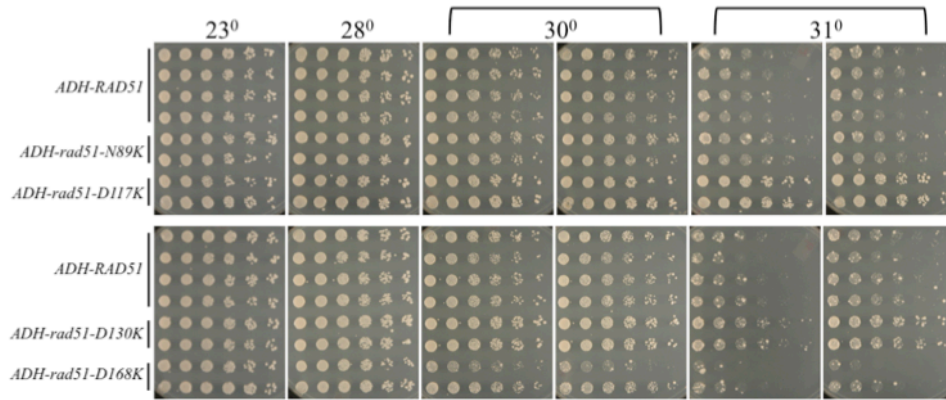
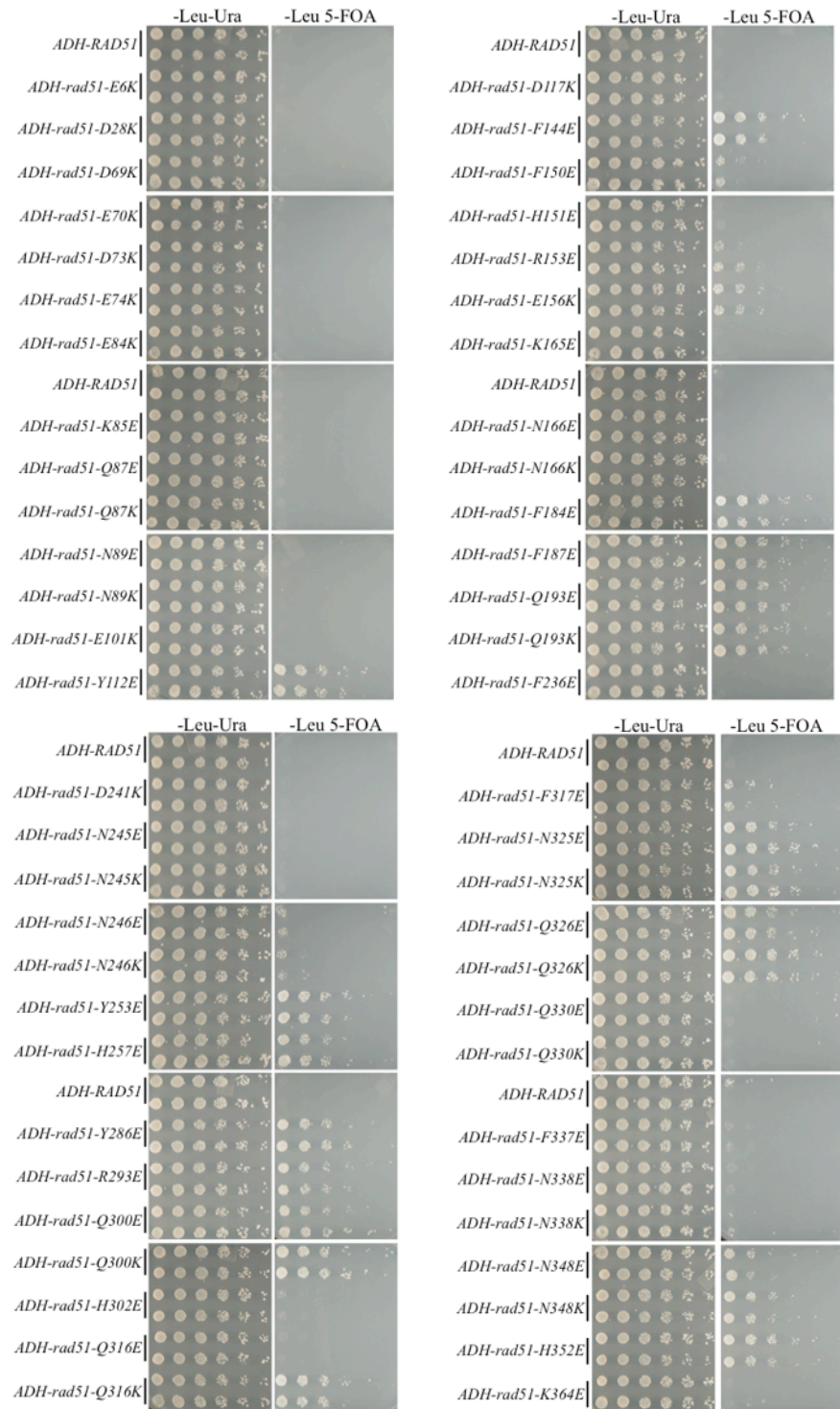


Figure C.1: Over-expression of *rad51* mutations in a *cdc2-2* strain (continued).



A



**Figure C.2: Over-expression of *rad51* mutations in an *sgs1*- $\Delta$  *mus81*- $\Delta$  strain.** High-copy plasmids containing *rad51* mutations under the control of the ADH promoter were transformed into an *sgs1*- $\Delta$  *mus81*- $\Delta$  strain containing an *SGS1* covering plasmid. Upon loss of the *SGS1* covering plasmid (on 5-FOA), the strain is inviable, unless *RAD51* is impaired. (A) Pictures taken after 3 days. (C) Pictures taken after 3 and 5 days.

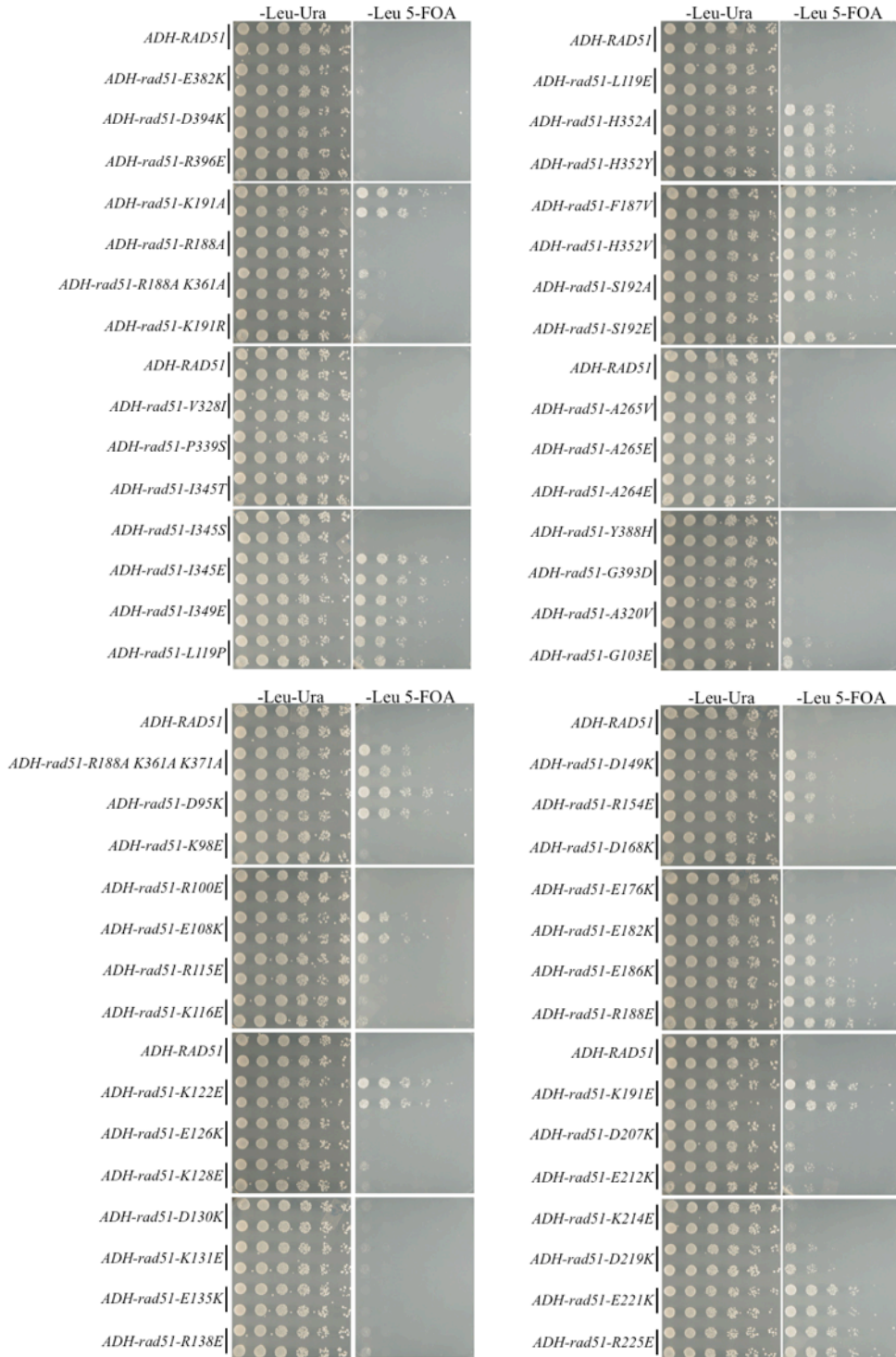


Figure C.2: Over-expression of *rad51* mutations in an *sgs1*- $\Delta$  *mus81*- $\Delta$  strain (continued).

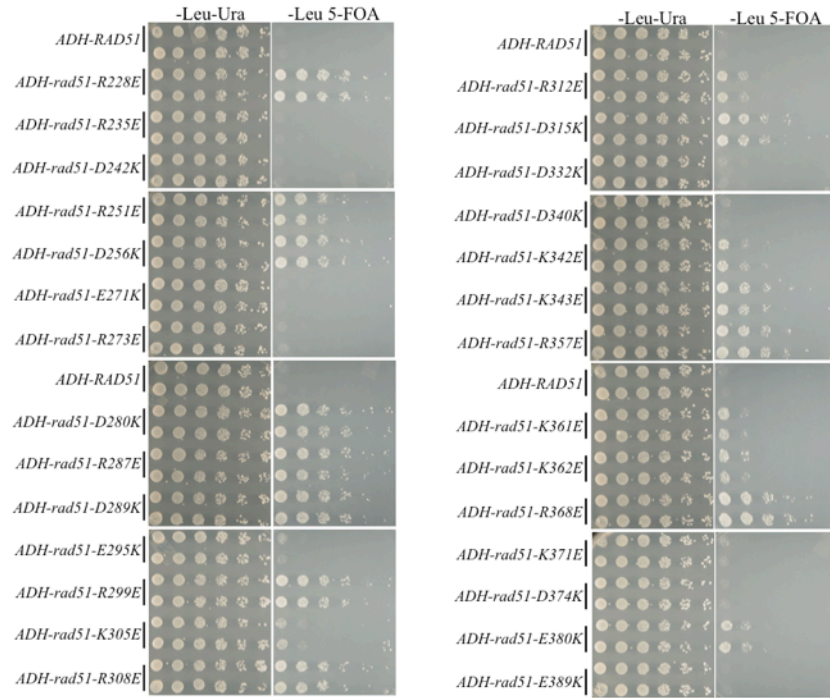


Figure C.2: Over-expression of *rad51* mutations in an *sgs1*- $\Delta$  *mus81*- $\Delta$  strain (continued).

B

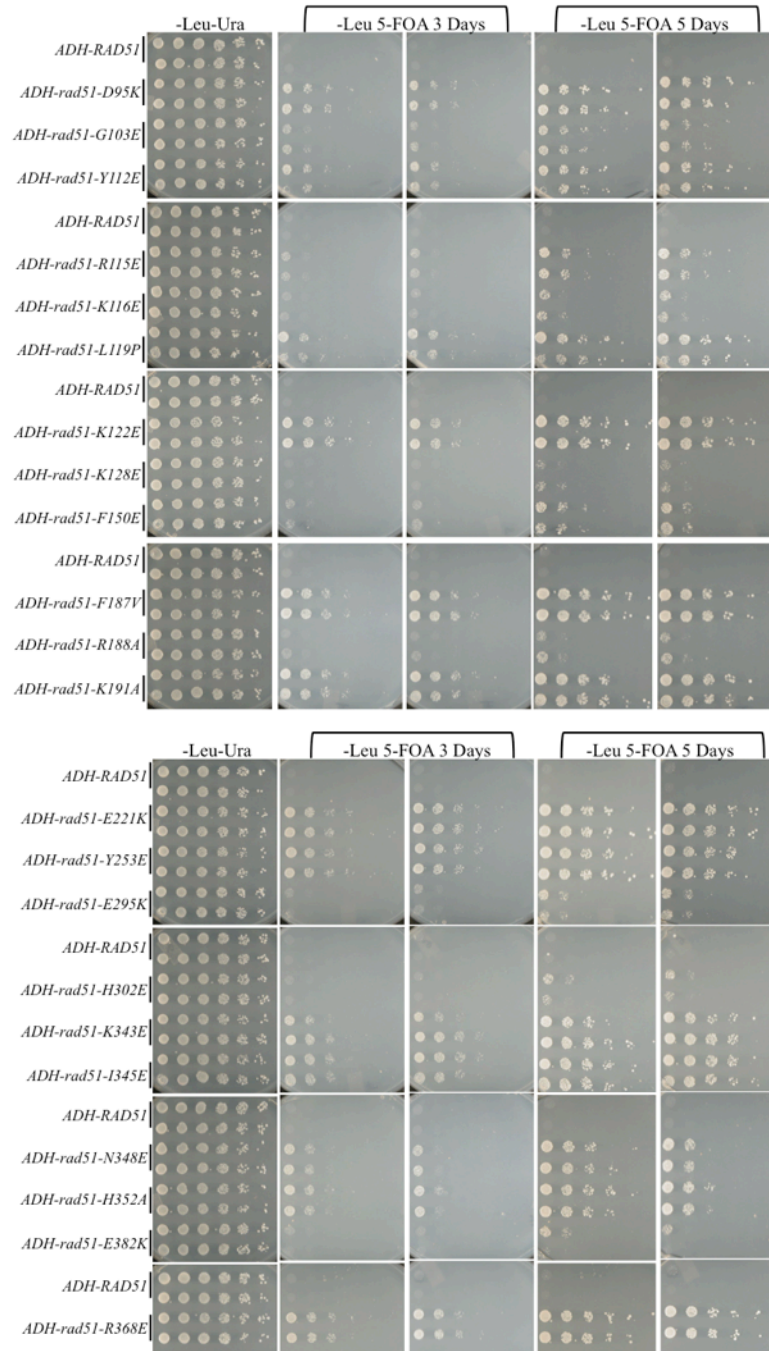


Figure C.2: Over-expression of *rad51T* mutations in an *sgs1-Δ mus81-Δ* strain (continued).

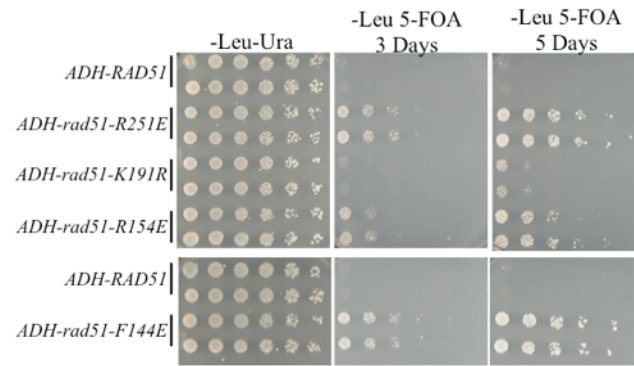


Figure C.2: Over-expression of *rad51* mutations in an *sgs1*- $\Delta$  *mus81*- $\Delta$  strain (continued).

**Table C.1: Summary of the *rad51* mutant phenotypes.**

Mutation	<i>cdc9-1</i>	<i>cdc2-2</i>	<i>sgs1-Δ mus81-Δ</i>	Hydroxyurea
E6K		Blue	Blue	
D28K		Blue	Blue	
D69K		Blue	Blue	
E70K		Blue	Blue	
D73K		Blue	Blue	
E74K		Blue	Blue	
E84K		Blue	Blue	
K85E		Blue	Blue	
Q87E		Blue	Blue	
Q87K		Blue	Blue	
N89E		Blue	Blue	
N89K		Blue	Blue	
D95K	Red	Red	Red	Red
K98E		Orange	Blue	Blue
R100E		Blue	Blue	
E101K		Blue	Blue	
G103E	Red	Red	Orange	Red
E108K	Red	Red	Orange	Red
Y112E	Red	Red	Red	Red
R115E		Orange	Orange	Red
K116E	Red	Red	Orange	Blue
D117K		Green	Blue	Blue
L119P	Red	Red	Red	Red
L119E		Orange	Blue	Blue
K122E		Orange	Red	Red
E126K		Blue	Blue	Blue
K128E	Red	Red	Blue	Red
D130K		Green	Blue	Blue
K131E		Blue	Blue	
E135K		Blue	Blue	
R138E		Blue	Blue	
D149K		Orange	Orange	Red
F144E	Red	Red	Orange	Red
F150E	Red	Red	Orange	Red
H151E		Blue	Blue	Orange
R153E	Red	Red	Orange	Red
R154E	Red	Red	Orange	Red
E156K	Red	Red	Orange	Red
K165E		Blue	Blue	
N166E		Blue	Blue	
N166K		Blue	Blue	
D168K		Blue	Blue	
E176K		Blue	Blue	
E182K	Red	Red	Orange	Red

**Table C.1: Summary of the *rad51* mutant phenotypes (continued).**

Mutation	<i>cdc9-1</i>	<i>cdc2-2</i>	<i>sqs1-Δ mus81-Δ</i>	Hydroxyurea
<b>WALKER A BOX</b>				
F184E		Orange	Red	Red
E186K		Orange	Red	Red
F187E		Orange	Red	Red
F187V		Orange	Red	Red
R188E		Orange	Red	Red
R188A	Red	Red	Blue	White
R188A K361A K371A	Red	Red	Orange	Red
K191A	Purple	Purple	Purple	Red
S192A	Purple	Purple	Purple	Red
Q193K	Red	Red	Red	Red
Q193E		Orange	Red	Red
D207K		Blue	Blue	White
E212K		Orange	Orange	White
K214E		Blue	Blue	White
D219K		Orange	Orange	White
E221K	Red	Red	Red	White
R225E	Red	Red	Red	White
R228E		Orange	Red	White
R235E		Blue	Blue	White
F236E		Blue	Blue	White
D241K		Blue	Blue	White
D242K		Blue	Blue	White
N245E		Blue	Blue	White
N245K		Blue	Blue	White
N246E		Blue	Blue	White
N246K		Blue	Blue	White
R251E	Red	Red	Red	Red
Y253E	Red	Red	Red	Red
D256K		White	Red	Red
H257E		Orange	Red	Red
A264E		Blue	Blue	White
A265V		Blue	Blue	White
A265E		Blue	Blue	White
E271K		Blue	Blue	White
R273E		Red	Blue	White
<b>WALKER B BOX</b>				
D280K	Red	Red	Red	White
Y286E		Orange	Red	Red
R287E	Red	Red	Red	Red
D289K		Orange	Red	Red
R293E		Red	Red	Red
E295K		Orange	Blue	Orange
R299E		White	Red	White
Q300E		Orange	Red	White

**Table C.1: Summary of the *rad51* mutant phenotypes (continued).**

Mutation	<i>cdc9-1</i>	<i>cdc2-2</i>	<i>sqs1-Δ mus81-Δ</i>	Hydroxyurea
Q300K	ODN-Strong	ODN-Mild	ODN-Strong	No phenotype
H302E	ODN-Strong	ODN-Mild	ODN-Strong	No phenotype
K305E	ODN-Strong	ODN-Mild	ODN-Strong	No phenotype
R308E	ODN-Strong	ODN-Mild	ODN-Strong	No phenotype
R312E	ODN-Strong	ODN-Mild	ODN-Strong	No phenotype
D315K	ODN-Strong	ODN-Mild	ODN-Strong	No phenotype
Q316E	ODN-Strong	ODN-Mild	ODN-Strong	No phenotype
Q316K	ODN-Strong	ODN-Mild	ODN-Strong	No phenotype
F317E	ODN-Strong	ODN-Mild	ODN-Strong	No phenotype
A320V	ODN-Strong	ODN-Mild	ODN-Strong	No phenotype
N325E	ODN-Strong	ODN-Mild	ODN-Strong	ODN-Strong
N325K	ODN-Strong	ODN-Mild	ODN-Strong	No phenotype
Q326E	ODN-Strong	ODN-Mild	ODN-Strong	No phenotype
Q326K	ODN-Strong	ODN-Mild	ODN-Strong	No phenotype
V328I	ODN-Strong	ODN-Mild	ODN-Strong	No phenotype
Q330E	ODN-Strong	ODN-Mild	ODN-Strong	No phenotype
Q330K	ODN-Strong	ODN-Mild	ODN-Strong	No phenotype
D332K	ODN-Strong	ODN-Mild	ODN-Strong	No phenotype
F337E	ODN-Strong	ODN-Mild	ODN-Strong	No phenotype
N338E	ODN-Strong	ODN-Mild	ODN-Strong	No phenotype
N338K	ODN-Strong	ODN-Mild	ODN-Strong	No phenotype
P339S	ODN-Strong	ODN-Mild	ODN-Strong	No phenotype
D340K	ODN-Strong	ODN-Mild	ODN-Strong	No phenotype
K342E	ODN-Strong	ODN-Mild	ODN-Strong	No phenotype
K343E	ODN-Strong	ODN-Mild	ODN-Strong	No phenotype
I345T	ODN-Strong	ODN-Mild	ODN-Strong	No phenotype
I345S	ODN-Strong	ODN-Mild	ODN-Strong	No phenotype
I345E	ODN-Strong	ODN-Mild	ODN-Strong	No phenotype
N348E	ODN-Strong	ODN-Mild	ODN-Strong	No phenotype
N348K	ODN-Strong	ODN-Mild	ODN-Strong	No phenotype
I349E	ODN-Strong	ODN-Mild	ODN-Strong	No phenotype
H352E	ODN-Strong	ODN-Mild	ODN-Strong	No phenotype
H352A	ODN-Strong	ODN-Mild	ODN-Strong	No phenotype
H352Y	ODN-Strong	ODN-Mild	ODN-Strong	No phenotype
H352V	ODN-Strong	ODN-Mild	ODN-Strong	No phenotype
R357E	ODN-Strong	ODN-Mild	ODN-Strong	No phenotype
K361E	ODN-Strong	ODN-Mild	ODN-Strong	No phenotype
K362E	ODN-Strong	ODN-Mild	ODN-Strong	No phenotype
K364E	ODN-Strong	ODN-Mild	ODN-Strong	No phenotype
R368E	ODN-Strong	ODN-Mild	ODN-Strong	No phenotype
K371E	ODN-Strong	ODN-Mild	ODN-Strong	No phenotype
D374K	ODN-Strong	ODN-Mild	ODN-Strong	No phenotype
E380K	ODN-Strong	ODN-Mild	ODN-Strong	No phenotype
E382K	ODN-Strong	ODN-Mild	ODN-Strong	No phenotype
Y388H	ODN-Strong	ODN-Mild	ODN-Strong	No phenotype
E389K	ODN-Strong	ODN-Mild	ODN-Strong	No phenotype
D390K	ODN-Strong	ODN-Mild	ODN-Strong	No phenotype
G393D	ODN-Strong	ODN-Mild	ODN-Strong	No phenotype
D394K	ODN-Strong	ODN-Mild	ODN-Strong	No phenotype
R396E	ODN-Strong	ODN-Mild	ODN-Strong	No phenotype
D399K	ODN-Strong	ODN-Mild	ODN-Strong	No phenotype

N.T.	
No phenotype	
ODP	
ODN-Mild	
ODN-Moderate	
ODN-Strong	
ODN-Severe	



## **Appendix D:**

Applying the RepFC assay to monitor telomerase processivity *in vivo*

A major question in telomere biology is regarding the processivity of telomerase. While its activity has been studied *in vitro* (Cohn and Blackburn 1995), these studies fail to assess the role of regulatory subunits and their interactions have on processivity. Additionally, these experiments cannot make conclusions as to whether the observed nucleotide addition is the result of one processive telomerase molecule, or several successive elongation events by multiple telomerase molecules.

To study telomerase processivity *in vivo*, the Lingner lab used an assay (2T-STEX) to determine the processivity of a single telomerase molecule by using an alternative template sequence in *Tlc1* (Chang et al. 2007). While their experimental design was elegant, they relied on strain mating and cell cycle timing to conclude “yeast telomerase is generally nonprocessive for repeat addition except at extremely short telomeres”, and had a rather small sample size of observable elongation events (~20).

In the Lundblad lab, using the RepFC assay described in Appendix B, we have seen extensive telomerase elongation events occur at telomeres of all lengths. This challenged some of the previous conclusions made by Chang et al. and warranted further investigation. By using the RepFC assay with an additional *TLCI* gene, bearing an alternative template sequence and integrated into the genome, I was able to visualize the activity of a single telomerase molecule acting during one cell division. My initial results confirmed their finding that telomerase is generally nonprocessive, however, this does not seem to be dependent on the length of the telomere.

## Results

Using the RepFC assay described previously, I integrated a second copy of *TLC1* into the genome with single nucleotide changes in its template region so that addition by this template would be distinct from the additions of wild-type telomerase. In this way, if telomerase is highly processive, one should observe only one TLC1 RNA template being used in the first cell division following a replication fork collapse. If one were to observe alternating wild-type and *tlc1<sup>-</sup>* sequence additions, as Chang et al. observed, this would argue that multiple telomerase molecules are acting on the same telomere and telomerase is non-processive.

Previous studies have shown telomerase is capable of incorporating nucleotides from a mutated TLC1 RNA sequence (Lin et al. 2004; Förstemann et al. 2003; Paschini 2015), so I used a viable template mutation (*tlc1-alt2*) when introducing the second *TLC1* into the genome (Figure D.1). The mutation was introduced into the template region of *TLC1* on a plasmid, which was then integrated into the genome of the RepFC strain, adjacent to the wild-type copy of *TLC1*.

### *tlc1-alt2* template mutations are incorporated in the RepFC assay

It has previously been observed that *tlc1-alt2* is capable of incorporating the alternative sequence to telomeric repeats (Paschini Thesis 2015) in a slightly different assay. I was also able to observe the incorporation of the alternative sequence in the RepFC assay (Figure D.2). I plated colonies of the RepFC strain containing *TLC1* and *tlc1-alt2* and sequenced the internal telomeric tract from the red portion of half-sectors, as previously described for the RepFC assay in Appendix B. Of the 8 half-sectors analyzed,

6 showed mutant sequence incorporation. Telomerase acted in the first cell division on two of these half sectors.

*Both wild-type and mutant templates are incorporated in a single cell division*

In both instances in which telomerase acted in the first cell division, both wild-type *TLC1* template sequence and *tlc1-alt2* template sequence was observed in this single elongation event (Figure D.3). These results are in-line with the results observed in Chang et al., and argue that multiple telomerase molecules act on a single telomere in one cell division.

*Template mutations affect telomere length homeostasis*

An important caveat to note in these experiments is the effect the template mutation had on telomere length homeostasis. Strains bearing different template mutations did show decreased telomere length phenotypes, and this was exacerbated when *TLC1* was not present (Figure D.4). The change in telomere length could be a result of decreased processivity of the mutant telomerase, or could be from the sequence change affecting telomere recognition by replication fork stabilizing proteins (i.e. t-RPA), and/or the structural stability of the telomere. I believe the latter explanation is more likely for two reasons. One, telomeres have evolved to have a specific sequence that distinguishes them from double strand breaks and allows them to be recognized by certain proteins. Altering this sequence undoubtedly has an effect on telomeric integrity. Secondly, the wild-type telomerase acted first, followed by the mutant in the half sector in Figure D.3B. If wild-type telomerase were highly processive, it would have had an

extensive elongation event and the mutant telomerase would not have acted. If the template mutation was the cause of the non-processive phenotype, I should have only observed an elongation event with alternating sequence if wild-type telomerase acted after the mutant failed to add repeated additions.

## **Discussion**

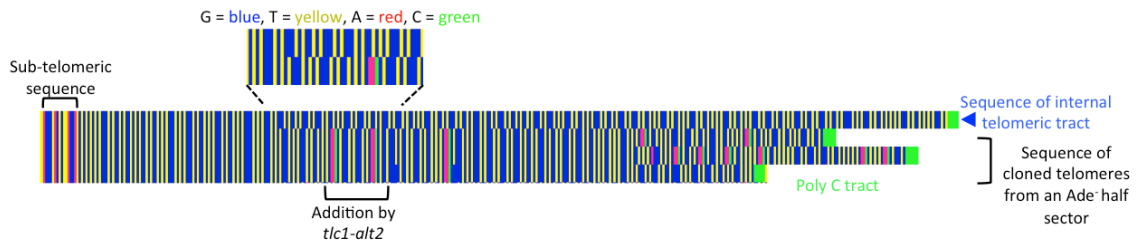
The RepFC assay allows for the observation of telomerase activity *in vivo* in a single cell division. In theory, this assay should help to answer long-standing questions about telomerase. The results from the experiments presented in this appendix are consistent with the conclusion made by Chang et al., that telomerase is non-processive. More than one telomerase acts on a single telomere in one cell division.

Unfortunately, the alternative templates in telomerase had a negative effect on telomere length regulation, which limited the usefulness of this experimental design for drawing further conclusions, such as how mutations in the telomerase proteins affect its processivity.

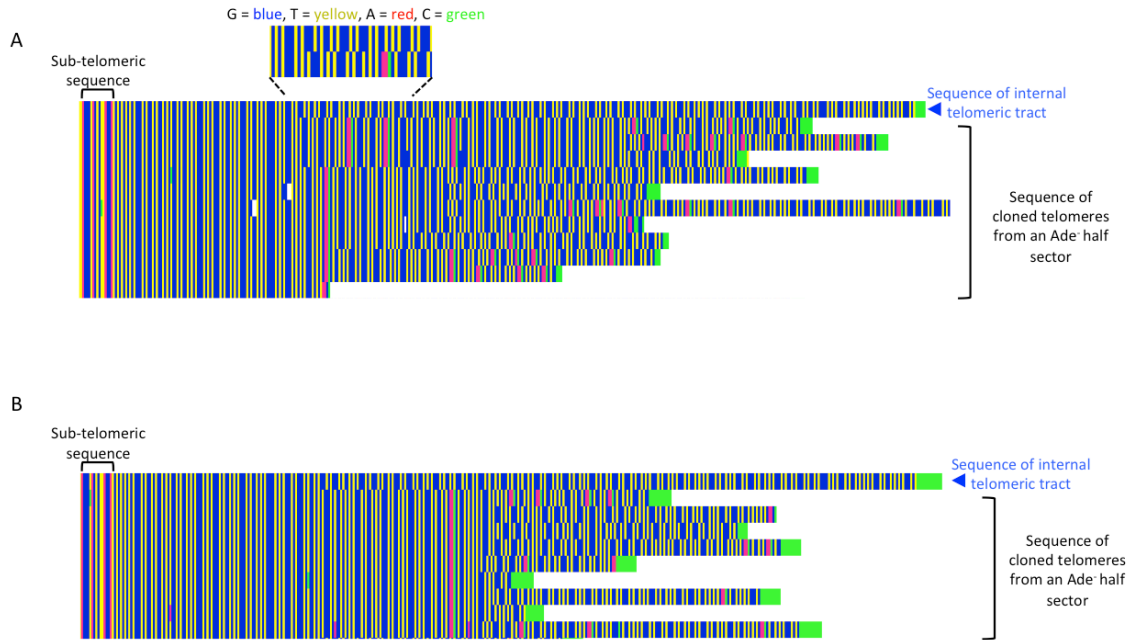
## Figures

WT TIC1:	3'-ACAC <u>CCAC</u> ACCAC-5'
WT telo repeat:	5'-TGTGGGGTGTGGTG-3'
<i>tcl1-alt2</i> :	3'-ACAC <u>TTG</u> CACCAC-5'
predicted telo repeat:	5'-TGTG <u>AAC</u> GTGGTG-3'

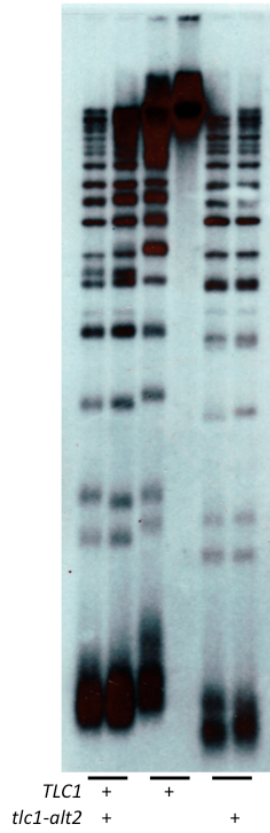
**Figure D.1: Mutation in the core template region of *TLC1* (adapted from Paschini Thesis 2015).** The *TLC1* template region (nt 472-479) is underlined, with the core sequence in bold. The mutation made is indicated in blue, with the predicted incorporation sequence in red.



**Figure D.2: Alternative template sequence is incorporated by *tcl1-alt2*.** An example of 3 cloned sequences, from a single red half-sector, aligned against the sequence of the telomeric tract. The point of sequence divergence indicates telomerase activity. The incorporation of the mutant nucleotides is where *tcl1-alt2* acted.



**Figure D.3: Both *TLC1* and *tlc1-alt2* add telomeric sequence at the same replication fork collapse event.** (A) and (B) are cloned sequences from two different red half-sectors. The sequence that is homologous to the clones, yet diverges from the internal telomeric tract, is indicative of where telomerase acted in the first cell division. Both wild-type and mutant sequence is incorporated, meaning more than one telomerase molecule acted on a single telomere. (B) Shows a replication fork collapse event where wild-type telomerase acted first, followed by the mutant.



**Figure D.4: Telomere length of the RepFC strains.** Telomere length assessment by southern blot of the strains used in the RepFC assay. The strains had either *TLC1*, *tlc1-alt2*, or both. *tlc1-alt2* caused a moderate telomere length defect that was exacerbated when *TLC1* was no longer present.



## REFERENCES

- Anderson, E.M., Halsey, W.A., and Wuttke, D.S. (2002). Delineation of the high-affinity single-stranded telomeric DNA-binding domain of *Saccharomyces cerevisiae* Cdc13. *Nucleic Acids Res* 30: 4305–4313.
- Antoniacci, L. M., Kenna, M. A., and R. V. Skibbens. (2007). The nuclear envelope and spindle pole body-associated Mps3 protein bind telomere regulators and function in telomere clustering. *Cell Cycle* 6: 75-79.
- Armanios, M. and Blackburn, E.H. (2012). The telomere syndromes. *Nat Rev Genet* 13: 693–704.
- Ashkenazy, H., Erez, E., Martz, E., Pupko, T., and Ben-Tal, N. (2010) ConSurf 2010: calculating evolutionary conservation in sequence and structure of proteins and nucleic acids. *Nucleic Acids Res* 38: W529-33.
- Askree, S.H., Yehuda, T., Smolikov, S., Gurevich, R., Hawk, J., Coker, C., Krauskopf, A., Kupiec, M., and McEachern, M.J. (2004). A genome-wide screen for *Saccharomyces cerevisiae* deletion mutants that affect telomere length. *PNAS* 101: 8658–8663.
- Baker, C. M., and Grant, G. H. (2007). Role of aromatic amino acids in protein-nucleic acid recognition. *Biopolymers* 85: 456–470.
- Ballew, B.J. and Lundblad, V. (2013). Multiple genetic pathways regulate replicative senescence in telomerase-deficient yeast. *Aging Cell* 12: 719-27.
- Beranek, D.T. (1990). Distribution of methyl and ethyl adducts following alkylation with monofunctional alkylating agents. *Mutat. Res.* 231: 11–30.
- Berjanskii, M.V. and Wishart, D.S. (2005). A simple method to predict protein flexibility using secondary chemical shifts. *J Am Chem Soc* 127: 14970–14971.
- Bianchi, A., S. Negrini, and Shore, D. (2004). Delivery of yeast telomerase to a DNA break depends on the recruitment functions of Cdc13 and Est1. *Mol. Cell* 16: 139–146.
- Blackburn, E. H. (1991). Structure and function of telomeres. *Nature* 350: 569–573
- Blackburn, E. H. (2001). Switching and signaling at the telomere. *Cell* 106: 661–673
- Bodnar, A.G., Ouellette, M., Frolkis, M., Holt, S.E., Chiu, C.P., Morin, G.B., Harley, C.B., Shay, J.W., Lichtsteiner, S., Wright, W.E. (1998). Extension of life-span by introduction of telomerase into normal human cells. *Science* 279: 349–352.
- Britt-Compton, B., Capper, R., Rowson, J., and Baird, D. M. (2009). Short telomeres are preferentially elongated by telomerase in human cells. *FEBS Lett.* 583: 3076–3080.
- Bupp, J. M., Martin, A. E., Stensrud, E. S., and S. L. Jaspersen. (2007). Telomere anchoring at the nuclear periphery requires the budding yeast Sad1-UNC-84 domain

- protein Mps3. *J Cell Biol.* 179: 845-854.
- Chang, M., Arneric, M., and Lingner, J. (2007). Telomerase repeat addition processivity is increased at critically short telomeres in a Tel1-dependent manner in *Saccharomyces cerevisiae*. *Genes Dev.* 21: 2485-2494.
- Chappell, A.S. and Lundblad, V. (2004). Structural elements required for association of the *Saccharomyces cerevisiae* telomerase RNA with the Est2 reverse transcriptase. *Mol Cell Biol* 24: 7720–7736.
- Chen K. and Tjandra, N. (2012). The use of residual dipolar coupling in studying proteins by NMR. *Top Curr Chem* 326: 47–67.
- Chen, C.C., Hwang, J.K., Yang, J.M. (2006). (PS)<sup>2</sup>: Protein structure prediction server. *Nucleic Acids Res* 34: W152-7.
- Chen, H., Xue, J., Churikov, D., Hass, E.P., Shi, S., Lemon, L.D., Luciano, P., Bertuch, A.A., Zappulla, D.C., Geli, V., Wu, J., and Lei, M. (2018). Structural insights into yeast telomerase recruitment to telomeres. *Cell* 172: 331-343.
- Cohn, M. and Blackburn, E. H. (1995). Telomerase in yeast. *Science* 269: 396–400.
- Croy, J.E. and Wuttke, D.S. (2006). Themes in ssDNA recognition by telomere-end protection proteins. *Trends Biochem Sci* 31: 516–525.
- Doreleijers, J.F., Sousa da Silva, A.W., Krieger, E., Nabuurs, S.B., Spronk, C.A., Stevens, T.J., Vranken, W.F., Vriend, G., and Vuister, G.W. (2012). CING: An integrated residue-based structure validation program suite. *J Biomol NMR* 54: 267-283.
- Dujon, B. (2010). Yeast evolutionary genomics. *Nat. Rev. Genet.* 11: 512–524.
- Engbrecht, J., Hirsch, J., and G.S. Roeder. (1990). Meiotic gene conversion and crossing over: their relationship to each other and to chromosome synapsis and segregation. *Cell* 62: 927-937.
- Esposito, D. and Chatterjee, D.K. (2006). Enhancement of soluble protein expression through the use of fusion tags. *Curr Opin Biotechnol* 17: 353–358.
- Evans, S. K. and Lundblad, V. (1999). Est1 and Cdc13 as comediators of telomerase access. *Science* 286: 117– 120.
- Evans, S.K. and Lundblad, V. (2002) The Est1 subunit of *Saccharomyces cerevisiae* telomerase makes multiple contributions to telomere length maintenance. *Genetics* 162: 1101–1115.
- Feng, J., Funk, W.D., Wang, S.S., Weinrich, S.L., Avilion, A.A., Chiu, C.P., Adams, R.R., Chang, E., Allsopp, R.C., Yu, J., *et al.* (1995). The RNA component of human

telomerase. *Science* 269: 1236–1241.

Ferguson, J. L., Chao, W. C., Lee, E., and Friedman, K. L. (2013). The anaphase promoting complex contributes to the degradation of the *S. cerevisiae* telomerase recruitment subunit Est1p. *PLoS One* 8: e55055.

Fernández, C. and Wider, G. (2003). TROSY in NMR studies of the structure and function of large biological macromolecules. *Curr. Opin. Struct. Biol.* 13: 570–580.

Fisher, T.S., Taggart, A.K., and Zakian, V.A. (2004). Cell cycle-dependent regulation of yeast telomerase by Ku. *Nat. Struct. Mol. Biol.* 11: 1198-1205.

Ford, A. S., Guan, Q., Neeno-Eckwall, E., and Culbertson, M. R. (2006). Ebs1p, a negative regulator of gene expression controlled by the Upf proteins in the yeast *Saccharomyces cerevisiae*. *Eukaryot. Cell* 5: 301–312.

Förstemann, K., Zaug, A.J., Cech, .T.R., and Lingner, J. (2003). Yeast telomerase is specialized for C/A-rich RNA templates. *Nucleic Acids Res.* 31:1646-55.

Fukuhara, N., Ebert, J., Unterholzner, L., Lindner, D., Izaurrealde, E., and Conti, E. (2005). SMG7 is a 14-3-3-like adaptor in the nonsense-mediated mRNA decay pathway. *Mol. Cell* 17: 537–547.

Gao, H., Cervantes, R. B., Mandell, E. K., Otero, J. H., and Lundblad, V. (2007). RPA-like proteins mediate yeast telomere function. *Nat. Struct. Mol. Biol.* 14: 208–214.

Gardner, K.H. and Kay, L.E. (1998). Modern Techniques in Protein NMR, eds Krishna NR, Berliner LJ (Plenum, New York), pp 27–74.

Gelinas, A. D., Paschini, M., Reyes, F. E., Heroux, A., Batey, R. T., Lundblad, V., and Wuttke, D.S. (2009). Telomere capping proteins are structurally related to RPA with an additional telomere-specific domain. *PNAS* 106: 19298– 19303.

Glaser F., Pupko, T., Paz, I., Bell, R.E., Bechor-Shental, D., Martz, E., and Ben-Tal, N. (2003). ConSurf: Identification of functional regions in proteins by surface-mapping of phylogenetic information. *Bioinformatics* 19: 163–164.

Greider, C. W. and Blackburn, E. H. (1987). The telomere terminal transferase of tetrahymena is a ribonucleoprotein enzyme with two kinds of primer specificity. *Cell* 51: 887–898.

Greider, C.W. (2016). Regulating telomere length from the inside out: the replication fork model. *Genes Dev.* 30: 1483–1491.

Güntert, P., Mumenthaler, C., and Wüthrich, K. (1997). Torsion angle dynamics for NMR structure calculation with the new program DYANA. *J Mol Biol* 273: 283–298.

- Ha, T., Kozlov, A.G. and Lohman, T.M. (2012). Single-Molecule Views of Protein Movement on Single-Stranded DNA. *Annu. Rev. Biophys* 41: 295-319.
- Hawkins, C., and Friedman, K. L. (2014). Normal telomere length maintenance in *Saccharomyces cerevisiae* requires nuclear import of the ever shorter telomeres 1 (Est1) protein via the importin alpha pathway. *Eukaryot. Cell* 13: 1036–1050.
- Helder, S., Blythe, A. J., Bond, C. S., and Mackay, J. P. (2016). Determinants of affinity and specificity in RNA-binding proteins. *Curr. Opin. Struct. Biol.* 38: 83–91.
- Herskowitz, I. (1987). Functional inactivation of genes by dominant negative mutations. *Nature* 329: 219–222.
- Holm, L. and Rosenström, P. (2010). Dali server: Conservation mapping in 3D. *Nucleic Acids Res* 38: W545-9.
- Hsu, M., Yu, E. Y., Spruňanský, O., McEachern, M. J., and Lue, N. F. (2012). Functional analysis of the single Est1/Ebs1 homologue in *Kluyveromyces lactis* reveals roles in both telomere maintenance and rapamycin resistance. *Eukaryot. Cell* 11: 932–942.
- Hug, N. and Lingner, J. (2006). Telomere length homeostasis. *Chromosoma* 115: 413–425.
- Jiang, J., Chan, H., Cash, D.D., Miracco, E.J., Loo, R. R., Upton, H.E., Cascio, D., Johnson, R.O., Collins, K., Loo, J.A., Zhou, Z.H., and Feigon, J. (2015). Structure of *Tetrahymena* telomerase reveals previously unknown subunits, function, and interactions. *Science* 350: 6260.
- Jones, S., Daley, D. T. A., Luscombe, N. M., Berman, H. M., and Thornton, J. M. (2001). Protein–RNA interactions: a structural analysis. *Nucleic Acids Res.* 29: 943–954.
- Kim, N.W., Piatyszek, M.A., Prowse, K.R., Harley, C.B., West, M.D., Ho, P.L., Coviello, G.M., Wright, W.E., Weinrich, S.L., and Shay, J.W. (1994). Specific association of human telomerase activity with immortal cells and cancer. *Science* 266: 2011–2015.
- Koç, A., Wheeler, L.J., Mathews, C.K., and Merrill, G.F. (2004). Hydroxyurea Arrests DNA Replication by a Mechanism That Preserves Basal dNTP Pools. *J. Biol. Chem.* 279: 223-230.
- Landau, M., Mayrose, I., Rosenberg, Y., Glaser, F., Martz, E., Pupko, T., and Ben-Tal, N. (2005) ConSurf 2005: The projection of evolutionary conservation scores of residues on protein structures. *Nucleic Acids Res.* 33: W299-302.
- Lange, O.F., Rossi, P., Sgourakis, N.G., Song, Y., Lee, H.W., Aramini, J.M., Ertekin, A., Xiao, R., Acton, T.B., Montelione, G.T., and Baker, D. (2012). Determination of solution structures of proteins up to 40 kDa using CS-Rosetta with sparse NMR data

- from deuterated samples. *PNAS* 109: 10873–10878.
- Laskowski, R.A., MacArthur, M.W., Moss, D.S., and Thornton, J.M. (1993). PROCHECK: A program to check the stereochemical quality of protein structures. *J. Appl. Cryst.* 26: 283-291.
- Lee, J. S., Mandell, E. K., Tucey, T. M., Morris, D. K., and Lundblad, V. (2008). The Est3 protein associates with yeast telomerase through an OB-fold domain. *Nat. Struct. Mol. Biol.* 15: 990–997.
- Lee, J., Mandell, E.K., Rao, T., Wuttke, D.S., and Lundblad, V. (2010). Investigating the role of the Est3 protein in yeast telomere replication. *Nucleic Acids Res* 38: 2279–2290.
- Lemieux, B., Laterreur, N., Perederina, A., Noël, J. F., Dubois, M. L., Krasilnikov, A.S., and Wellinger, R.J. (2016). Active yeast telomerase shares subunits with ribonucleoproteins RNase P and RNase MRP. *Cell* 165: 1171– 1181.
- Lendvay, T. S., Morris, D. K., Sah, J., Balasubramanian, B., and Lundblad, V. (1996). Senescence mutants of *Saccharomyces cerevisiae* with a defect in telomere replication identify three additional EST genes. *Genetics* 144: 1399–1412.
- Levy, M. Z., Allsopp, R. C., Futcher, A. B., Greider, C. W., and Harley, C. B. (1992). Telomere end-replication problem and cell aging. *J. Mol. Biol.* 225: 951–960.
- Lin, J., Smith, D.L., and Blackburn, E.H. (2004). Mutant telomere sequences lead to impaired chromosome separation and a unique checkpoint response. *Mol. Biol. Cell* 15: 1623–1634.
- Lin, K. W., McDonald, K. R., Guise, A. J., Chan, A., Cristea, I.M., Zakian, V.A. (2015). Proteomics of yeast telomerase identified Cdc48-Npl4-Ufd1 and Ufd4 as regulators of Est1 and telomere length. *Nat. Commun.* 6: 8290.
- Lingner, J., Cech, T. R., Hughes, T. R., and Lundblad, V. (1997). Three Ever Shorter Telomere (EST) genes are dispensable for in vitro yeast telomerase activity. *PNAS* 94: 11190–11195.
- Lingner, J., Hughes, T. R., Shevchenko, A., Mann, M., Lundblad, V., and Cech, T. R. (1997). Reverse Transcriptase Motifs in the Catalytic Subunit of Telomerase. *Science* 276: 561–567.
- Livengood, A. J., Zaug, A. J., and Cech, T. R. (2002). Essential regions of *Saccharomyces cerevisiae* telomerase RNA: separate elements for Est1p and Est2p interaction. *Mol. Cell. Biol.* 22: 2366–2374.
- Lubin, J.W., Rao, T., Mandell, E.K., Wuttke, D.S., and Lundblad, V. (2013). Dissecting protein function: An efficient protocol for identifying separation-of-function mutations that encode structurally stable proteins. *Genetics* 193: 715–725.

- Lubin, J.W., Tucey, T. M., and Lundblad, V. (2012). The interaction between the yeast telomerase RNA and the Est1 protein requires three structural elements. *RNA* 18: 1597–1604.
- Lubin, J.W., Tucey, T.M., and Lundblad, V. (2018). Using separation-of-function mutagenesis to define the full spectrum of activities performed by the Est1 telomerase subunit *in Vivo*. *Genetics* 208: 97-110.
- Lue, N.F., Yu, E.Y., and Lei, M. (2013). A popular engagement at the ends. *Nat Struct Mol Biol* 20: 10–12.
- Luke, B., Azzalin, C. M., Hug, N., Deplazes, A., Peter, M., and Lingner, J. (2007). *Saccharomyces cerevisiae* Ebs1p is a putative ortholog of human Smg7 and promotes nonsense-mediated mRNA decay. *Nucleic Acids Res.* 35: 7688–7697.
- Lundblad, V. and Szostak, J.W. (1989). A mutant with a defect in telomere elongation leads to senescence in yeast. *Cell* 57: 633-43.
- Marblestone, J.G., Edavettal, S.C., Lim, Y., Zuo, X., and Butt, T.R. (2006). Comparison of SUMO fusion technology with traditional gene fusion systems: Enhanced expression and solubility with SUMO. *Protein Sci* 15: 182–189.
- Murzin, A.G. (1993). OB(oligonucleotide/oligosaccharide binding)-fold: Common structural and functional solution for non-homologous sequences. *EMBO J* 12: 861–867.
- Nakamura, T. M., Morin, G.B., Chapman, K.B., Weinrich, S.L., Andrews, W.H., Lingner, J., Harley, C.B., and Cech, T.R. (1997). Telomerase catalytic subunit homologs from fission yeast and human. *Science* 277: 955–959.
- Nandakumar J., Bell, C.F., Weidenfeld, I., Zaug, A.J., Leinwand, L.A., and Cech, T.R. (2012). The TEL patch of telomere protein TPP1 mediates telomerase recruitment and processivity. *Nature* 492: 285–289.
- Nguyen, L. (2013). Defining the functional surface of the Est2 catalytic subunit of yeast telomerase. *UC San Diego*. ProQuest ID: Nguyen\_ucsd\_0033M\_13431.
- Nugent, C.I., Hughes, T.R., Lue, N.F., and Lundblad, V. (1996) Cdc13p: a single-strand telomeric DNA-binding protein with a dual role in yeast telomere maintenance. *Science* 274: 249-252.
- Osterhage, J. L., Talley, J. M., and Friedman, K. L. (2006). Proteasome-dependent degradation of Est1p regulates the cell cycle-restricted assembly of telomerase in *Saccharomyces cerevisiae*. *Nat. Struct. Mol. Biol.* 13: 720–728.
- Palm, W. and de Lange, T. (2008). How shelterin protects mammalian telomeres. *Annu. Rev. Genomics Hum. Genet.* 42: 301–334.

- Paschini, M. (2015). A telomere-dedicated RPA complex is essential for the replication of duplex telomeric DNA. *UC San Diego*. ProQuest ID: Paschini\_ucsd\_0033D\_14759.
- Paschini, M., Reyes, C.M., Mandell, E.K., Glustrom, L.W., Lewis, K.A., Wuttke, D.S. and Lundblad, V. Replication fork collapse drives telomere length homeostasis in wild type cells. *Nature*, submitted.
- Paschini, M., Toro, T. B., Lubin, J.W., Braunstein-Ballew, B., Morris, D. K., and Lundblad, V. (2012). A naturally thermolabile activity compromises genetic analysis of telomere function in *Saccharomyces cerevisiae*. *Genetics* 191: 79–93.
- Pennock, E., Buckley, K., and Lundblad, V. (2001). Cdc13 delivers separate complexes to the telomere for end protection and replication. *Cell* 104: 387–396.
- Raman S., Lange, O.F., Rossi, P., Tyka, M., Wang, X., Aramini, J., Liu, G., Ramelot, T.A., Eletsky, A., Szyperski, T., Kennedy, M.A., Prestegard, J., Montelione, G.T., and Baker, D. (2010). NMR structure determination for larger proteins using backbone-only data. *Science* 327: 1014–1018.
- Rao, T., Lubin, J.W., Armstrong, G. S., Tucey, T. M., Lundblad, V., and Wuttke, D.S. (2014). Structure of Est3 reveals a bimodal surface with differential roles in telomere replication. *Proc. Natl. Acad. Sci. USA* 111: 214–218.
- Ritchie, K.B., Mallory, J.C., and Petes, T.D. (1999). Interactions of *TLC1* (which encodes the RNA subunit of telomerase), *TEL1*, and *MEC1* in regulating telomere length in the yeast *Saccharomyces cerevisiae*. *Mol. Cell. Biol.* 19: 6065–6075.
- Rohl C.A. (2005). Protein structure estimation from minimal restraints using Rosetta. *Methods Enzymol* 394:244–260.
- Schmidt, J. C. and Cech, T. R. (2015). Human telomerase: biogenesis, trafficking, recruitment, and activation. *Genes Dev.* 29: 1095–1105.
- Schober, H., Ferreira, H., Kalck, V., Gehlen, L. R., and S. M. Gasser. (2009). Yeast telomerase and the SUN domain protein Mps3 anchor telomeres and repress subtelomeric recombination. *Genes Dev.* 23: 928-938.
- Schramke, V., Luviano, P., Brevet, V., Guillot, S., Corda, Y., Longhese, M.P., Gilson, E., and Géli, V. (2004). RPA regulates telomerase action by providing Est1p access to chromosome ends. *Nat Genet.* 36: 46-54.
- Schrödinger, LLC. The PyMOL Molecular Graphics System, Version 1.5.0.4. Available at [www.pymol.org](http://www.pymol.org).
- Sealey, D. C., Kostic, A. D., LeBel, C., Pryde, F., and Harrington, L. (2011). The TPR-containing domain within Est1 homologs exhibits species-specific roles in telomerase interaction and telomere length homeostasis. *BMC Mol. Biol.* 12: 45.



- Seto, A. G., Livengood, A. J., Tzfati, Y., Blackburn, E. H., and T. R. Cech. (2002). A bulged stem tethers Est1p to telomerase RNA in budding yeast. *Genes Dev.* 16: 2800–2812.
- Seto, A. G., Zaug, A. J., Sobel, S. G., Wolin, S. L., and Cech, T. R. (1999). *Saccharomyces cerevisiae* telomerase is an Sm small nuclear ribonucleoprotein particle. *Nature* 401: 177–180.
- Sexton, A.N., Youmans, D.T., and Collins K. (2012). Specificity requirements for human telomere protein interaction with telomerase holoenzyme. *J Biol Chem* 287: 34455–34464.
- Shen, Y., Delaglio, F., Cornilescu, G., and Bax, A. (2009). TALOS+: A hybrid method for predicting protein backbone torsion angles from NMR chemical shifts. *J Biomol NMR* 44: 213–223.
- Shen, Y., Vernon, R., Baker, D., and Bax A. (2009). De novo protein structure generation from incomplete chemical shift assignments. *J Biomol NMR* 43: 63–78.
- Sievers, F., Wilm, A., Dineen, D., Gibson, T.J., Karplus, K., Li, W., Lopez, R., McWilliam, H., Remmert, M., Soding, J., Thompson, J.D., and Higgins, D.G. (2011) Fast, scalable generation of high-quality protein multiple sequence alignments using Clustal Omega. *Mol Syst Biol* 7: 539.
- Smith, J., Zou, H., and Rothstein, R. (2000). Characterization of genetic interactions with RFA1: the role of RPA in DNA replication and telomere maintenance. *Biochimie* 82, 71-78.
- Smogorzewska, A., and de Lange, T. (2004). Regulation of telomerase by telomeric proteins. *Annu Rev Biochem* 73: 177–208.
- Spellman, P. T., Sherlock, G., Zhang, M. Q., Iyer, V. R., Anders, K., Eisen, M.B., Brown, P.O., Botstein, D., Futcher, B. (1998). Comprehensive identification of cell cycle-regulated genes of the yeast *Saccharomyces cerevisiae* by microarray hybridization. *Mol. Biol. Cell* 9: 3273–3297.
- Stewart, S. A. and Weinberg, R. A. (2006). Telomeres: Cancer to Human Aging. *Annu. Rev. Cell Dev. Biol.* 22: 531– 557.
- Sun, J., Yu, E. Y., Yang, Y., Confer, L. A., Sun, S. H., Wan, K., Lue, N.F., and Lei, M. (2009). Stn1-Ten1 is an Rpa2-Rpa3-like complex at telomeres. *Genes Dev.* 23: 2900–2914.
- Takata, H., Kanoh, Y., Gunge, N., Shirahige, K., and Matsuura, A. (2014). *Mol. Cell* 14: 515–522.
- Takata, H., Tanaka, Y., and Matsuura, A. (2005). Late S Phase-Specific Recruitment of Mre11 Complex Triggers Hierarchical Assembly of Telomere Replication Proteins in *Saccharomyces cerevisiae*. *Mol. Cell* 17: 573–583.

- Teixeira, M.T., Arneric, M., Sperisen, P., and Lingner, J. (2004). Telomere length homeostasis is achieved via a switch between telomerase- extendible and - nonextendible states. *Cell* 117:323–335.
- Tong, X.-J., Li, Q. J., Duan, Y. M., Liu, N. N., Zhang, M. L., and Zhou, J. Q. (2011). Est1 protects telomeres and inhibits subtelomeric Y'-element recombination. *Mol. Cell. Biol.* 31: 1264-1274.
- Tucey, T. M. and Lundblad, V. (2013). A yeast telomerase complex containing the Est1 recruitment protein is assembled early in the cell cycle. *Biochemistry* 52: 1131–1133.
- Tucey, T. M. and Lundblad, V. (2014). Regulated assembly and disassembly of the yeast telomerase quaternary complex. *Genes Dev.* 28: 2077–2089.
- Tugarinov, V., and Kay, L.E. (2003). Ile, Leu, and Val methyl assignments of the 723-residue malate synthase G using a new labeling strategy and novel NMR methods. *J Am Chem Soc* 125: 13868–13878.
- Virta-Pearlman, V., Morris, D. K., and Lundblad, V. (1996). Est1 is a single-strand telomeric DNA binding protein required for the yeast telomerase pathway. *Genes Dev.* 10: 3094–3104.
- Wang, F., Podell, E.R., Zaug, A.J., Yang, Y., Baciou, P., Cech, T.R., and Lei, M. (2007). The POT1-TPP1 telomere complex is a telomerase processivity factor. *Nature* 445: 506–510.
- Webb, C. J. and Zakian, V. A. (2012). Schizosaccharomyces pombe Ccq1 and TER1 bind the 14–3-3-like domain of Est1, which promotes and stabilizes telomerase-telomere association. *Genes Dev.* 26: 82–91.
- Wolfe, K. H. and Shields, D. C. (1997). Molecular evidence for an ancient duplication of the entire yeast genome. *Nature* 387: 708–713.
- Wu, R. A., Upton, H. E., Vogan, J. M., and Collins, K. (2017). Telomerase mechanism of telomere synthesis. *Annu. Rev. Biochem.* 86: 439–460.
- Yu, E.Y., Wang, F., Lei, M., and Lue, N.F. (2008). A proposed OB-fold with a protein-interaction surface in Candida albicans telomerase protein Est3. *Nat Struct Mol Biol* 15: 985–989.
- Zappulla D.C. and Cech, T.R. (2004). Yeast telomerase RNA: A flexible scaffold for protein subunits. *PNAS* 101: 10024–10029.
- Zhang, M. L., Tong, X.J., Fu, X. H., Zhou, B. O., Wang, J., Liao, X.H., Li, Q.J., Shen, N., Ding, J., Zhou, J.Q. (2010). Yeast telomerase subunit Est1p has guanine quadruplex-promoting activity that is required for telomere elongation. *Nat. Struct. Mol. Biol.* 17: 202–209.

Zhong F.L., Batista, L.F., Freund, A., Pech, M.F., Venteicher, A.S., and Artandi, S.E. (2012). TPP1 OB-fold domain controls telomere maintenance by recruiting telomerase to chromosome ends. *Cell* 150: 481–494.

Zhou, J., Lloyd, S.A., and Blair, D.F. (1998). Electrostatic interactions between rotor and stator in the bacterial flagellar motor (flagella motility energy transduction) *PNAS* 95: 6436–6441.

Zhou, P. and Wagner, G. (2010). Overcoming the solubility limit with solubility-enhancement tags: Successful applications in biomolecular NMR studies. *J Biomol NMR* 46: 23–31.

Zou, L. and Elledge, S.J. (2003). Sensing DNA damage through ATRIP recognition of RPA-ssDNA complexes. *Science* 300:1542-8.